



National Library
of Canada

Bibliothèque nationale
du Canada

Canadian Theses Service Service des thèses canadiennes

Ottawa, Canada
K1A 0N4

NOTICE

The quality of this microform is heavily dependent upon the quality of the original thesis submitted for microfilming. Every effort has been made to ensure the highest quality of reproduction possible.

If pages are missing, contact the university which granted the degree.

Some pages may have indistinct print especially if the original pages were typed with a poor typewriter ribbon or if the university sent us an inferior photocopy.

Previously copyrighted materials (journal articles, published tests, etc.) are not filmed.

Reproduction in full or in part of this microform is governed by the Canadian Copyright Act, R.S.C. 1970, c. C-30.

AVIS

La qualité de cette microforme dépend grandement de la qualité de la thèse soumise au microfilmage. Nous avons tout fait pour assurer une qualité supérieure de reproduction.

S'il manque des pages, veuillez communiquer avec l'université qui a conféré le grade.

La qualité d'impression de certaines pages peut laisser à désirer, surtout si les pages originales ont été dactylographiées à l'aide d'un ruban usé ou si l'université nous a fait parvenir une photocopie de qualité inférieure.

Les documents qui sont déjà l'objet d'un droit d'auteur (articles de revue, tests publiés, etc.) ne sont pas microfilmés.

La reproduction, même partielle, de cette microforme est soumise à la Loi canadienne sur le droit d'auteur, SRC 1970, c. C-30.

THE UNIVERSITY OF ALBERTA

Modelling of Dispersion in Porous Media

BY

Christopher G. Voigt

A THESIS

SUBMITTED TO THE FACULTY OF GRADUATE STUDIES AND RESEARCH IN
PARTIAL FULFILMENT OF THE REQUIREMENTS FOR THE DEGREE OF

MASTER OF SCIENCE

DEPARTMENT OF CHEMICAL ENGINEERING

EDMONTON, ALBERTA

Fall 1988

Permission has been granted to the National Library of Canada to microfilm this thesis and to lend or sell copies of the film.

The author (copyright owner) has reserved other publication rights, and neither the thesis nor extensive extracts from it may be printed or otherwise reproduced without his/her written permission.

L'autorisation a été accordée à la Bibliothèque nationale du Canada de microfilmer cette thèse et de prêter ou de vendre des exemplaires du film.

L'auteur (titulaire du droit d'auteur) se réserve les autres droits de publication; ni la thèse ni de longs extraits de celle-ci ne doivent être imprimés ou autrement reproduits sans son autorisation écrite.

ISBN 0-315-45526-8

THE UNIVERSITY OF ALBERTA

RELEASE FORM

NAME OF AUTHOR: Christopher G. Voigt

TITLE OF THESIS: Modelling of Dispersion/in Porous Media

DEGREE: Master of Science

YEAR THIS DEGREE GRANTED: 1988

Permission is hereby granted to THE UNIVERSITY OF ALBERTA LIBRARY to reproduce single copies of this thesis and to lend or sell such copies for private, scholarly or scientific research purposes only.

The author reserves other publication rights, and neither the thesis nor extensive extracts from it may be printed or otherwise reproduced without the author's written permission.

Christopher G. Voigt

Calgary, Alberta

DATE: May 1988

THE UNIVERSITY OF ALBERTA

FACULTY OF GRADUATE STUDIES AND RESEARCH

The undersigned certify that they have read, and recommend to the Faculty of Graduate Studies and Research for acceptance, a thesis entitled "Modelling of Dispersion in Porous Media" submitted by Christopher G. Voigt in partial fulfilment of the requirements for the degree of Master of Science in Chemical Engineering.

Paul Hays

(Supervisor)

W. H. Jones

W. H. Jones

Date: 30 May 1988

ABSTRACT

Breakthrough data is presented for dispersion in two dimensional flow for particle Peclet numbers in the range of 30 to 8000. Numerical simulations to predict the breakthrough for various convection-dispersion models are shown and compared to the experimental results. Higher longitudinal dispersion rates than previously reported in the literature for Peclet numbers above 150 are successfully modelled as proportional to $4.5 \cdot Pe_p$, and roughly equivalent results are obtained if the factor of 4.5 is replaced by the natural log of the product of porosity and Peclet number, along the form predicted by Koch & Brady (1985). Both the transient and the path length dependent forms for the longitudinal dispersion coefficient are shown to reduce the overall dispersion, and not to cause tailing in the breakthrough curves. Simulation results are shown to be unaffected by choice of boundary condition for the convection-dispersion equation (Danckwerts versus fixed), or choice of definition of average particle diameter (arithmetic, geometric, etc.). A blank identification method of deconvolution is shown to be superior to the traditional discrete deconvolution scheme.

ACKNOWLEDGEMENT

For their encouragement, advice and assistance I wish to thank especially Bob Hayes, Kumar Nandakumar, Bob Barton and Tim Spanos.

TABLE OF CONTENTS

Chapter		Page
1.	Introduction.....	1
	1.1 Equations of Change.....	3
	1.2 Dispersion.....	10
	1.3 Residence Time Requirement.....	14
	1.4 Convection-Dispersion Equation Boundary Conditions.....	20
	1.5 Porosity and Particle Size Variation Effects.....	25
	1.6 Tensor Form of the Convection-Dispersion Equation.....	33
	1.7 Stability Criteria.....	36
2.	Dispersion Models.....	39
	2.1 Convection-Dispersion Models.....	39
	2.2 Alternatives to the Convection-Dispersion Equation.....	60
	2.2.1 Capacitance Model.....	60
	2.2.2 Capacitance Type Correlation.....	62
	2.2.3 Alternating Flow Model (AFM).....	66

Chapter	Page
3. Experimental Results.....	68
3.1 Experimental Design and Apparatus.....	68
3.2 Deconvolution.....	87
4. Numerical Simulations.....	106
4.1 Finite Element Method.....	106
4.2 Simulation Results.....	110
4.3 Conclusions and Recommendations.....	185
References.....	189
Appendix A.....	204

LIST OF TABLES

Table		Page
1	Core Simulations.....	76
2	Run Conditions.....	86
3	Deconvolution Pairs.....	99
4	Run #1 Simulations.....	125
5	Run #6 Simulations.....	128
6	Run #7 Simulations.....	133
7	Run #11 Simulations.....	135
8	Run #20 Simulations.....	137
9	Run #22 Simulations.....	138
10	Run #23 Simulations.....	139
11	Run #27 Simulations.....	140
12	Run #32 Simulations.....	142

LIST OF FIGURES

Figure		Page
1	Core Design.....	74
2	Experimental Apparatus.....	78
3	Drain Valve Breakthrough.....	80
4	Spectrophotometer Calibration.....	83
5	Non-Loading Cascaded Elements.....	88
6	Block Diagram of System.....	89
7	Block Diagram of Lumped System.....	90
8	Identification Test.....	100
9	Reproducibility of Deconvolution.....	101
10	3x1 Inch Core Runs.....	102
11	3x1.5 Inch Core Runs.....	103
12	6x1 Inch Core Runs.....	104
13	6x1.5 Inch Core Runs.....	105
14	Run #1 d_p Variation.....	143
15	Run #6 d_p Variation.....	144
16	Boundary Condition Effect.....	145
17	Time Step Small Core.....	146
18	Time Step Large Core.....	147
19	Mesh Effects.....	148
20	Mesh Uniformity Effects.....	149

Figure		Page
21	Injector Mesh Effects.....	150
22	Numerical Dispersion Effects.....	151
23	Transverse Dispersion Effects.....	152
24	Limit of Transverse Effects.....	153
25	Transient Variations.....	154
26	Transient Effects.....	155
27	Length Dependence Effects.....	156
28	FC Variations.....	157
29	Cutoff Effects on FC(2).....	158
30	Model Type Comparison Run #1.....	159
31	KB Variations.....	160
32	FC Variations.....	161
33	Model Type Effects.....	162
34	FC Variations.....	163
35	Cutoff Effects on FC(2).....	164
36	Model Type Effects.....	165
37	KB Variations.....	166
38	FC Variations.....	167
39	Cutoff Effect on FC(2).....	168
40	Model Type Effect.....	169
41	KB Variations.....	170
42	FC Variations Run #22.....	171
43	Model Type Effects.....	172
44	FC Variations.....	173

Figure		Page
45	Model Type Variations.....	174
46	KB Variations.....	175
47	FC Variations.....	176
48	Model Type Variations.....	177
49	KB Variations.....	178
50	FC Variations.....	179
51	Model Type Variations.....	180
52	KB Variations.....	181
53	FC Variations.....	182
54	Model Type Variation.....	183
55	KB Variations.....	184

Appendix A

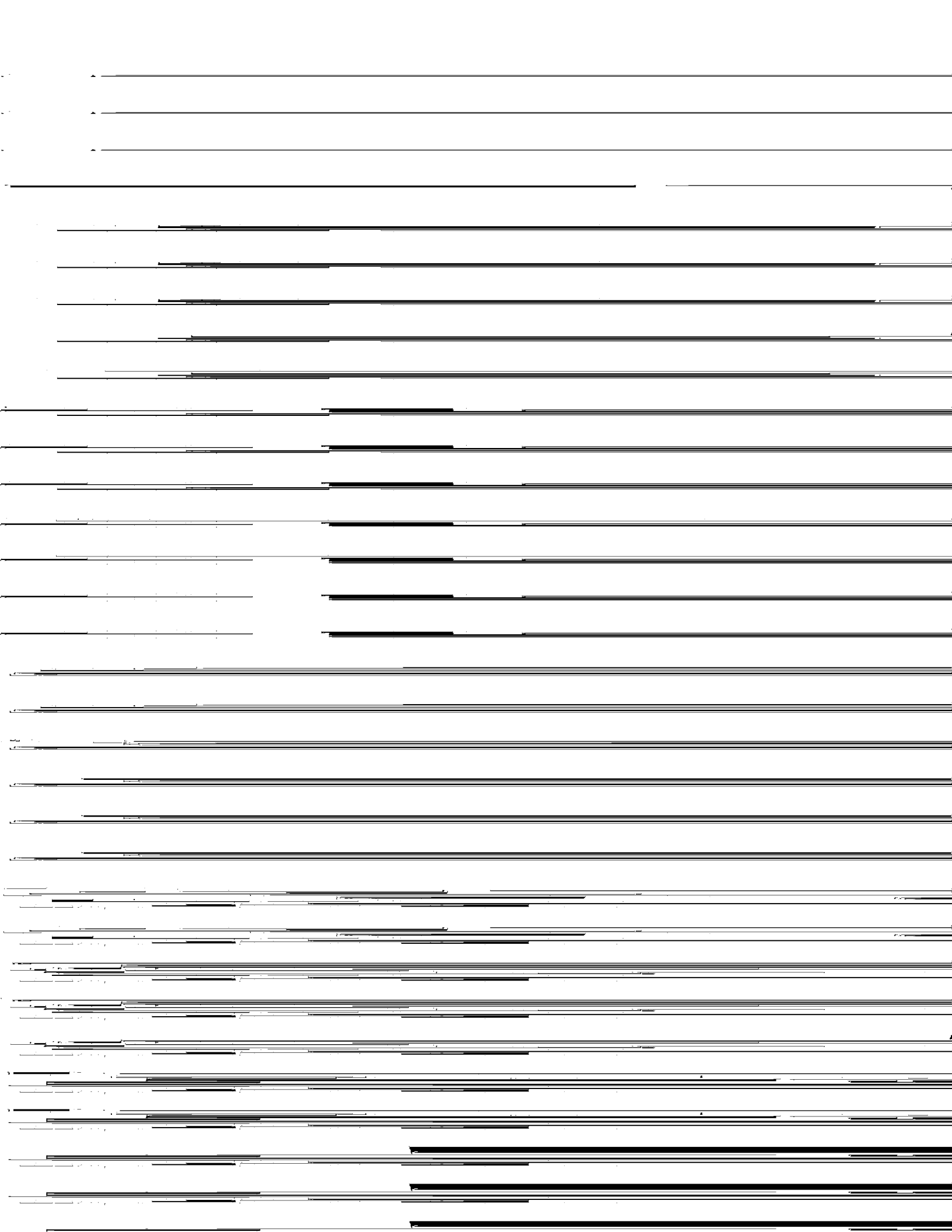
A.1	Raw Data for 3x1 Inch Core.....	205
A.2	Raw Data for 3x1.5 Inch Core.....	206
A.3	Raw Data for 6x1 Inch Core.....	207
A.4	Raw Data for 6x1.5 Inch Core.....	208
A.5	Raw Data for Blank Runs.....	209

NOMENCLATURE

a	<ul style="list-style-type: none">* aspect ratio, in equation (1.5.10)* parameter of transience, equation (4.2.1)
a_1 to a_4	Constants in equation (1.5.3)
\bar{a}_s	mean area of mass transfer relative to void volume, cm^2/cm^3 , in equation (2.2.2.7)
a_{ld}	parameter of length dependence, equation (4.2.2)
A	<ul style="list-style-type: none">* Bed cross-sectional area* Constant in Ergun equation, (1.1.16)* Absorbance, equation (3.2.6)
A_b	Absorbance data for blank runs, equation (3.2.7)
A_p	Total surface area of particles in bed
B	Constant in Ergun equation, (1.1.16)
C	<ul style="list-style-type: none">* Interstitial concentration* deLigny parameter, equation (2.1.32)
C_c	<ul style="list-style-type: none">* Feed concentration* Concentration of fast moving fluid, in equation (2.2.2.7)
C_m	Mean interstitial concentration
C_0	Concentration at Z equal to zero
C_s	Concentration of slow moving fluid in equation (2.2.2.7)
C^*	Concentration at $Z = Z^*$
C_1	Concentration in dead end pores, equation (2.2.1.1)
d_c	Column diameter
d_h	Hydrodynamic particle diameter, equation (2.2.2.2)
d_p	Particle diameter (\bar{d}_p is average)
\bar{D}, D_{ij}	Dispersion matrix, tensor

D_f	Diffusion coefficient
D_l	Longitudinal dispersion coefficient
D_t	Transverse dispersion coefficient
D^m	Contribution to dispersion from difference in diffusivities between particle and surrounding fluid, equation (2.1.18)
D^T	Convective contribution to dispersion, equation (2.1.18)
D^α	Diffusive contribution to dispersion, equation (2.1.18)
D^*	Dispersion coefficient of Chandrasekhara <i>et al.</i> (1980), equation (2.1.43)
e	White noise, equation (3.2.8)
f	* Flowing fraction, equation (2.2.1.3) * Input function, equation (3.2.1)
f_c	Forchheimer's coefficient
f_s	Step input, equation (3.2.6)
F	Formation resistivity factor, so tortuosity is $(F\phi)^{-1}$
g	Gravitational constant
G	Transfer function
G_c	Transfer function of packed core, equation (3.2.6)
G_f	Transfer function of fittings <i>etc.</i> , equation (3.2.6)
h	* Head pressure * Model parameter, defined in (1.5.9)
j	Molar flux, equation (1.4.3)
k	* Intrinsic permeability * Time step, equation (3.2.7)
K_h	Hydraulic conductivity, $k \rho g/\mu$
K_0	Diffusion coefficient for tracer in a porous medium
\bar{K}_{fs}	Mean overall mass transfer coefficient at interface of flowing and stagnant regions, equation (2.2.2.7)
l	Distance; pore length in Pe_s

L	Bed length
m	* Number of concentric cylindrical layers in thickness equal to $d_p/2$, equation (1.5.10) * Ratio of tracer solubilities, equation (2.1.28)
M	Mass transfer coefficient, equation (2.2.1.4)
n	Constant in Ergun equation, (1.1.16)
n_i	Number fraction in equation (1.5.6)
na	Order of polynomial PA, equation (3.2.9)
nb	Order of polynomial PB, equation (3.2.10)
nk	Number of time steps in delay, equation (3.2.8)
N_T	Total number of spheres in the bed
p	Pressure
PA	Polynomial in Z for output function, equation (3.2.8)
PB	Polynomial in Z for the input function, equation (3.2.8)
Pe_h	Hydrodynamic Peclet number, equation (2.2.2.4)
Pe_{hl}	Dynamic longitudinal Peclet number, equation (2.2.2.1)
Pe_{ht}	Dynamic transverse Peclet number, equation (2.2.2.3)
Pe_k	Peclet number based on screening length, $U d_p k^{1/2}/D_f$
Pe_p	Particle Peclet number, $U d_p/D_f$
$Pe_{p,Han}$	Peclet number of Han <i>et al.</i> (1985), $\phi Pe_p/(1-\phi)$
Pe_s	Peclet number based on pore length, $U l/D_f$
r	Thickness of concentric cylindrical layer
q_s	Molar flux along streamline direction, equation (1.6.2)
q_t	Molar flux along direction transverse to streamline, equation (1.6.3)
Q	Total volumetric flow rate
R	* Reynolds' number for equation (2.1.43) * Rate of reaction or adsorption, equation (1.2.1) * Tube radius, equation (1.2.6)



Greek Nomenclature

α_k	Diffusivity ratio parameter, equation (2.1.19)
α_1	Adjustable parameter (≈ 0.5) in Fried & Combarous (1971) dispersion model, equation (2.1.2)
α_t	Adjustable parameter (≈ 0.025) in Fried & Combarous (1971) dispersion model, equation (2.1.3)
β	Parameter in equations (2.1.7) & (2.1.8)
β_1	Adjustable power (≈ 1.2) in Fried & Combarous (1971) dispersion model, equation (2.1.2)
β_t	Adjustable power (≈ 1.1) in Fried & Combarous (1971) dispersion model, equation (2.1.3)
γ	* Koch & Brady (1985) parameter, eqn. (2.1.28) * de Ligny (1970) dispersion parameter, eqn. (2.1.32)
Γ	core wall boundary, equation (4.1.2b)
Γ'	boundary open to flow, equation (4.1.2a)
θ	* Time, equation (2.2.2.8) * Dimensionless group for residence time, eqn. (1.2.4)
λ	de Ligny (1970) dispersion parameter, eqn. (2.1.32)
λ_1	Dispersion (longitudinal) parameter in equation (2.1.4)
λ_t	Dispersion (transverse) parameter in equation (2.1.5)
λ_0	Dispersion parameter in equation (2.1.43)
μ	Viscosity
ν	Kinematic viscosity, ρ/μ
Ω	domain of core, equation (4.1.1)
ρ	density
σ	* Non-homogeneity factor in equation (2.1.9) * $h/k^{1/2}$, equation (2.1.43)
τ	* Tortuosity, $(F\phi)^{-1}$

- * Dummy variable of integration, equation (3.2.1)
- ϕ * Porosity
- * Potential in equation (1.6.8)
- ϕ_b Bulk porosity
- ϕ_f Volume fraction of flowing fluid, eqn. (2.2.2.6)
- ϕ_s * Volume fraction of stagnant fluid, eqn. (2.2.2.6)
- * Solids volume fraction, Koch & Brady (1985) dispersion model
- ψ Stream function, equation (1.6.8)

1. INTRODUCTION

Dispersion in porous media is a subject of interest to many, including engineers, chromatographers and geo-scientists. Given the ease and successful use of Fick's equation for diffusion, the goal has been to find a similarly convenient result for the dispersion of tracers in a fluid flowing in a porous medium. It would have the same form (flux proportional to concentration gradient) except that the dispersion coefficient, replacing the diffusion coefficient as the proportionality factor, would be primarily a function of velocity and various porous medium dependent parameters. Applications include modelling of residence-time distributions for packed bed reactors, groundwater contamination by hydrologists, the transition zone between salt water and fresh water in coastal aquifers, movement of chemicals through the soil, chromatography and miscible displacement in enhanced oil recovery (EOR) techniques.

There have been many papers on this subject since the early 1960's, including several reviews. Among the most recent of the reviews are Patel (1983), Dullien (1979), Greenkorn (1983), Cluff and Hawkes (1976), Rose (1977), Fried (1975), Schwartz (1977) and Stalkup (1983). Greenkorn (1981) also presented a review on flow through porous media with a short review on dispersion. Cluff presents a chromatographer's viewpoint; Schwartz, a geoscientist's; and Rose, a soil scientist's. Of the more recent papers, the one by Han *et al.* (1985), on column length and

particle size distribution effects, and especially the Koch & Brady (1985, 1987 a & b) presentation of a theoretical dispersion model for randomly packed unconsolidated porous media, are the most interesting. These papers are discussed at length in later sections.

The objective of this study is to review and evaluate the models proposed for the dispersion coefficients, with an emphasis on finding one that gives both reasonable results in practice and has a sound physical basis. The first chapter contains the relevant background information on the equations of flow and dispersion for porous media, choice of boundary conditions, residence time requirement, porosity and particle size variation effects, tensor formulation and stability theory. The various dispersion models are described in the second chapter. The third chapter details the experimental work, including an in-depth look at a topic (deconvolution) that has not been well presented in the literature on dispersion. The fourth chapter contains the results of the numerical simulations, which provide the testing ground for the dispersion models, and their comparison to the experimental data. Conclusions and recommendations are then given concerning the experimental work, deconvolution, and dispersion models.

1.1 EQUATIONS OF CHANGE

For porous media, Reynolds' number is usually defined as:

$$Re_p = \frac{\phi U d_p \rho}{\mu} \quad (1.1.1)$$

where ϕ is the porosity, U is the interstitial or pore velocity, d_p is the (average) particle diameter, ρ is density and μ is viscosity. Porosity may be a function of position and pressure; for an ideal non-deformable, homogeneous, isotropic porous medium, it is usually assumed to be constant (Cheng, 1985). It varies from near unity at the wall to a constant value at five to seven particle diameters into the bed. Porosity is discussed in detail later, as it has been a topic of recent discussion in the literature.

Different definitions of average particle sizes have been used. One is the geometric average defined by Fair and Hatch (1933):

$$\bar{d}_p = \left[\sum_i \frac{X_i}{d_{m,i}} \right]^{-1} \quad (1.1.2)$$

where X_i is the mass fraction of the total sample sieved, or the ratio of mass on a tray to the sample mass, and $d_{m,i}$ is the geometric mean of the rated sizes (root of the product of the sizes) of adjacent sieve trays. A second common average is that

of Han et al. (1985):

$$\bar{d}_p = \frac{\sum_i \left[\frac{X_i}{\rho_i} \right]}{\sum_i \left[\frac{X_i}{\rho_i d_{p,i}} \right]} \quad (1.1.3)$$
$$= 6 \frac{V_p}{A_p}$$

where ρ_i is the density of a particle, $d_{p,i}$ is the diameter of a particle, V_p is the volume of the particles in the bed and A_p is the surface area of the particles. This is also the average proposed, for cases of constant porosity, by MacDonald et al. (1979) in their review. A third definition is presented in Allen (1981) as:

$$\bar{d}_p = \sum_i X_i d_{p,i} \quad (1.1.4)$$

The dimensionless group used to characterize dispersion processes is the Peclet number:

$$Pe_p = \frac{U d_p}{D_f} \quad (1.1.5)$$

where D_f is the diffusion coefficient of the solute. Other definitions that have been used include using the superficial velocity instead of the pore velocity, e.g. as in Koch & Brady (1985, 1987), or using the quantity defined in (1.1.5) multiplied by a ratio involving the porosity. For example, Han *et al.* (1985) use:

$$Pe_{p, \text{Han}} = \frac{\phi Pe_p}{(1-\phi)} \quad (1.1.6)$$

The equation of continuity, modified for porous media, is (Bird *et al.*, 1960):

$$\phi \frac{\partial \rho}{\partial t} = - \bar{\nabla} \cdot \rho \bar{U}_0 \quad (1.1.7)$$

\bar{U}_0 is the bed average or superficial velocity vector.

For flow in porous media, the commonly used equation of motion is Darcy's law (Cheng, 1985):

$$U_0 = \frac{Q}{A} = - K_h \frac{\Delta h}{\Delta l} \quad (1.1.8)$$

where

$$\Delta h = \Delta z + \frac{\Delta p}{\rho} \quad (1.1.9)$$

Q is the total flow rate, A is the bed cross-sectional area, Z is

elevation and l is distance. K_h is the hydraulic conductivity, given by:

$$K_h = \frac{k \rho g}{\mu} \quad (1.1.10)$$

where g is the gravitational constant. The intrinsic permeability, k , is essentially dependent only on the medium microstructure and is independent of temperature. For three-dimensional flow, $1/k$ is assumed to be a second-order tensor whose elements' values depend on the pore structure. Darcy's law is commonly written as, using matrix notation (double overbar for a matrix and a single overbar for a vector):

$$\bar{q} = - \frac{\bar{k}}{\mu} (\bar{\nabla}p - \rho \bar{g}) \quad (1.1.11)$$

The ratio k/μ is often termed the mobility in the petroleum engineering literature.

The flow regime in which Darcy's law is valid is given as Re_p less than ten by Bird *et al.* (1960) and as Re_p less than one by Greenkorn (1981). Others, e.g. Fand *et al.* (1986), put the limit on this as being between one and ten. Fand *et al.* as well consider the flow regimes in porous media to be:

- (1) Pre-Darcy: $Re_p < \text{approximately } 10^{-5}$
- (2) Darcy Flow: $10^{-5} < Re_p < 3$, approximately.
- (3) Transition from Darcy to Forchheimer flow

- (4) Forchheimer Flow: $3 < Re_p < 100$
- (5) Post-Forchheimer flow: $Re_p > 100$.

Turbulence is significant in this last regime. Bear (1973) explains the phenomenon of a "pre-Darcy" flow regime as being due to the non-Newtonian behaviour of fluids and to small currents that run counter to the main flow in the pores. This classification may not be of much interest since it occurs at such a low value of Re_p , and has therefore avoided debate; it has not been widely accepted in any case.

The equation for one-dimensional Forchheimer flow is (Cheng, 1985):

$$U_0 + \frac{f_c \rho U_0^2}{\mu} = - \frac{k}{\mu} \frac{dp}{dl} \tag{1.1.12}$$

where f_c is Forchheimer's coefficient. Based on experimental data for isothermal flow of water at Re_k (or $Re_p k^{1/2} d_p^{-1}$) less than 18.1, the following ratio was determined (Cheng, 1985):

$$\frac{f_c}{k^{1/2}} = 0.55 \tag{1.1.13}$$

Alternatives to Darcy's Law include the Ergun equation (Cheng, 1985):

$$-\frac{dp}{dl} + \frac{150(1-\phi)^2}{\phi^3} \frac{\mu U_0}{d_p^2} + \frac{1.75(1-\phi)}{\phi^3} \frac{\rho U_0^2}{d_p} \quad (1.1.14)$$

It is used to obtain estimates of k and of f_c as

$$k = \frac{d_p^2 \phi^3}{150(1-\phi)^2} \quad (1.1.15)$$

and

$$f_c = \frac{1.75 d_p}{150(1-\phi)} \quad (1.1.16)$$

from equation (1.1.12).

MacDonald *et al.* (1979) presented a modified Ergun equation for smooth particles:

$$\frac{\text{grad } P}{U_0^2} \frac{\bar{d}_p}{(1-\phi)} \frac{\phi^n}{(1-\phi)} = \frac{A(1-\phi)}{\text{Re}_p} + B \quad (1.1.17)$$

where n is 3, A is 180 and B is 1.8. For the specific case of smooth uniform spherical particles, A and B have the values of 146 and 1.47, respectively. Using n equal to 3.6 is suggested for best results.

For three-dimensional flow, Forchheimer's equation is written

as (Cheng, 1985):

$$\bar{U}_0 + \frac{\rho f_c \bar{U}_0}{\mu} |\bar{U}_0| = - \frac{\bar{k}}{\mu} (\bar{\nabla}P - \rho \bar{g}) \quad (1.1.18)$$

This reduces to Darcy's law when f_c is zero.

In using Darcy's law, the velocity obtained for a wall or boundary is non-zero given a non-zero pressure gradient at that location. The many boundaries in dilute or highly porous media make the inclusion of a viscous term necessary in order to model the flow properly. An empirical modification of Darcy's Law, proposed by Brinkman (1947), that allows for this viscous effect is given in Bird *et al.* (1960) as:

$$-(\bar{\nabla}P - \rho \bar{g}) = \frac{\mu \bar{U}_0}{k} - \mu \nabla^2 \bar{U}_0 \quad (1.1.19)$$

The viscous term, $\mu \nabla^2 \bar{U}_0$, affects the velocity profile to give a momentum boundary layer of thickness on the order of $k^{1/2}$ (Haber *et al.*, 1983; Chandrasekhara *et al.*, 1979). Darcy's law gives quite similar results (Haber *et al.*, 1983) if the boundary condition at the wall, normally taken as a pressure condition, is replaced with:

$$U_n = \sqrt{k} \bar{\nabla}_t \cdot \bar{U}_t \quad (1.1.20)$$

where "n" and "t" refer to the normal and tangential directions, respectively, to the wall. It is expected that the effect of the boundary layer are insignificant if large tube to particle diameter ratios are used. Brinkman's and Haber's corrections may then be omitted safely.

Vafai & Tien (1981) presented the following general equation that uses Forchheimer's coefficient, as presented in Cheng (1985):

$$-\bar{\nabla}p = \frac{\mu \bar{U}_0}{k} + \frac{\rho f_c \bar{U}_0}{k} |\bar{U}_0| - \frac{\mu}{\phi} \nabla^2 \bar{U}_0 \quad (1.1.21)$$

Darcy's law is relatively convenient to use in view of the type of corrections or alternatives that are available. It has become the form most commonly used due to both its convenience and its reasonable results for a wide range of flow conditions.

1.2 DISPERSION

The dispersion-convection equation is obtained by a mass balance as:

$$\phi \frac{\partial C}{\partial t} + \bar{\nabla} \cdot (\bar{U}C\phi) = \bar{\nabla} \cdot (\phi \bar{D} \bar{\nabla} C) + R \quad (1.2.1)$$

where \bar{U} is the interstitial velocity vector, R is the rate of

adsorption or reaction and C is the pore or interstitial concentration. \bar{D} is the dispersion matrix, which is generally characterized by Pe_p for a given porous medium. The convection term, $\bar{v} \cdot (\bar{U} \nabla \phi)$, is often written as $\bar{U} \cdot \bar{\nabla} \phi$ for incompressible fluids by making use of the continuity expression (1.1.7). The magnitude of the dispersion effect depends on the flow velocity and type of porous media, and can include effects from mixing due to obstructions and velocity gradients in the fluid phase, as well as adsorption and diffusion to and from stagnant regions such as dead end pores, areas of closed streamlines and hydrodynamic boundary layers. If the (Darcy scale) velocity field is one dimensional through the packed bed, the dispersion matrix reduces to a diagonal form often denoted as having the longitudinal (in the direction of flow) component, D_l , and the transverse (perpendicular to the direction of flow) component, D_t . The analogous equation for heat transfer is obtained by using enthalpy and thermal diffusivity, respectively, instead of concentration and mass diffusivity in the above form (Koch & Brady, 1985).

Applying this equation to the dispersion of a slug of tracer in a tube was first done by Taylor (1953, 1954) in an attempt to explain the experimental observations of Griffiths (1911), who noticed that a slug of tracer injected into laminar tube flow of water eventually spreads out in a symmetrical manner about the plane moving with the average velocity of the water. Taylor realized that two aspects of this needed explanation. First, the maximum speed of the water occurs at the centre of the tube for

laminar flow profiles and this maximum speed is twice the mean speed of the water. This means the clear water around the centre of the tube approaches the slug of tracer, absorbs it as it passes through, then leaves it behind to become clear water again when it exits the slug. Second, the velocity profile is parabolic and hence asymmetric about the plane moving at the mean velocity, yet the dispersion of the slug is symmetric about that plane. For large values of time, one dimensional flow and using the coordinate moving with the mean speed of flow as

$$x = x' - U_m t \quad (1.2.2)$$

Taylor obtained the equation:

$$\frac{\partial C_m}{\partial t} = D_1 \frac{\partial^2 C_m}{\partial x^2} \quad (1.2.3)$$

The residence time constraint necessary is:

$$\theta = \frac{D_1 t}{l^2} \gg 0.14 \quad (1.2.4)$$

C_m is the mean concentration at distance x and time t and l is given the value of R , the tube radius. This tube dispersion problem has the solution, for initial slug concentration C_f :

$$\frac{C_m}{C_f} = \frac{1}{2(\pi D_1 t)^{1/2}} \exp\left[\frac{-(x-U_m t)^2}{4 D_1 t}\right] \quad (1.2.5)$$

which satisfies Griffiths' observation of symmetric flow. Taylor found an explicit formula for D_1 for the case where diffusion is neglected; Aris (1956) extended this to include diffusion to obtain:

$$D_1 = D_f + \frac{U_m^2 R^2}{48 D_f} \quad (1.2.6)$$

It shows dispersion to increase quickly with velocity and with tube radius.

Certain aspects of the Taylor-Aris theory presented above are useful later in describing other models. Those dispersion models are presented here in varying levels of detail, in accordance with the following objective. For this study, a comparison of the various practical dispersion models is the primary goal and so their many different derivations are not dealt with in detail here; they are well presented in the reviews already mentioned. Emphasis is on evaluating models that may be used for practical calculations. Given that the general form of the dispersion equation (1.2.1) can be derived (Greenkorn, 1983) by statistical methods (Scheidegger, 1963), mixing cell models (Kramers *et al.*, 1953) and volume averaging (Carbonell *et al.*, 1983; Whitaker,

1967), as well as by the mass balance method already stated, the various geometric models (capillary, spatially periodic, etc.) that have been proposed in attempts mainly to show the effects of porous medium structure on dispersion, rather than to give practical models for dispersion calculations (Greenkorn, 1983), are of secondary concern.

1.3 RESIDENCE TIME REQUIREMENT

A tacit assumption of many dispersion models is that D_l and D_t are not functions of residence time or position in the packed bed. It should not be so quickly overlooked, as even in Taylor's original analysis of dispersion in a capillary tube a "long time" assumption (equation 1.2.4) had to be made before a solution could be obtained. A number of papers consider this, including Gill and Sankarasubramanian (1970), Brenner (1980), Paine *et al.* (1983) and Carbonell & Whitaker (1983). More recently, Dieulin *et al.* (1981), Reis *et al.* (1979), Han *et al.* (1985) and Koch & Brady (1985, 1987 a & b) have explored the implications of a time-dependent dispersion tensor. Dieulin *et al.* assume that the longitudinal dispersion coefficient is a function of time but that the transverse coefficient is not. They demonstrate this method for a simple, one-dimensional dispersion and obtained excellent results, better than those obtained by a non-transient "classical" model or a "capacitance" model (the dispersion models are

described in detail later). The works by Han *et al.* (1985) and Koch & Brady (1987 a & b) are the most comprehensive and so are discussed in detail below.

Han *et al.* (1985) developed the following semi-empirical expression for the residence time requirement:

$$\theta = \frac{L}{d_p} \frac{1}{Pe_p} \frac{(1-\phi)^2}{\phi^2} \geq 0.3 \quad (1.3.1)$$

Here L is intended to be the path length through the bed (not related to tortuosity but to the overall flow pattern) and Pe_p is based on the average interstitial velocity of a particle along that path to the point in question. Their data show D_l to grow with residence time until it reaches its asymptotic value. Thus, for a given Pe_p , the ratio of bed length to particle diameter must be large enough to satisfy this criterion. If it is met, then D_l will be within $\pm 10\%$ of its asymptotic value. If it is not met, then the asymptotic value for D_l will be underestimated. Han *et al.* (1985) consider much of the published data for longitudinal dispersion coefficients at high Pe_p to be too low because this criterion was not met. The transverse coefficient, D_t , was found experimentally not to exhibit any transience. By adhering to this constraint in the design of an experiment, Han *et al.* predict that the long-time asymptotic longitudinal dispersion coefficients will be reliably obtained. They do not supply a time-dependent expression for D_l or D_t . It should be noted that the form of this

constraint was derived in Carbonell & Whitaker (1983) as $D_t t / l^2$ being much greater than unity, where l is a characteristic length of the pores. This is the same as that obtained by Taylor (1953, 1954) for a capillary tube (equation 1.2.4).

Koch & Brady (1985, 1987 a & b) use ensemble averaging techniques and statistical methods on the basic equations of motion for random porous media in a new approach to the problem. Their 1987 papers present a solution for the transience or, as they refer to it, the "non-local dispersion". Koch & Brady (1987b) treats the "non-mechanical" aspect, while Koch & Brady (1987a) describes the additional, albeit minor, contribution of convection to transience. Their 1985 paper briefly discussed transience and managed to show that although D_t is transient, it actually achieves its asymptotic value much more quickly than does D_1 . This is due to the stagnant volume and boundary layer contributions to transient dispersion affecting only the longitudinal and not the transverse processes. Their 1987 papers do not give explicitly the non-local response curve for a step input, which is the experimental condition for this study, but do for pulse inputs at high values of Pe_p for both porous and non-porous particles. Their results warrant some elaboration.

In Figure (2) of Koch & Brady (1987a) is shown, for cores of different length:

- (1) the basic non-local solution for the pulse response if stagnant volume and boundary layer effects are ignored,
- (2) the solution obtained using non-local theory and

(3) the solution obtained using the asymptotic form of the equations for D_1 & D_t , or local theory, from the Koch & Brady (1985) paper.

These solutions were developed for a ϕPe_p of 10,000. The main feature of these plots that concerns this work is that they show how the breakthrough curves predicted using the non-local theory tend to converge to their local-solutions as the core length, residence time, is increased. If the boundary-layer and stagnant volume contributions are omitted there is substantial error. This implies that the non-transient or "local" theory may be used provided certain residence-time criteria are met, which are specified in Koch & Brady (1987b) as:

$$L \gg d_p (\phi Pe_p)^{1/3} \quad (1.3.2)$$

for boundary layer dispersion effects and

$$L \gg d_p (\phi Pe_p) \quad (1.3.3)$$

for holdup dispersion. The latter is most significant if porous particles or consolidated media is used, which contain a significant amount of stagnant fluid. These criteria were derived, in a manner similar to Han's, from the ratio of the time for a tracer to be convected the length of the bed to the time for it to diffuse into the boundary layers and the time to diffuse into stagnant volumes, respectively. For this, as Paine *et al.*

(1983) and Carbonell *et al.* (1983) found, the quasi-steady state assumption appropriate is that the magnitude of the spatial deviations in concentration, do not vary greatly in time when compared to convective and diffusive effects (equations 29 to 31 in Carbonell, *et al.*, 1983). *i.e.* In order to use the non-transient expression, the time necessary for a particle to diffuse to the boundary layers and stagnant volumes must be much less than the time for it to pass through the bed. The smaller this ratio is, the smaller is the effect on the breakthrough curve of the diffusion to stagnant areas or areas of closed streamlines and the non-local or transient solution tends to converge to the local or non-transient solution.

Koch & Brady's (1987) constraints (1.3.2 and 1.3.3) are similar to that (equation 1.3.1) employed by Han *et al.* (1985) as they can be rearranged to the form:

$$\frac{L}{d_p} \cdot \frac{1}{Pe_p^n} \gg \phi^n \quad (1.3.4)$$

It is easy to see that, if n is unity (corresponding to the holdup value in equation 1.3.3), the inequality changed to a less stringent "greater than or equal to" and ϕ is given a "typical value" of 0.37 for unconsolidated media, the above expression becomes very similar to the semi-empirical result, equation (1.3.1), of Han *et al.* (1985). In the latter, a constant of approximately 0.1 (for ϕ of 0.37) was found instead of 0.37; this includes the additional factor in equation (1.3.1) involving

porosity, which is effectively constant at about three for a given porous medium. Whether the experimental result actually matches the boundary layer (equation 1.3.2) or the holdup constraint (equation 1.3.3) is another question, as Koch & Brady do not relax their "much greater than" inequality. Since the power on Pe_p in (1.3.2) is only one-third, the length requirement for the boundary layer contribution is less than that for the holdup dispersion, and experimental results might be expected to be dominated by holdup dispersion whenever it is present. The expression obtained by Han *et al.* (1985) presumably includes the holdup effect since it has the same functional dependence on Pe_p as that predicted by Koch & Brady (1987) for holdup dispersion. However, from the description of the experimental method used by Han *et al.* (1985) - impermeable spheres, moderately high Pe_p (10^2 to 10^4 for d_p as large as 1.58 cm), non-adsorbing & non-reacting tracer and one-dimensional flow - holdup dispersion would not be expected to be significant. There is not much stagnant volume. This implies that the expression (1.3.1) supplied by Han *et al.* must match the boundary layer contribution constraint (1.3.2) of Koch & Brady (1987); however, the functional dependence is on Pe_p in the former and on $Pe_p^{1/3}$ in the latter. The experimental result of Han *et al.* (1985), if accepted, may therefore be limited to their tested range of Pe_p between 10^2 and 10^4 . It may be that their probes interfered with the local flow pattern and the resulting measured dispersion was greater at that point than should have been recorded.

An interesting result of Koch & Brady's (1987b) non-local model is that it predicts a bi-modal pulse response if the residence time is very short. The first peak of this type of breakthrough is due to the convected part of the dispersion; the bulk of the input tracer is convected through the bed. The second peak is due to the tracer that was initially put into the slow moving boundary layer or stagnant region and had to diffuse out slowly before being convected through the bed. This result is similar to that obtained by Paine *et al.* (1983) for the case of reversible adsorption on a capillary tube model using a volume-averaging technique.

Finally it should be noted that this non-local model compares well with the relatively small amount of experimental data, as given by Han *et al.* (1985) for unconsolidated media and by Charlaix *et al.* (1987) for consolidated media (sintered glass beads). The data of Charlaix *et al.* are in press and this comparison is as related by Koch & Brady (1987).

1.4 CONVECTION-DISPERSION EQUATION BOUNDARY CONDITIONS

The choice of boundary conditions for the convective - dispersion equation (1.2) is not obvious and has been studied by several workers, including Patel (1983), Patel & Greaves (1987), Coats & Smith (1964), Danckwerts (1953), Kreft & Zuber (1978), Rasmuson (1986c), Parker (1984) and Pearson (1959). Kreft & Zuber

(1978) are the most comprehensive.

A common choice of boundary condition for the inlet to the packed bed for a step input of feed is:

$$C = C_f \quad (1.4.1)$$

This condition is used by Patel (1983), Patel *et al.* (1987), Coats & Smith (1964) and Rasmuson (1986c); however, its use means that the dispersion coefficient is not continuous over the domain of the packed bed because it would be going from non-zero in the bed to zero at the boundary.

The convection dispersion equation (1.2.1) may be written in the form:

$$\phi \frac{\partial C}{\partial t} + \bar{v} \cdot \bar{j} = 0 \quad (1.4.2)$$

where

$$\bar{j} = \bar{U} C \phi - \phi \bar{D} \cdot \bar{v} C \quad (1.4.3)$$

The correct boundary condition to use for the inlet is based on equation (1.4.3); it is, as proposed by Danckwerts (1953):

$$U C_f = U C - D_1 \frac{\partial C}{\partial z} \quad (1.4.4)$$

where one dimensional flow and dispersion is assumed. C is the interstitial concentration within the packed bed, including the boundaries, and D_1 is continuous over the same domain. This equation may be used in numerical work only if one-dimensional dispersion may be assumed at the inlet; then it may be integrated from the boundary ($Z = 0; C = C_0$) to a point just across the boundary that is a short distance into the packed bed, $Z = Z^*$. Assuming that the velocity is constant (one-dimensional) over this very short distance implies:

$$\int_{Z=0}^{Z=Z^*} dZ = - \int_{C_0}^{C^*} \frac{D_1 dC}{U (C_f - C)} \quad (1.4.5)$$

This has the solution:

$$C_0 = C_f - (C_f - C^*) \exp\left[\frac{-U Z^*}{D_1}\right] \quad (1.4.6)$$

which has

$$C_0 \rightarrow C_f \text{ as } D_1 \rightarrow 0 \quad (1.4.7)$$

and

$$C_0 \rightarrow C_f \text{ as } C^* \rightarrow C_f \quad (1.4.8)$$

These last two equations show the limiting cases; namely, for piston flow with no dispersion the concentration is everywhere equal to the feed and, for large times, the concentrations at the entrance and just inside the entrance converge to the feed concentration.

Coats and Smith (1964) and Rasmuson (1986C) show analytical solutions for the one-dimensional dispersion for each case of inlet boundary condition. While they examined slightly different problems, as Rasmuson included particle diffusion effects, they have different opinions regarding the effects of the choice of boundary conditions. For Coats *et al.*, the solutions were "roughly" the same accuracy; for Rasmuson, whose solution involves a difficult numerical integration of a rapidly oscillating integrand, the solutions were more substantially different. Patel (1983) and Patel *et al.* (1987) studied the case numerically and found that there was only a slight difference in the breakthrough curves, when a moderately long bed and large aspect ratio are used (67.2 centimetres bed length and ratio of tube diameter to d_p of 228, in their case); these conditions make the effect of the boundary condition less marked.

The Danckwerts boundary condition may be applied at the exit of the bed as well (Parker, 1984); however in that case C_f represents the concentration outside the bed and C inside the bed,

both of which are unknown. To deal with this, the common assumption made for finite beds is to set the two concentrations equal, or equivalently, set the derivative to zero:

$$\left. \frac{\partial C}{\partial Z} \right|_{Z=L} = 0 \quad (1.4.9)$$

Physically, this corresponds to the condition (Coats *et al.*, 1964):

$$D_1 \Big|_{\text{Exit Chamber}} \ll D_1 \Big|_{\text{Bed}} \quad (1.4.10)$$

i.e., that mixing in the exit chamber or tube is much less than the mixing that occurs inside the packed bed. It is also used as the exit condition for semi-infinite beds:

$$\lim_{Z \rightarrow \infty} \frac{\partial C}{\partial Z} = 0 \quad (1.4.11)$$

As an exit condition, the following has also been employed (Coats and Smith, 1964):

$$\lim_{Z \rightarrow \infty} C(Z) = 0 \quad (1.4.12)$$

Coats & Smith find it to be slightly superior to equation (1.4.11) for the semi-infinite case. The zero slope condition, equation

(1.4.9), is physically more realistic for finite beds:

1.5 POROSITY AND PARTICLE SIZE VARIATION EFFECTS

Recently the effects of porosity and particle size variations on flow processes have been subject to renewed interest; neither effect has been completely characterized to date. Their existence is well established for both heat and mass transfer; the concern here is that small differences in void fraction (Carbonell, 1979, 1980) and the width of the particle size distribution (Han *et al.*, 1985) may have strong effects on the value of the longitudinal dispersion coefficient. Regarding the former, the channelling caused by the wall effects on porosity is greater (Chandrasekhara *et al.*, 1979) than that caused by the non-linear term in Forchheimer's equation.

As one of the original experimental works (Benenati *et al.*, 1962) showed, the radial variation within a packed bed of uniform spheres has been found to vary sinusoidally from unity at the wall to about 38% in the bulk or centre of the bed. This is due to the layer of spheres nearest to the wall tending to be highly ordered, the next layer having somewhat less order and so on until the bulk of the bed where they are randomly located. Experimental work since then shows the same pattern, with the heavily damped oscillations reaching their bulk value at about four or five particle diameters into the bed, as long as the

aspect ratio, d_c/d_p , is greater than about ten (Govindarao *et al.*, 1986; Cohen & Metzner, 1981). If the aspect ratio is less than about six, a bulk or steady value for porosity is not reached. This same effect was also observed for a binary mixture of spheres for systems with particle diameter ratios greater than 0.4, provided that the average diameter is properly chosen (Ridgeway *et al.*, 1966). For beds with a wider distribution of sizes it is obvious that this oscillatory variation will be unpredictable and probably much more heavily damped since the smaller particles may fit between the larger ones and significantly decrease the voidage, especially in the wall area.

Among the papers on the porosity variation, useful reviews are given by Govindarao *et al.* (1986) and Cohen *et al.* (1981). Govindarao describes the currently available methods for dealing with porosity variations as using either the experimental data of Benenati *et al.* (1962), or as using various semi-empirical equations such as an exponential type (Chandrasekhara *et al.*, 1979; Vortmeyer *et al.*, 1983; Cheng *et al.*, 1986), a tri-regional trigonometric type (Cohen *et al.*, 1981), or even simply sub-dividing the bed into regions of constant porosity (Carbonell, 1980). Stanek *et al.* (1972) deal with regions of different but constant porosity (not due to wall effects) and shows the very strong effects of moderate porosity variations on flow patterns.

For the simple sub-division method described by Carbonell (1980), the bulk 90% of total area in the centre of the bed was assumed to have a constant porosity of 0.40, while the remaining

wall region was at 0.50. This was enough to result in the order of magnitude decrease in Nusselt number at low Peclet numbers (less than ten) as obtained by previous investigators. Porosity variation at the wall similarly affects dispersion; Stephenson *et al.* (1986) used their experimental data averaged over subdivisions to obtain an oscillatory profile for porosity; their measured values of D_1 for air in water did not vary along the cross-section. However, their values of D_t dropped monotonically from a bulk value to zero at the wall, which is surprising in that the rate dispersion is expected to follow the Pe_p (which depends on ϕ) variations.

The exponential equations used by Vafai *et al.* (1984), Chandrasekhara *et al.* (1979), Vortmeyer *et al.* (1983) and Cheng *et al.* (1986) are all of the form:

$$\phi = \phi_b \left[1 + c_1 \exp \left[\frac{-N_1 y}{d_p} \right] \right] \quad (1.5.1)$$

where ϕ_b is the bulk value of the porosity, and both c_1 and N_1 are empirical constants which depend slightly on the aspect ratio, d_c/d_p . For flow between plates, Cheng chose values of unity and two for c_1 and N_1 , respectively. Cheng also used this form for the resulting permeability variation, taking values of twenty and four for c and N , respectively, by comparison to the Ergun-type permeability expression (1.1.15).

Cohen et al.'s (1981) semi-empirical tri-regional model applies for packed beds whose aspect ratio, d_c/d_p , is in the range of seven to sixty:

$$\frac{1-\phi}{1-\phi_b} = 4.5 \left[X - \frac{7}{9} X^2 \right] \quad (1.5.2)$$

for $X \leq 0.25$.

$$\frac{\phi-\phi_b}{1-\phi_b} = a_1 \exp(-a_2 X) \cdot \cos(a_3 X - a_4) \pi \quad (1.5.3)$$

for $0.25 < X < 8$.

$$\phi = \phi_b \quad (1.5.4)$$

for $8 \leq X < \infty$.

Here X is the number of particle diameters from the wall, ϕ is the local porosity and the constants a_1 to a_4 are, respectively:

$$\begin{aligned} a_1 &= 0.3463 \\ a_2 &= 0.4273 \\ a_3 &= 2.4509 \end{aligned} \quad (1.5.5)$$

and

$$a_4 = 2.2011$$

For beds with an aspect ratio less than ten, only the wall and

transition region equations (1.5.2 and 1.5.3) are used. When the aspect ratio is greater than thirty for Newtonian fluids (fifty for power law), wall corrections for average mass flux are unnecessary (Cohen *et al.*, 1981).

Govindarao *et al.* (1986) present a new, somewhat elaborate, semi-empirical model that is based on dividing the cylindrical bed into a number of concentric layers of equal thickness. In this method, the porosity in each layer is determined by the fraction of the total number of spheres in the bed that have their centre in that layer. For the layers that are up to four or five particle diameters from the wall, the number fractions are correlated with the aspect ratio using experimental data from the literature. His results are:

$$\phi_1 = 1 - \frac{h}{g_1} \left[n_{i+m} + (m-1/4) + 3 \sum_{j=m+1}^{i+m-1} X n_j b_{i,j} \right] \quad (1.5.6)$$

for $i = 1$ to $2m$.

$$\phi_1 = 1 - \frac{h}{g_1} \left[(n_{i-m} + n_{i+m})(m-1/4) + 3 \sum_{j=i-m+1}^{i+m-1} X n_j b_{i,j} \right] \quad (1.5.7)$$

for $i \geq 2m$. Here

$$b_{i,j} = m^2 - i^2 + j(2i-j) - \frac{1}{6} \quad (1.5.8)$$

for $i \ll am$.

In the above equations, X is number of sphere diameters from the wall, n_i is the number fraction in the i^{th} layer and

$$h = \frac{N_T \Delta r}{3L} \quad (1.5.9)$$

where N_T is the total number of spheres in the bed, r is the thickness of a concentric cylindrical layer (CCL) and L is the bed length. As well

$$g_i = 2am - 2i + 1 \quad (1.5.10)$$

where "a" is the aspect ratio and m is the number of CCL's in a thickness equal to d_p/z . The quantity N_T/L can be estimated from:

$$\frac{N_T}{L} = \frac{3}{4m^3 \Delta r} \left[\sum_{i=1}^q (1-\phi_1) g_i + (1-\phi_b)(a_m - q)^2 \right] \quad (1.5.11)$$

where q is the number of CCL's being used. This method does not work if the aspect ratio is small or infinite; it does work well for large aspect ratios.

Particle size variations present a number of problems; they affect transport properties markedly (Han *et al.*, 1985; Carbonell, 1979 a & b), are not readily correlated (LeGoff *et al.*, 1985) for even the bulk porosity of the bed (much less the wall-induced

variation) and are themselves not always reliably measured or characterized by standard sieving techniques (Allen, 1981).

Early work on this was done by Niemann (1969). As related by Greenkorn *et al.* (1969), Niemann used a glass-beads media, which had an approximately logarithmic distribution of diameters, and found that the effective load diameter to be used in permeability calculations was slightly above the 10% value in the number distribution. Most authors (Greenkorn, 1969) take the 50% value for dispersion calculations. His model for dispersion is presented in equation (2.1.15); it shows that the dispersion can be correlated to show a dependence on permeability, interstitial velocity, and the variance of the particle size distribution.

Other early experimental work was correlated in Perkins *et al.* (1963) to give equations (2.1.9) and (2.1.10) for the dispersion coefficients, in which an average particle diameter is used as well as an empirically based inhomogeneity factor. His result is different from Niemann's, showing a need for more work in this area.

More recent attempts to capture the effect of pore-size distributions by Carbonell (1979, a & b) involve a capillary model, in which a moment analysis yields a longitudinal model for dispersion that depends strongly on the standard deviation of the pore size distribution. This suggests that Niemann's approach may be more fruitful for actual random porous media as his form includes the variance of the particle size distribution.

In the most recent work, Han *et al.* (1985) obtained

experimental results for random unconsolidated porous media. They tested for the effects of using uniform spheres, spheres with a narrow size distribution (ratio of maximum to minimum diameter of 2.2) and spheres with a wide size distribution (ratio of 7.3). Most experiments in the literature have been done with a very narrow size distribution over $\phi Pe_p / (1-\phi)$ in the range of 10^2 to 10^4 for both longitudinal and lateral dispersivities. For the cases of uniform particle size and narrow size distribution, the longitudinal dispersivities obtained experimentally by Han *et al.* were quite similar. The wide size distribution, however, resulted in values of D_1 that were two to three times larger than those obtained for uniform spheres. As well, the length of the bed, or the residence time requirement to measure steady dispersion values, was greater for wider size distributions. They suggest that this is indicative of the media having a characteristic length larger than $\bar{d}_p \phi / (1-\phi)$ for cases with wide size distributions. It should be noted that virtually the same porosity and \bar{d}_p were obtained for all three size distributions, indicating that the width of the distribution is the important factor (Han *et al.*, 1985). Their column had a square cross-section (27 cm in width) and the range of particle sizes was 0.25 cm to 1.58 cm, hence the range of their aspect ratio was approximately 108 to 17. As noted previously in this section, aspect ratios less than 30 have significant porosity variations at the walls with respect to the average mass flux; these low aspect ratio runs may have given the higher dispersion values due to

channelling at the walls rather than due to just the wide distribution of particle sizes.

1.6 TENSOR FORM OF THE CONVECTION-DISPERSION EQUATION

Various papers use the following form of the convection-dispersion equation for cartesian coordinate systems (Bachmat and Bear, 1964; Fattah *et al.*, 1985; Li *et al.*, 1967; Guin *et al.*, 1972; Bear, 1961; Greenkorn, 1981):

$$\frac{\partial C}{\partial t} + U_i \frac{\partial C}{\partial X_i} = \frac{\partial}{\partial X_i} \left[D_{ij} \frac{\partial C}{\partial X_j} \right] \quad (1.6.1)$$

The coordinate system X_i may be set up for one-dimensional flow so that one axis coincides with the direction of flow, thus reducing the dispersion tensor D_{ij} to its principal components, D_l and D_t (i.e. $D_{ij} = 0$ for $i \neq j$).

If the flow is not one-dimensional, then all components of D_{ij} may have non-zero values. The tensor form of the dispersion term may be used to account for this, but the same result can be obtained geometrically, as shown in Peaceman (1966). In that paper, the off-diagonal components for the dispersion matrix are straightforwardly calculated by rotating the coordinate axes and summing the contributions along each from both the streamline flux, q_s , and the transverse flux, q_t . This is done by noting

that the longitudinal dispersion is proportional to the streamline concentration gradient, $\partial C / \partial X_s$, by

$$q_s = -D_1 \frac{\partial C}{\partial X_s} \quad (1.6.2)$$

and transverse dispersion is proportional to the concentration gradient, $\partial C / \partial X_t$, that is perpendicular or transverse to the streamline and parallel to the potential,

$$q_t = -D_t \frac{\partial C}{\partial X_t} \quad (1.6.3)$$

Since X_s and X_t are not parallel everywhere to their corresponding axes in the chosen coordinate system, i.e. the flow is not one-dimensional, there are net mass flux contributions from both D_1 and D_t along each axis. The calculations are somewhat tedious.

The alternative process is to use the following general tensor form of the dispersion-convection equation (with subscripts for covariant components and superscripts for contravariant ones):

$$\frac{\partial C}{\partial t} = \frac{\partial}{\partial X^i} \left[D^{ik} \frac{\partial C}{\partial X^k} - U^i C \right] \quad (1.6.4)$$

In order to write the matrix form of the dispersion tensor D^{ik} for the case of a cylindrical coordinate system (r, z) with no

rotational (θ) dependence, the potential-streamline (ϕ, ψ) form is first given as:

$$\bar{D} = \begin{bmatrix} D_t & 0 \\ 0 & D_1 \end{bmatrix} \quad (1.6.5)$$

To transform a contravariant tensor to another coordinate system, the following identity is used (Spiegel, 1974):

$$\bar{A}^{pr} = \frac{\partial \bar{X}^p}{\partial X^q} \frac{\partial \bar{X}^r}{\partial X^s} A^{qs} \quad (1.6.6)$$

where \bar{X} and X represent different coordinate systems. Here, stream function and potential are nondimensionalized with the total volumetric flow rate and total pressure drop, respectively, and then are redimensionalized (to length) using the radius and core length, respectively.

In matrix form, equation (1.6.6) becomes:

$$\begin{bmatrix} \bar{A}^{11} & \bar{A}^{12} \\ \bar{A}^{21} & \bar{A}^{22} \end{bmatrix} = \begin{bmatrix} \frac{\partial \bar{X}^1}{\partial X^1} & \frac{\partial \bar{X}^1}{\partial X^2} \\ \frac{\partial \bar{X}^2}{\partial X^1} & \frac{\partial \bar{X}^2}{\partial X^2} \end{bmatrix} \begin{bmatrix} A^{11} & A^{12} \\ A^{21} & A^{22} \end{bmatrix} \begin{bmatrix} \frac{\partial \bar{X}^1}{\partial X^1} & \frac{\partial \bar{X}^2}{\partial X^1} \\ \frac{\partial \bar{X}^1}{\partial X^2} & \frac{\partial \bar{X}^2}{\partial X^2} \end{bmatrix} \quad (1.6.7)$$

The (r, z) form of the dispersion tensor is then:

$$D^{ik} = \begin{bmatrix} \frac{\partial r}{\partial \phi} & \frac{\partial r}{\partial \psi} \\ \frac{\partial z}{\partial \phi} & \frac{\partial z}{\partial \psi} \end{bmatrix} \begin{bmatrix} D_t & 0 \\ 0 & D_1 \end{bmatrix} \begin{bmatrix} \frac{\partial r}{\partial \phi} & \frac{\partial z}{\partial \phi} \\ \frac{\partial r}{\partial \psi} & \frac{\partial z}{\partial \psi} \end{bmatrix} \quad (1.6.8)$$

and, finally:

$$\bar{D} = \begin{bmatrix} D_t \left(\frac{\partial r}{\partial \phi} \right)^2 + D_1 \left(\frac{\partial r}{\partial \psi} \right)^2 & D_t \frac{\partial z}{\partial \phi} \frac{\partial r}{\partial \phi} + D_1 \frac{\partial z}{\partial \psi} \frac{\partial r}{\partial \psi} \\ D_t \frac{\partial z}{\partial \phi} \frac{\partial r}{\partial \phi} + D_1 \frac{\partial z}{\partial \psi} \frac{\partial r}{\partial \psi} & D_t \left(\frac{\partial z}{\partial \phi} \right)^2 + D_1 \left(\frac{\partial z}{\partial \psi} \right)^2 \end{bmatrix} \quad (1.6.9)$$

This may also be obtained using the geometric approach previously mentioned.

1.7 STABILITY CRITERIA

When the densities and viscosities of the displacing and displaced fluid do not meet a certain stability criteria, the displacing fluid will finger through the displaced fluid. That is, as the displacement process begins there is initially a rather well defined front or transition zone between the displacing and displaced fluids; in an unstable situation, the displacing fluid

will not maintain this front but will develop various isolated protusions or fingers into the displaced fluid. This process is not described by the convection-dispersion equation. The displaced fluid will have its concentration in the bed drop asymptotically to zero, with islands of it left in the bed that are difficult to move.

The case has been studied by Saffman and Taylor (1958) and Chuoke *et al.* (1959) for the case of immiscible fluids, with both arriving at the form:

$$\left[\frac{\mu_2}{K_2'} - \frac{\mu_1}{K_1'} \right] U + (\rho_2 - \rho_1) g \cos(z') > 0 \quad (1.7.1)$$

The velocity, U , is positive for liquid 1 displacing liquid 2, K_1' and K_2' are the effective permeabilities to their respective fluids and $\cos(z')$ is the direction cosine between the vertical axis and the axis normal to the (initially plane) interface between the two liquids. Generally, if the driving fluid's viscosity and density are both greater than that of the displaced fluid, there will be no unstable growths or fingers.

Miscible displacement tends to be more stable than immiscible due to a transition zone, rather than a sharp interface, that exists between the two pure fluids. Even if small fingers are formed momentarily, diffusion tends to make them join and so retards their growth. Experimental work is presented by Perkins

and Johnston (1963), Crane *et al.* (1963), Fried & Combarous (1971) and Chen (1987). More recently, Chang *et al.* (1987) presented a stability analysis for miscible displacements and reviewed the previous work in this field. Unlike that previous work, (*e.g.* Heller, 1966), Chang *et al.* did not limit the problem to a porous media that is unbounded in the direction of flow. Their motivation for considering a semi-infinite porous media comes from the recognition that entrance effects can cause the instabilities to grow if the system is unstable. In the Chang *et al.* analysis, it is concluded that if the viscosity ratio, μ_1/μ_2 , is less than one then the displacement in the porous medium will be stable to small perturbations as long as the two fluids have equal densities and are miscible. However, the displacement will not necessarily be unstable if the viscosity ratio is greater than one. If the concentration is changed sufficiently slowly with time, the displacement will be stable, no matter how unfavourable the mobility ratio.

2. DISPERSION MODELS

The models presented in this section deal primarily with the convection-dispersion equation (1.2.1). There have been other defining equations proposed, most notably the "capacitance" model, and some of these are discussed at the end of the chapter.

The convection-dispersion equation is solved numerically using these dispersion models and those simulation results are presented in the fourth chapter.

2.1 CONVECTION-DISPERSION MODELS

Dimensionless groups to be used in dispersion models were found by dimensional analysis (Fried and Combarous, 1971), assuming:

- (1) mixing occurs without a volume change,
- (2) the diffusion coefficient is constant and is denoted as K_0 for a porous medium and
- (3) the dispersion does not depend on the mixture viscosity, but only on the individual viscosities of the fluids before they are mixed.

Considering experimental results, they found that the dimensionless group, D/D_r , and the Peclet number, Pe_p , can be used to adequately characterise the dispersion phenomenon. Here D is the dispersion coefficient.

For unconsolidated porous media, these dimensionless groups can be used in correlations to describe five different dispersion regimes. These are (Fried and Combarrous, 1971):

- (1) $Pe_p < 0.15$, approximately. There is essentially only pure diffusion in the porous medium, where

$$K_0 = \frac{D_l}{D_f} \Big|_0 = \frac{D_t}{D_f} \Big|_0 \approx 0.67 \quad (2.1.1)$$

The magnitude varies for different packings. There are no velocity gradients, and particles in the porous medium block or impede the diffusion process. The subscript "0" denotes the low velocity or diffusion asymptote.

- (2) $0.15 < Pe_p < 6$, approximately. Here mechanical dispersion begins to superimpose onto the diffusion process for both longitudinal and transverse processes. No correlation was given, but equations (2.1.2) and (2.1.3) may be assumed.
- (3) $6 < Pe_p < 260$, approximately. The general forms of the dispersion models are given as:

$$\frac{D_l}{D_f} = \frac{D_l}{D_f} \Big|_0 + \alpha_1 Pe_p^{\beta_1} \quad (2.1.2)$$

and

$$\frac{D_t}{D_f} = \frac{D_t}{D_f} \Big|_0 + \alpha_t Pe_p^{\beta_t} \quad (2.1.3)$$

Approximations for α_1 , α_t , β_1 and β_t are given as 0.5, 0.025, 1.2 and 1.1, respectively; practical values corresponding to particular experimental data are found by curve-fitting. The effect of mechanical dispersion is predominant over the diffusive process in this region. The longitudinal parameter values differ from the transverse values even for an isotropic porous medium, hence they cannot merely be medium properties (Dullien, 1979). The value of the exponent " β " may be roughly stated to lie in the range $1 \leq \beta \leq 1.2$, for a general dispersion model applicable over $6 < Pe_p < 2 \times 10^5$. For a capillary tube, β_1 is two; this would be the theoretical upper limit for porous media.

(4) $260 < Pe_p < 2 \times 10^5$, approximately. Here the diffusion contribution is insignificant compared to the mechanical dispersion. Generally,

$$\frac{D_l}{D_f} = \lambda_1 Pe_p \quad (2.1.4)$$

where $\lambda_1 = 1.8 \pm 0.4$ and

$$\frac{D_t}{D_f} = \lambda_t Pe_p \quad (2.1.5)$$

where λ_t is approximately the same as α_t . The transverse and longitudinal forms can be seen here to be equivalent to those in regime (3), except that the exponent " β " now has a value of unity.

(5) $2 \times 10^5 < Pe_p$, approximately. Here the flow may be becoming turbulent and Darcy's law is no longer valid. Darcy's law is considered valid for Re_p up to about the range of 1 to 10 (Bird *et al.*, 1960). For porous media, turbulence is more significant at Re_p around 100. There are few results in this range and even some of these do not satisfy the residence time limitation of Han *et al.* (1985); they must therefore be considered as possibly being underestimated. There are other correlations available that are similar to the forms of equations (2.1.2) and (2.1.3). One of these is referred to as the power-law model (Patel, 1983):

$$\frac{D_t}{D_f} = \frac{1}{F \phi} + \frac{\alpha_1}{D_f} U^\beta \quad (2.1.6)$$

where F is the formation electrical resistivity factor, $F\phi$ is the flow tortuosity, and α_1 and β are constants. The tortuosity term is usually insignificant for a velocity less than 10^{-4} cm/sec

(Patel, 1983). Bear (1972) suggested that longitudinal and transverse dispersion were directly proportional to the pore velocity by the medium characteristic parameters α_l and α_t as described by Dullien (1979), this model has been generalized for use in hydrogeology to the form:

$$D_l = \alpha_l U^\beta \quad (2.1.7)$$

and

$$D_t = \alpha_t U^\beta \quad (2.1.8)$$

where the parameters α_l , α_t and β are again obtained by curve fitting. This may work and give consistent values for the parameters as long as the same media and tracer are used. However, the dimensionless-group form of equations (2.1.2) to (2.2.5) demonstrates their more substantial physical basis; the adjustable parameters there should be more reliable when different particle sizes and tracer diffusion coefficients are being considered.

More similar to the classical model, that being the one described by Fried and Combarous (1971), is the model of Perkins and Johnston (1963) for uniform and non-uniform media:

$$\frac{D_1}{D_f} = \frac{1}{F \phi} + 0.5 \text{Pe}_p \sigma \quad (2.1.9)$$

for $\text{Pe}_p < 50$ and

$$\frac{D_t}{D_f} = \frac{1}{F \phi} + 0.055 \text{Pe}_p \sigma \quad (2.1.10)$$

for Pe_p less than 100. The non-homogeneity factor, σ , is based on data from Raimondi *et al.* (1959) for non-uniform media. It has a value of unity for ideal packing; experimentally they show it to increase as d_p gets smaller, due to bridging and the wider particle size distribution common of smaller particles. For beads of approximately 0.3 or 0.4 mm in diameter, σ is 3.5 to 4.0 as read from Figure 18, p. 79, Perkins & Johnston (1963). Thus, while this model has the same form as that presented by Fried and Combarros (1971), its parameters have substantially different values.

One of the earlier correlations presented was that of Harleman *et al.* (1963), which used Reynolds' number based upon the interstitial velocity:

$$D_1 = 0.66 \nu \left[\frac{\text{Re}_p}{\phi} \right]^{1.2} \quad (2.1.11)$$

and

$$D_t = 0.036 \nu \left[\frac{Re_p}{\phi} \right]^{0.7} \quad (2.1.12)$$

for $10^{-3} < Re_p / \phi < 10$, where Re_p is based on the average particle diameter, \bar{d}_p . The upper limit is that for laminar flow. Here \bar{d}_p is the average by weight as per Han *et al.* (1985). To show a Pe_p and Re_p dependence, this model may be rewritten in the form:

$$\frac{D_l}{D_f} = 0.66 Pe_p \left[\frac{Re_p}{\phi} \right]^{0.2} \quad (2.1.13)$$

and

$$\frac{D_t}{D_f} = 0.036 Pe_p \left[\frac{Re_p}{\phi} \right]^{-0.3} \quad (2.1.14)$$

A more recent model that incorporates both the permeability and the particle size distribution is that of Niemann (1969), as presented by Greenkorn (1983). He found that the longitudinal dispersion coefficient was a function of the permeability, velocity, and slope of the particle size distribution, S , in the following manner:

$$D_1 \propto S \frac{U^{m_1}}{k^{m_2}} \quad (2.1.15)$$

where m_1 was correlated as $\{0.70 + 0.54 \log(k)\}$ and m_2 has a value of 0.07. These results have also been shown in the form where D_1 is proportional to Re_k^m (Greenkorn, 1969). Previous to Niemann's work, the only other model to explicitly include the effect of particle size distributions was based on the data of Brigham *et al.* (1961); there, Perkins *et al.* (1963) relied upon an average diameter and an inhomogeneity factor in their semi-empirical relation presented earlier in this section. Most models are used with an average diameter for this work.

Koch and Brady (1985, 1987 a & b) give asymptotic solutions to the dispersion problem. In their first paper is derived a model that shows reasonable agreement, as they judge it, for both longitudinal and transverse dispersion coefficients when compared to the experimental data as presented in Fried *et al.* (1971). Their 1987 paper deals with the transient nature of dispersion and will be discussed later; it does support their 1985 model, but is applicable to cores of any length and not just the sufficiently long cores required of the previous model. The major feature of these (1985 & 1987) models is that they may be used without adjustable parameters, eliminating curve-fitting to breakthrough data. Actually, they leave room for adjustment but in effect offer a prediction for that correction factor. A second, possibly

very useful, attribute is that they also apply for permeable particles.

The physical mechanisms described by Koch & Brady (1985) for the dispersion are significant to varying degrees in different flow regimes. There is a convective mechanism due to the velocity variations that is most significant at high Peclet numbers. The resulting effective diffusivities, D/D_f , grow linearly with ϕPe_p . At low ϕPe_p , the zero velocity regions that exist inside permeable particles cause D/D_f to grow as $\phi^2 Pe_p^2$. At high ϕPe_p , the low velocity regions inside the boundary layer and regions of closed streamlines gives terms that grow as $\phi Pe_p \ln(\phi Pe_p)$ and $\phi^2 Pe_p^2$, respectively.

To obtain these results, Brinkman's equation is used instead of Darcy's law; it is integrated over the volume surrounding a point particle. Two particle interaction effects are added when necessary. The resulting asymptotic forms for the longitudinal and transverse dispersion coefficients are given in Table 1 of Koch & Brady (1985). Upon inspection of their derivation it was decided to use the full form of their solution. i.e. Where their scale or order-of-magnitude analysis did not definitely show some terms, which they drop, to be negligible in the flow regimes of interest here, those terms were reinserted and the resulting more general equations used. This is described in more detail later, once the model has been completely presented.

For their analysis, ϕ_s is defined as the solid volume fraction (porosity is then $1-\phi_s$), m is the ratio of the

solubilities of the solute in the fluid to that in the particles (m^{-1} is zero for impermeable particles) and α_k is the ratio of diffusivity in the particle to that in the fluid, all divided by m , giving $D_p / (D_f m)$. α_k is zero for impermeable particles. For dilute beds they use dimensionless permeability, k , as given by:

$$k = \frac{2}{9} \phi^{-1} \quad (2.1.16)$$

The square root of the permeability is known as the screening length. A Peclet number based on screening length is:

$$Pe_k = \frac{\phi U k^{1/2}}{D_f} d_p = \phi Pe_p k^{1/2} \quad (2.1.17)$$

Their dispersion model contains three terms:

$$D = D^m + D^\alpha + D^* \quad (2.1.18)$$

where D^m is the diffusion contribution, D^α is the particle effects from the difference in diffusivities and D^* is the convective contribution. The dispersion model, as presented in Table 1 of Koch & Brady (1985), is as follows:

(1) For $\phi Pe_p \ll \phi_s^{1/2} \ll 1$,

$$\frac{D_i}{D_f} = 1 + \frac{3(\alpha_k - 1)\phi}{\alpha_k + 2} + \frac{2^{1/2} \phi^2 Pe_p^2}{15 \phi_s^{1/2}} \quad (2.1.19)$$

and

$$\frac{D_t}{D_f} = 1 + \frac{3(\alpha_k - 1)\phi}{\alpha_k + 2} + \frac{2^{1/2} \phi^2 Pe_p^2}{60 \phi_s^{1/2}} \quad (2.1.20)$$

In these equations, the first term is the diffusive contribution, D^m . The second is the contribution from the difference in diffusivities inside and outside the particles, D^α . In their calculations (p. 420, Koch & Brady, 1985) was included an extra term to this, the "Jeffrey correction", giving:

$$D^\alpha = -1.5 \phi_s + 0.588 \phi_s^2 \quad (2.1.21)$$

for impermeable (α_k of zero) particles. That term is included as well for this study. The third term, containing Pe_k^2 , is the convective contribution, D^c .

(2) For $\phi_s^{3/4} \ll \phi Pe_p \ll 1$,

$$\frac{D_1}{D_f} = 1 + D^\alpha + k^{-1/2} \left[\frac{3}{4} |Pe_k|^{-2} - \frac{3}{2} |Pe_k|^{-1} + 3 |Pe_k|^{-2} \right. \\ \left. + 3 \left[|Pe_k|^{-1} - |Pe_k|^{-3} \right] \ln \left[|Pe_k| + 1 \right] \right] \quad (2.1.22)$$

and

$$\frac{D_t}{D_f} = 1 + D^\alpha + k^{-1/2} \left[\frac{1}{4} + \frac{3}{4} |Pe_k|^{-1} - \frac{3}{4} |Pe_k|^{-2} \right. \\ \left. + \frac{3}{2} \left[|Pe_k|^{-3} - \frac{1}{2} |Pe_k|^{-1} \right] \ln \left[|Pe_k| + 1 \right] \right] \quad (2.1.23)$$

(3) For $\phi_s^{1/2} \ll \phi Pe_p \ll 1$ (or $Pe_k \gg 1$),

$$\frac{D_1}{D_f} = 1 + \frac{3}{4} |\phi Pe_p| \quad (2.1.24)$$

and

$$\frac{D_t}{D_f} = 1 + \frac{3\sqrt{2}}{8} \phi_s^{1/2} \quad (2.1.25)$$

(4) For $\phi Pe_p \gg 1$,

$$\frac{D_1}{D_f} = 1 + \frac{3}{4} |\phi Pe_p| + \frac{1}{6} \pi^2 \phi_s |\phi Pe_p| \ln |\phi Pe_p| + \frac{1}{15} (1 + \gamma)^2 \frac{D_f}{mD_p} \phi_s \phi^2 Pe_p^2 \quad (2.1.26)$$

and

$$\frac{D_t}{D_f} = 1 + \frac{63 \sqrt{2}}{320} \phi_s^{1/2} |\phi Pe_p| \quad (2.1.27)$$

where

$$\gamma = \frac{\phi_s (1 - m^{-1})}{1 - \phi_s (1 - m^{-1})} \quad (2.1.28)$$

For D_1 in (2.1.26), the natural log term is the boundary layer contribution; Koch & Brady state that the functional form of this equation is correct, but that its constant pre-multiplier may be adjusted, as necessary, to fit beds that have a different microstructure. *i.e.* The Stokes' drag assumed for its derivation may not be a reasonable approximation and so a certain amount of adjusting of the result is expected to be necessary. Along the same line of reasoning, the dilute bed permeability (equation 2.1.16) may also be subject to some reasonable variation, such as to that predicted by Ergun's equation. The last term is the

stagnant volume or "holdup" contribution. In their calculations, equations (2.1.26) and (2.1.27) were used with a value of unity for ϕPe_p as an arbitrary lower limit. The experimental data obtained here are for an average ϕPe_p above unity and so these (2.1.26 and 2.1.27) are the most relevant equations for this study. However, Koch and Brady have over simplified them as they are presented. The D^α term is therefore retained, including its Jeffrey correction. As well, the term that is first order in ϕPe_p , the first mechanical contribution of D^* , is to be used in its full form instead of the form shown just above. To do this, the full form of equation (3.14.10) of Koch & Brady (1985) is used for D_1^* in the derivation of (2.1.26) & (2.1.27). i.e. All the terms in equation (2.1.22) except the terms corresponding to D^m and D^α are used to replace the $(3/4)\phi Pe_p$ term, giving the following complete expression for longitudinal dispersion:

$$\begin{aligned} \frac{D_1}{D_f} = & 1 + D^\alpha + k^{-1/2} \left[\frac{3}{4} |Pe_k|^{-2} - \frac{3}{2} |Pe_k|^{-1} + 3 |Pe_k|^{-2} \right. \\ & \left. + 3 \left[|Pe_k|^{-1} - |Pe_k|^{-3} \right] \ln \left[|Pe_k| + 1 \right] \right] \\ & + \frac{1}{6} \pi^2 \phi_s^2 |\phi Pe_p| \ln |\phi Pe_p| + \frac{1}{15} (1+\gamma)^2 \frac{D_f}{mD_p} \phi_s^2 \phi Pe_p^2 \quad (2.1.29) \end{aligned}$$

To get D_t , first consider equation (4.11a) of Koch & Brady (1985):

$$D_t = 1 + \frac{21\sqrt{2}}{80} \phi_s^{1/2} D_1 + \frac{9\sqrt{2}}{80} D_t \phi_s^{1/2} \quad (2.1.30)$$

The factor of $\phi_s^{1/2}$ has been added to the last term on the right-hand side as they apparently had a misprint. Substituting the new form for D_1 just described (equation 2.1.29) into equation (2.1.30) produces the following complete form for D_t :

$$\begin{aligned} \frac{D_t}{D_f} = & \left[1 + \frac{21\sqrt{2}}{80} \left\{ 1 + D^\alpha + k^{-1/2} \left[\frac{3}{4} |Pe_k|^{-2} - \frac{3}{2} |Pe_k|^{-1} \right. \right. \right. \\ & + 3 |Pe_k|^{-2} + 3 \left[|Pe_k|^{-1} - |Pe_k|^{-3} \right] \ln \left[|Pe_k| + 1 \right] \left. \left. \left. \right] \right. \right. \\ & + \left. \left. \left. \frac{1}{6} \pi^2 \phi_s \left| \phi Pe_p \right| \ln \left| \phi Pe_p \right| + \frac{1}{15} (1+\gamma)^2 \frac{D_f}{mD_p} \phi_s \phi^2 Pe_p^2 \right\} \right] \\ & + \left[1 - \frac{9\sqrt{2}}{80} \phi_s^{1/2} \right] \end{aligned} \quad (2.1.31)$$

Due to the similarity between these equations (2.1.29 & 2.1.31) for D_1 and D_t , the computational effort to use them is not as much as it might at first seem. One note: if permeable particles are used and it is desired to use the Jeffrey (1973) correction, then the value of the correction coefficient for the ϕ^2 term for D_t must be changed as per that paper.

One model that can be looked upon as being classical with a correction factor on the Peclet number term is that of de Ligny (1970), which was derived by a statistical means:

$$D = \gamma D_f + \frac{\lambda \bar{d}_p U}{1 + C D_f / (\bar{d}_p U)} \quad (2.1.32)$$

Here U is the pore velocity and γ , λ and C are constants. He gives the order of magnitude of γ as 0.7. For spherical packing and liquid fluid λ_1 is 2.5, C_1 is 8.8 and λ_t is 0.08. He does not give a value for C_t although by derivation it is expected to equal C_1 . However, he found experimentally that C_t is about an order of magnitude above C_1 for gaseous fluids. In any case, this parameter may be adjusted to get the best curve fit to experimental data. Similarly, Edwards and Richardson (1968) found:

$$\frac{D_1}{D_f} = 0.73 + \frac{0.5 Pe_p}{1 + 9.7 / Pe_p} \quad (2.1.33)$$

for $0.0377 < \bar{d}_p < 0.60$ cm., $0.02 < Pe_p < 130$ and $0.008 < Re_p < 50$. This data was correlated from data obtained in experiments using an argon tracer in air in a packed bed of spheres.

Previous to Koch and Brady, Saffman (1960) presented a model based on random walks through straight, uniform and randomly

oriented capillary tubes. While the final expression he obtained for D_t overestimates its experimental value, the expression for D_1 does give reasonable results and has a form that is not entirely dissimilar to that of Koch and Brady (1985). Saffman obtained:

$$\frac{D_1}{D_f} = \frac{D_1}{D_f} \Big|_0 + \frac{4}{9} + \frac{Pe_s}{6} \left[\ln \left[\frac{3}{2} Pe_s \right] - \frac{17}{8} + \frac{1}{16} Pe_s \right] \quad (2.1.34)$$

and

$$\frac{D_t}{D_f} = \frac{D_t}{D_f} \Big|_0 + \frac{1}{3} + \frac{3}{16} Pe_s + \frac{1}{40} \left(\frac{RU}{D_f} \right)^2 \quad (2.1.35)$$

where Pe_s is given by Ul/D_f , l is the pore length, R is the pore radius and $(D/D_f)_0$ is the porous media diffusivity (approximated as $2D_f/3$). He uses l with a value equal to d_p and then R is taken as $l/5$. The range of applicability given is:

$$1 \ll Pe_s \ll 8 \left(\frac{l}{R} \right)^2 \quad (2.1.36)$$

For the approximation of l/R as 5, the above limits become:

$$1 \ll Pe_s \ll 200 \quad (2.1.37)$$

For $Pe_s \ll 1$, he found the form, similar to the classical of Fried

& Combarous (1971):

$$\frac{D_1}{D_f} = \frac{2}{3} + \frac{1}{15} Pe_s^2 \quad (2.1.38)$$

and

$$\frac{D_t}{D_f} = \frac{2}{3} + \frac{1}{40} Pe_s^2 \quad (2.1.39)$$

Dieulin *et al.* (1981) presented a model in which the longitudinal dispersion coefficient D_1 is a function of time while the transverse coefficient D_t is constant. They obtained very impressive results for a one-dimensional system, but do not show how to get the dispersion coefficients for higher dimensional systems. As mentioned previously, Han *et al.* (1985) found no time dependence experimentally for D_t yet did for D_1 , thus supporting the method of Dieulin *et al.* on that point. Koch and Brady (1985, 1987) show that both are functions of time, but since the transverse coefficient reaches its final value very quickly only the transience of the longitudinal coefficient is significant for most applications. Many of the non-transient models are similar in that the values of the dispersion coefficients are predicted using adjustable parameters found from experimental data. While the classical non-transient and capacitance (to be presented later) models use curve fitting to find two or three parameters characterizing breakthrough curve data, predictions by the

transient model of Dieulin *et al.* are procured using all of the experimental run data. It must be pointed out that the exact method used by Dieulin *et al.* is unclear, and their success may be due to the prior knowledge and use of particular experimental data. That is, they decompose D_1 into a product of two functions $\{f(U)*g(x)\}$ in a manner making use of breakthrough data, then use that product to "predict" that same breakthrough data.

Rose (1977) presents the following statistically-based model of Bear (1969) as having good agreement with the data of Pfannkuch (1963) for l/a having the value of unity:

$$\frac{D_1}{D_f} = K_0 + Pe_p \left[1 + \frac{2}{Pe_p} + \frac{4}{Pe_p} \left(\frac{l}{a} \right)^2 \right] \quad (2.1.40)$$

where l/a is taken to be the ratio of the mean pore length to the mean pore radius. The model for the porous medium is a random network of pores of varying length and radius. The expression for D_1 obtained above is given as valid for all values of Peclet number.

Cluff *et al.* (1976) reviewed some seven hundred and fifty data points $(D_1/D_f, Pe_p)$ of eighteen investigations and did a statistical analysis to obtain a correlating equation for each of the high and low velocity regimes. They not only included the previously mentioned dimensionless groups that characterize the dispersion phenomenon but also somewhat speculatively used various

physical parameters. This results in a relatively lengthy (for a correlation) and perhaps questionable formulation. For systems that have an integral-measuring technique, e.g. light-absorption over the column cross-section, they obtained the regression formulae:

For low velocity ($Re_p \leq 30$),

$$\frac{D_1}{D_f} = \frac{Pe_p}{2} \left[5.01 + 7.34 \times 10^{-4} Pe_p - 1.10 d_c - 0.134 Re_p - 2.79 \times 10^{-8} Pe_p^2 + 3.04 \times 10^{-13} Pe_p^3 + \frac{0.14}{Pe_p^2} - \frac{3.34 \times 10^{-3}}{Pe_p^3} + 0.089 d_c^2 \right] \quad (2.1.41)$$

For high velocity ($Re_p > 30$),

$$\frac{D_1}{D_f} = \frac{Pe_p}{2} \left[0.879 \log(Pe_p) - 1.22 \log(Re_p) - 3.00 \log(d_p) + 0.0196 d_c^2 \right] \quad (2.1.42)$$

It is to be expected that Pe_p and Re_p are statistically significant in the above correlation, but it is surprising to find that the column diameter, d_c , was as well. They state that d_c and

d_p both have units of centimeters; since $\log(d_p)$ appears it is not clear how the unit has been eliminated for that calculation. While porosity is not explicitly shown, it is implicit in the Pe_p and Re_p terms. The column length, L , was not found to be significant for integrated data, although it was for point-data. Perhaps this suggests that any non-local effects or transience are substantially reduced by using integrated measurements; more likely it is merely the result of the few improperly staged experiments, with respect to the residence time requirement, having been done using point measurement techniques. They do not give an expression for transverse dispersion. As chromatographers, they are less concerned with that aspect since they tend to use relatively long and thin columns in which transverse effects would be less marked.

Chandrasekhara *et al.* (1980) use Brinkman's equation to get the following expression for longitudinal dispersion in a porous medium between parallel plates.

$$\frac{2 D^*}{\bar{u}^* d_p} = \frac{1.8 R}{R+48S} \quad (2.1.43)$$

where

$$\bar{u}^* = U/\lambda_0$$

$$2h = \text{distance between plates}$$

$$\sigma = h/k^{1/2}$$

$$\lambda_0 = \sigma \cosh(\sigma) - 1$$

$$R = \frac{\bar{u}^* d \rho}{\mu}$$

and

$$S^{-1} = D_f / v$$

2.2 ALTERNATIVES TO THE CONVECTION-DISPERSION EQUATION

This section will describe a few of the alternative models available. Despite the various geometric models (capillary tube, spatially periodic, etc.) available, the ones described here were either only recently presented in the literature or have been more successful in terms of fitting breakthrough data.

2.2.1 CAPACITANCE MODEL

This is the first alternative appearing in the literature. As presented by Fried & Combarous (1971), two of the original papers to use this approach (Fatt *et al.*, 1960; Fatt and Goodnight, 1963) described dispersion with:

$$\frac{\partial C}{\partial t} = \frac{D_f}{\tau} \frac{\partial^2 C}{\partial X^2} - \frac{v_d}{v_1} \frac{\partial C_1}{\partial t} \quad (2.2.1.1)$$

and

$$\frac{\partial C_1}{\partial t} = \frac{D_f A_0}{l_0 V_c} (C - C_1) \quad (2.2.1.2)$$

where $C_1(X,t)$ is the concentration in the dead-end pores, τ is the tortuosity, V_1 is the volume of the flow channels, V_d is the total volume of the dead-end pores, V_c is the volume of one dead-end pore and l_0 and A_0 are the length and cross-sectional area of one dead-end pore, respectively. These equations are somewhat difficult to use because of the number of parameters involved.

Coats and Smith (1964) presented a simplified version of the dead-end pore model:

$$f \frac{\partial C}{\partial t} + U \frac{\partial C}{\partial X} = D_1 \frac{\partial^2 C}{\partial X^2} - (1-f) \frac{\partial C_1}{\partial t} \quad (2.2.1.3)$$

and

$$(1-f) \frac{\partial C_1}{\partial t} = M (C - C_1) \quad (2.2.1.4)$$

whose M is the mass transfer coefficient, f is the flowing fraction (without dead-end pores) and C_1 is the concentration in dead-end pores. This may easily be extended to a multidimensional model. As presented in Yellig and Baker (1981) and in Baker

(1977), these equations reduce to the convection-dispersion form by defining an effective dispersion coefficient as:

$$\frac{D_{1,eff}}{D_1} = 1 + \frac{(1-f)^2 U^2}{D_1 M} \quad (2.2.1.5)$$

provided that the following condition is met:

$$\lim_{X \rightarrow \infty} \frac{\partial^2 C_1}{\partial X^2} \bigg/ \frac{\partial^2 C}{\partial X^2} = 1 \quad (2.2.1.6)$$

This equation is essentially a length requirement.

These "dead-end pore" or "capacitance" models do fit the long, slowly converging tail associated with breakthrough curves but, as mentioned in the residence time requirement section, this may be handled to a certain degree using the non-local or transient model of Koch and Brady (1987) or Dieulin (1981).

2.2.2 CAPACITANCE TYPE CORRELATION

Miyauchi and Kikuchi (1975) present a model that is similar to the capacitance model in that they assume that there are stagnant and flowing regions; however, what they have provided is as well a correlation based on data taken from liquid and gaseous

systems for electrolyte, powder and other tracers. It may be used as a predictive equation.

They use a dynamic Peclet number, which is defined for longitudinal dispersion as:

$$Pe_{hl} = \frac{U d_h}{D_l} \quad (2.2.2.1)$$

where d_h is the hydrodynamic diameter,

$$d_h = \frac{2 \phi d_p}{3(1-\phi)} \quad (2.2.2.2)$$

For transverse processes,

$$Pe_{ht} = \frac{U d_h}{D_t} \quad (2.2.2.3)$$

and

$$Pe_h = \frac{U d_h}{D_f} \quad (2.2.2.4)$$

This last definition is given for the hydrodynamic Peclet number. For the region of correlation of interest here, Pe_p in the range of 1.0 to 10^4 , they use a Pe_{ht} of 0.17. They define tortuosity,

τ , as:

$$\tau = \frac{U_f \phi_f}{U} \quad (2.2.2.5)$$

where U_f is the mean velocity of the flowing fluid, and ϕ_f and ϕ_s are the volume fractions of the flowing and stagnant fluid, respectively, such that:

$$\phi_f + \phi_s = 1 \quad (2.2.2.6)$$

They present the non-dimensionalized system equations as:

$$\frac{D_f}{\tau^2} \frac{\partial^2 C_f}{\partial Z^2} - \frac{U}{\phi_f} \frac{\partial C_f}{\partial Z} - \frac{\bar{K}_{fs} \bar{a}_{fs}^{-1}}{\phi_f} (C_f - C_s) = \frac{\partial C_f}{\partial \theta} \quad (2.2.2.7)$$

and

$$\frac{D_f}{\tau^2} \frac{\partial^2 C_s}{\partial Z^2} + \frac{\bar{K}_{fs} \bar{a}_{fs}^{-1}}{\phi_s} (C_f - C_s) = \frac{\partial C_s}{\partial \theta} \quad (2.2.2.8)$$

where

C_f and C_s are the concentrations of the fast moving fluid and stagnant fluid, respectively,
 \bar{K}_{fs} is the mean overall mass transfer coefficient at the interface of the flowing and stagnant regions,

\bar{a}_{fB} is the mean area of mass transfer relative to void volume, cm^2/cm^3 ;

and

θ is time;

Their correlation for the region Pe_p belonging to the range $[10, 10^4]$ is:

$$\frac{1}{Pe_{hl}} = \frac{1}{\tau Pe_h} + \frac{1}{Pe_{ht} X} \left[1 - \frac{(1 - \exp(-2X))}{2X} \right] \quad (2.2.2.9)$$

where X is obtained by the correlation (Gunn, 1969):

$$X = \frac{55.5}{Pe_h} \quad (2.2.2.10)$$

They also present two other correlations for X which are not as dependent on Pe_h as Gunn's correlation:

For high Pe_h ,

$$X = \frac{35}{Pe_h^{6/7}} \quad (2.2.2.11)$$

and, for low Pe_h ,

$$X = \frac{22}{Pe_h^{2/3}} \quad (2.2.2.12)$$

2.2.3 ALTERNATING FLOW MODEL (AFM)

This is a very recently presented model from Klingman and Lee (1987). It predicts the breakthrough curves given a packing geometry, comparing well with data in the range ($5.6 < d_c/d_p < 54.4$) and ($100 < Re_p < 1000$) for both gases and liquids. They state that the AFM is therefore most useful for those packed beds with small aspect ratios.

The premise of this model is that the flow through a packed bed may be considered as ordered; the bed itself is considered as an ordered array of repeating cells. The cells are alternately offset so that the flow from one cell goes into the two cells downstream of it; the flow to that one cell comes from the two cells upstream of it. The flow through the bed is then a series of flows through alternating annular plugs, hence the name of the model. Within each cell, plug flow is assumed. Obviously, this may be better modelled if a developing flow profile were used for each cell, instead of assuming (fully developed laminar or) plug flow, but Klingman et al. did not consider this.

The model predicts the breakthrough curves for steady-state

and transient inputs for high Re_p conditions ($Re_p > 100$). It does not use a dispersion model; each cell is assumed to have a homogeneous concentration, i.e. perfect mixing. It cannot therefore be expected to give useful results for low Re_p flow. As the experimental conditions of this study do not include an ordered bed, low aspect ratio, or exclusively high values of Re_p , this algorithm is not discussed further here; for complete details see Klingman *et al.* (1987).

3. EXPERIMENTAL RESULTS

The experimental design and apparatus is presented first, followed by a section on data analysis. Experimental results are plotted at the end of this chapter.

3.1 EXPERIMENTAL DESIGN AND APPARATUS

There exists a great deal of experimental data on dispersion in the literature for one dimensional flow but little work has been published for multidimensional flow. Peaceman *et al.* (1962) worked on a theoretical problem involving two dimensional dispersion with fingering, but assumed one dimensional flow for their dispersion calculations. Since a more rigorous test of dispersion models can be done using a broad range of flow and dispersion conditions, experimental results for a multidimensional flow and dispersion situation were first obtained for this study. Specifically, data were collected for a two-dimensional dispersion in two-dimensional flow for a stable miscible displacement.

Sodium dodecylbenzene sulphonate (SDBS) initially was chosen to be used as the tracer compound. It is soluble in water (a readily available solvent) and has been considered in industry for the miscible displacement of oil. There is also a fair amount of technical information available in the literature. For example, it satisfies the clogging criteria of Herzig *et al.* (1970), *i.e.*

its diameter and the diameter of its micelles (Hiemenz, 1977; Cheng et al, 1982) are too small to clog the pores of the packed bed used in this study. Cheng et al. also give its aqueous diffusion coefficient over a range of temperature and salt concentrations. The salt stabilizes the ionic strength of the solution, giving more reproducible results. Kalpackci et al. (1981) discuss the flow of surfactants in porous media and the problems of permanent permeability modifications of the porous media, caused by the surfactants, for different surface characteristics of the medium. Trogus et al. (1977) and Ramirez et al. (1980) both considered adsorption of surfactants onto the porous medium, with the former also considering the specific case of petroleum sulphonates.

However, in preliminary experiments using SDBS it was found that the results were difficult to reproduce because of the tendency of the SDBS to adsorb strongly onto the tube walls. Leaving the system filled with distilled water overnight, to allow the SDBS to desorb, and rinsing it out over all of the following day still did not prevent blips caused by slowly desorbing surfactant. These runs could only be done at low Reynolds number, even at the maximum pump setting, so flushing out the system to do the next run was quite difficult. Since the breakthrough curves from the short cores were significantly distorted by the blips, it was decided that a non-absorbing tracer had to be used.

The next tracer chosen was the dye Amaranth, otherwise known as C.I. Acid Red 27 or FD & C Red #2. Tinghui et al. (1983) give

its radius and diffusion coefficient for aqueous solutions. El Mariah *et al.* (1984) also give its aqueous diffusion coefficient at various pH levels; their result is quite close to that of Tinghui *et al.* The original work on Amaranth was done by McKeown *et al.* (1954); in that is presented a value for D_f of 6.9×10^{-6} cm^2/s at 25°C in which is acceptable for use in this study. Amaranth is a red in colour for concentrations as low as 10^{-4} molar, which allows for a visual check on the progress of experiments if transparent tubes are used for the packed. That is, an asymmetric dispersion is readily noticed and data for that run reliably discounted. Another important attribute of this tracer is that it absorbs light in an area of the spectrum that is well away from that of its solvent (water), so there is no interference in the absorbance signal caused by minor variations in water quality. Finally, as Amaranth does not form micelles, it easily satisfies Herzig's clogging criteria.

The experimental method for this study was designed in part by considering a review (Cluff *et al.*, 1976) of the experimental techniques of eighteen investigators. Effects such as column diameter (d_c), particle diameter (d_p), aspect ratio (d_c/d_p), column length (L), particle type, fluid and tracer used, injection method (step or pulse) and mode of measurement (point or integrated, absolute or relative) were evaluated. They obtained a correlation for D_1 based on most of these factors, as presented previously. Qualitatively, one of their findings was that measurements taken at two points, one before and one after the

core, gives a relative value for D_1 that surprisingly tends to be higher than the value obtained by just measuring the "absolute" value in one location, that being just after the core. There might have been increased dispersion caused by the additional detectors in the relative measurements, however. It is expected that measurements obtained by absolute methods would be higher than those obtained by a relative means unless those absolute values are deconvolved, in a manner described later in this chapter, in order to remove the effects on dispersion caused by fittings and lines. A second and more significant result of their study was that the values of D_1 obtained by point measurement techniques (e.g. conductivity probes) consistently were lower than those obtained by integrated techniques such as light absorption over the cross-section of the tube. This may have been due in part to velocity effects on dispersion near the wall of a tube that were not picked up by point measurements taken at the centre of the tube. Another consideration is that there may have been some flow distortion effects caused by small inhomogeneities in the packing as well as by the point measurement probe itself, leading to inaccurate results at the probe location. Integrated measurements therefore are likely to be more reliable. They could not be conclusive, but suggest that the step input results may be better than pulse since it is easier to design a system that has a sharp front upon injection for a step than for a pulse. It was found that the experiments done with step inputs tended to produce lower values for D_1 ; since those same experiments were done

unfortunately only with point measurements, the results may have been strongly influenced as described above. Considering these points, the experimental procedure designed for this study employed integrated (absorption) absolute (single measuring point after the core) measurements for step-inputs of concentration, with Amaranth as the tracer.

The size of the core relative to the particle for a given Pe_p is an important parameter, as discussed in the sections on residence-time requirement and porosity variation effects. However, while the core dimensions are obviously known, neither of the choice of definition of average particle size, \bar{d}_p , nor the choice of method to use in sieving to obtain reliable mass fractions (Allen, 1981; Shergold, 1946) to be used in equations for \bar{d}_p is obvious. Following the suggested approach of Allen (1981), the (spherical glass) beads were dry sieved for nine minutes on a Tyler Ro-Tap sieving machine. The four sieves were nominally of sizes 425, 417, 355 and 300 microns (μm). The beads supplied were nominally in the range of 295 to 415 μm ; beads on the 300 to 417 μm trays were kept. An optimum load of about 150 grams to use for each sieving run on the Tyler Ro-Tap was determined by dry sieving successively smaller masses until further reductions in mass did not significantly affect the percent retained on each tray (Allen, 1981; Shergold, 1946). The final total weights used were 421.0 g at 417 μm , 384.8 g at 355 μm and 326.5 g at 300 μm to give a geometric \bar{d}_p of 362.8 μm using equation (1.1.2), an arithmetic average of 336.5 μm using equation

(1.1.3) and an average of $340.4 \mu\text{m}$ using the definition of Allen (1981), equation (1.1.4). The effect of particle diameter definition is shown in the chapter on numerical simulation.

The density of the glass beads was determined by measuring the volume of distilled water displaced by a known mass of beads, giving a value of 2.50 g/ml at room temperature. This agrees with the value given by the manufacturer (Rotair).

The packed beds were lucite cylindrical cores loaded with spherical glass beads, to form an unconsolidated porous medium. In order to facilitate testing of the predicted dispersion coefficients, four differently sized lucite cores were used. Their dimensions are given below in Table 1, corresponding to the diagram in Figure 1.

Two requirements on the design of the cores were that the flow through the resulting packed bed be homogeneous, and that they hold the beads in place and not allow shifting. The former condition was not easily obtained. It was found that any air bubbles that were trapped in the packing would markedly affect the flow pattern. The way to circumvent this was to remove all of the air in the void volume of a completely dry packed core by a vacuum pump and then fill this, using the vacuum, with deaerated water. There was one recurring problem; the glass beads tended to interfere with the operation of the inside o-ring by preventing it from compressing. This meant that a seal strong enough to hold a vacuum could not be formed; a second o-ring seal was added to the outside of each mesh endplate to give a doubly secure airtight

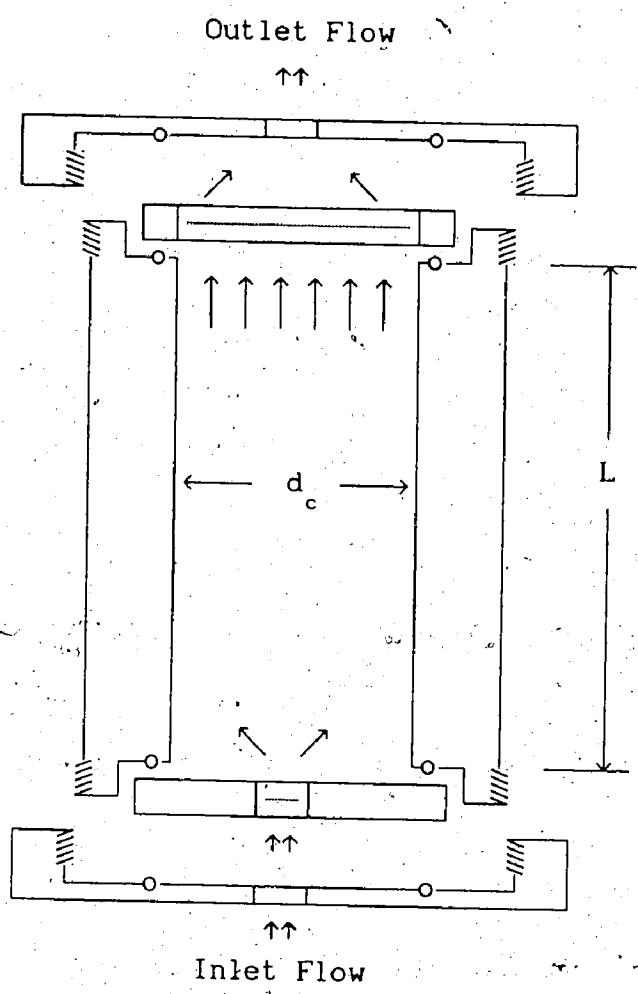


Figure 1: Core Design

seal. If the vacuum necessary to load the water was not made, attempts to fill the core with water would only partially saturate it. The beads would then have to be redried, in a process taking one or two days, before another attempt to load the core with water could be made. The second o-ring seal substantially limited the occurrence of this problem. This entire process is described in more detail in the next paragraph. The other requirement for a packed bed was more easily satisfied; mesh ring endplates nicely held the beads inside the core while allowing essentially unobstructed flow. The mesh rings had an opening for flow that was different for the inlet than for the outlet discs; for the inlet there was a relatively small inlet diameter (0.474 cm diameter), corresponding to the one quarter inch feedline to the core, while the outlet disc had as its inside diameter the same value as the inside core diameter. This allowed for a two-dimensional inlet flow but an essentially one-dimensional outlet flow. A 325 mesh (44 μm) mesh screen supported by a stronger mesh was used for the discs. The volume of the packed bed was slightly affected by the additional volume of the screens; the estimated contributions are listed below in Table 1.

CORE #	LENGTH (cm)	\bar{d}_c (cm)	MESH VOLUME (ml)	TOTAL VOLUME (ml)
1	7.54	2.88	1.23	50.42
2	7.51	3.90	2.89	92.5
3	15.00	2.88	1.23	99.1
4	15.05	3.90	2.89	182.3

Table 1: Core Dimensions

To fill a core with dry glass beads ready to be evacuated, one mesh endplate and cap were attached and the core then partially filled with water. Dry beads were added slowly, with tapping on the side of the core to help settle the beads. Damp beads were not used as they would stick together and carry air into the bed. The level of the water in the core was always kept above that of the beads, until the core was completely filled with the beads, so that no air could get trapped inside the bed. Once the core was filled with the beads, the water was allowed to drain out and the exit mesh endplate and cap then attached. The beads in the core were then dried by passing air through the bed at a low flowrate. This limited flowrate was unavoidable as a high pressure drop could not be sustained by the system. The core was deemed dry when measurements of its mass were essentially constant over four hours of drying. The entire drying process usually took

one or two days. A small electric vibrator, of the type commonly used in unconsolidated core experiments, was used in some preliminary runs to help pack the core but it gave no better results, as measured by porosity, than did the tapping method. Porosity was determined by noting the dry mass of beads added to the core; with the known volume of the core (including the mesh screen contribution) and the density of the beads, ϕ is found from:

$$\phi = \frac{(\text{mass of beads}) / (\text{density of beads})}{\text{total core volume}} \quad (3.1.1)$$

Consistent values of porosity were obtained.

Loading the dry packed core with the fluid to be displaced (water) was the next step. Boiled distilled water was used to minimize the effects of any contaminants and to prevent any dissolved air from appearing, and expanding, in the evacuated core. Once completely packed with dry beads, the core could be isolated using Quick-Connect fittings and then evacuated. By holding one end of the packed core under the surface of the water and opening its Quick-Connect fitting, the core void volume would fill with water. If no air bubbles appeared on the walls of the core, it was assumed that the core was air-free and ready for use. Finally, it was put online with the pump (see Figure 2) and distilled water sent through to the drain; any settling that the

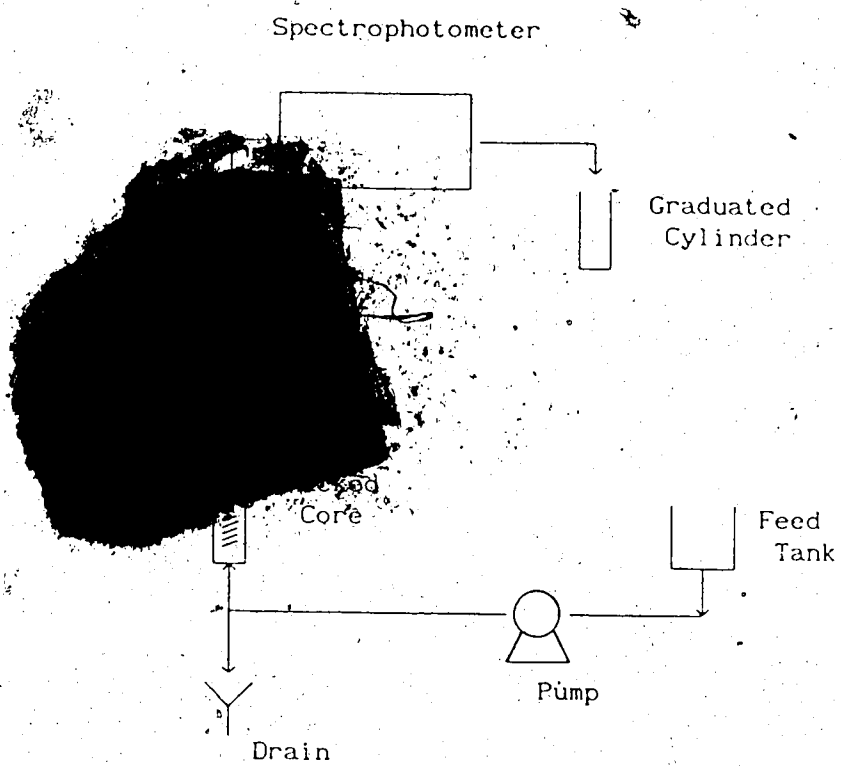


Figure 2: Experimental Apparatus

beads might do, or loss of fines, would happen at this time.

As shown in Figure 2, the feed stock solution of Amaranth was contained in a 10 centimetre diameter 2.2 litre tank which fed into an Eldex dual synchronous pump. It was pumped from there past a pulse damper and a two-way valve. The valve could be set to allow flow upwards to the core or down to a drain. Flow downward through the core was observed to be unstable; the Amaranth solution fingers through the distilled water. All experimental runs were therefore made with flow upwards through the packed core. Before starting a run, the entire system (from the pump through to the spectrophotometer) was filled with distilled water and rinsed until no residual tracer could be detected by the spectrophotometer. Then the valve was turned to direct flow to the drain and the feedstock solution of Amaranth pumped through the system, and out the drain until the concentration at the drain valve reached the feedtank concentration C_f . This rinse out time for Amaranth was determined by collecting effluent from that drain valve until its concentration effectively reached its asymptotic value of C_f . The drain valve breakthrough curve is shown in Figure 3. Based on this plot, a minimum time of fifteen minutes at the maximum flowrate was allowed for each run or blank run for rinsing out the system before the core. After the system was so saturated with the Amaranth solution up to the valve, a run was initiated by turning the valve to direct flow upwards to the core and switching on the pump to start the flow; run time was kept with a stopwatch

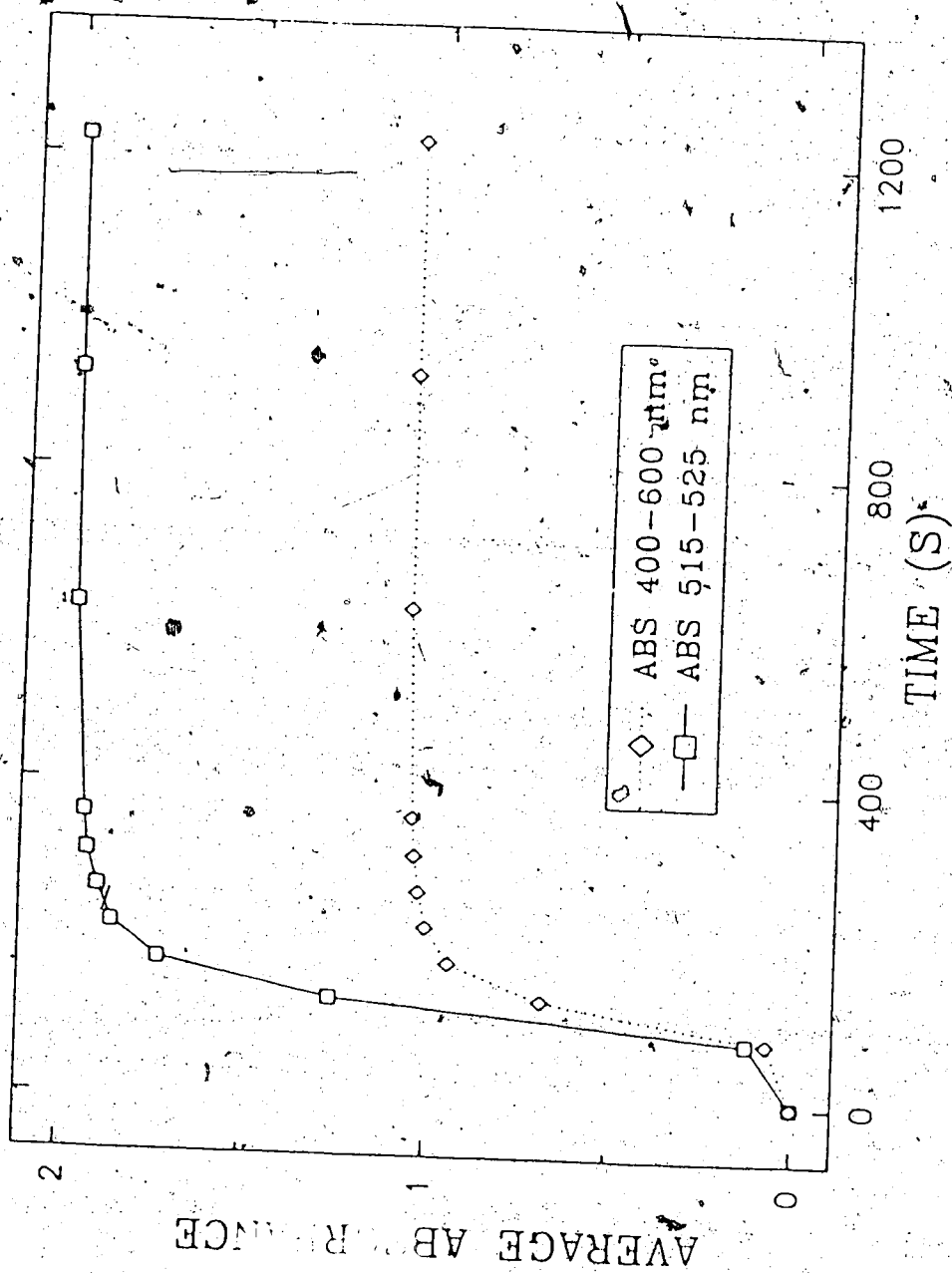


Figure 3: Drain Valve Breakthrough

beginning at the moment that the first drop of effluent fell into the 50 ml. buret. Once the stopwatch was going, the data collection program on the spectrophotometer was started. The average flow rate for the run was taken as the effluent volume divided by the run time as measured on the stopwatch. Blank runs were conducted in the same manner except that the core was removed from the line and a fitting, of roughly the same size as the entrance and exit fittings to the core together, was put in its place. The breakthrough curve of a blank run gives the dispersion caused by the fittings and lines of the system and does not include the dispersion caused by a packed bed; their use is discussed in some detail in the next section.

The tracer (Amaranth) did not adsorb onto either of the glass beads or the tube walls so a core packed and used in one run could be simply rinsed with distilled water, in order to recover its original pristine state, for use in the next run. If there were stagnant volumes that could not be rinsed out, then letting the core sit stagnant for a few hours (corresponding to the duration of the next planned run) would allow diffusion out of them to areas where convection did occur. If it was not properly rinsed, then upon the next startup of the pump there would have to be a blip or peak, on an otherwise flat baseline, caused by tracer reappearing from a stagnant volume. This rarely happened; when it did, the core was immediately dried out, reloaded with fresh water by vacuum and rinsed to make sure that neither tracer nor air bubbles were remaining. Through their flow distortion effect, air

bubbles present in the packing could lead to more stagnant volumes.

The measurement process was programmed in BASIC on the HP-8451A spectrophotometer. The measured variable, the absorbance in the visible region, varies linearly with the concentration of the tracer. Amaranth's peak absorbance, occurs at approximately 520 nanometres; a 515 to 525 nanometre average absorbance was employed because it produces a significantly stronger response than a 400 to 600 nanometre one, as shown in Figure 4. A concentration of 3×10^{-4} molar (aqueous Amaranth) was used. To allow for baseline drift, the average absorbance over the range 690 to 700 nanometres was subtracted from this amount. Due to the strong absorbance of water and its impurities in the range below 300 nanometres, measurements in that area were specifically avoided. The program on the HP8451A to measure the concentration used only a constant time step, as a limitation of the machine, so points could not be concentrated in the region of the sharp front. To speed the data storage, the results are stored on disc by giving the number of points, integration time and time step in the output file header information, followed by a single column of absorbance data. This was necessary as the steepness of the breakthrough makes it difficult for the spectrophotometer to measure and record the data when a small time step is used. All breakthrough data were normalized and smoothed using cubic splines before being used.

The flowrate was determined by measuring the effluent volume

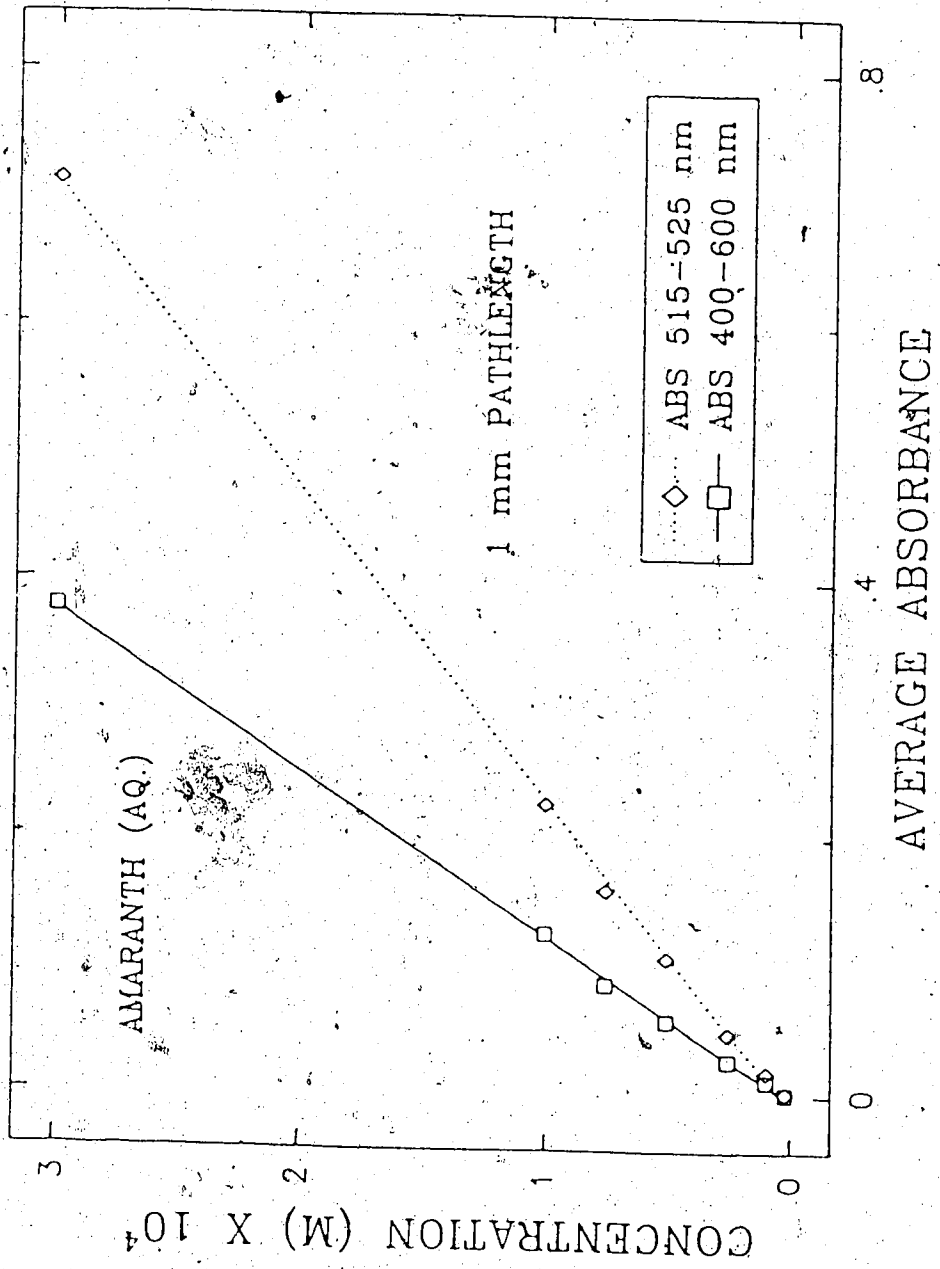


Figure 4: Spectrophotometer Calibration

for the time of the run. If an air bubble got into the system, e.g. through the on-line filter before the pump, the flowrate was markedly affected. Those runs could be discounted. Unfortunately, this meant redrying and refilling the core to make sure that there were no bubbles present in the core. The advantage of using transparent lucite cores is that the breakthrough profile is clearly seen; if it was not symmetric, possibly due to air bubbles, those runs could as well be discounted. Either of an unusual flowrate or an asymmetric breakthrough as seen through the core would be cause for discounting the result of a particular run.

Residence time considerations were difficult to satisfy using the criterion of Han *et al.* (1985) as that equation (1.3.1) explicitly only allows for one dimensional flow. In this study, the Peclet number varies from as high as 8730 at the core entrance to as low as 28 at the exit for the same core. Based on the entrance Pe_p , only a few runs (those below about 3.5 ml/min for the long cores, and the 1.5 ml/min runs for the short cores) were done which satisfy that constraint; based on the exit Pe_p , however, all of the runs easily meet the criterion. As the bulk of the core (about 2/3 for the short cores, 5/6 for the long cores) had one dimensional flow at the low Pe_p exit, strong tailing was not expected from this source.

Table 2 gives a list of the runs and the corresponding data. All runs were at room temperature (23 to 25°C) and effluent concentration was measured for seven to ten pore volumes. Some of

the earlier runs had measured porosities below 36%; otherwise most runs measured around 37%. The low porosity runs were the first runs actually done; it is believed that some fine beads that were not removed in the sieving process were lost in the bead washing step done between runs, resulting in the slightly higher porosities of subsequent runs.

Comparable magnitudes in the the dispersion for both run and blank data are the motivation for the deconvolution process and that is presented, along with the data, in the next section.

RUN #	FLOWRATE (ml/min)	POROSITY	CORE #	Exit P_e
1	6.73	0.355	1	237
3	6.73	0.355	1	237
4	6.73	0.358	1	235
6	3.58	0.361	1	124
7	1.56	0.361	1	54
8	2.40	0.361	1	83
10	0.82	0.355	1	29
11	6.72	0.373	2	123
12	4.70	0.373	2	86
13	2.98	0.373	2	54
16	4.71	0.373	2	86
18	3.6	0.377	3	119
20	6.72	0.369	3	227
21	3.03	0.366	2	56
22	3.02	0.366	2	56
23	6.73	0.370	4	124
25	4.69	0.370	4	86
27	3.02	0.370	4	56
28	4.71	0.370	4	87
31	2.42	0.365	3	83
32	1.58	0.365	3	54
33	0.80	0.365	3	27
34	6.74	0.370	4	124

Table 2: Run Conditions

3.2 DECONVOLUTION

Peculiar to small systems is the problem of the dispersion caused by tube fittings, lines and the concentration measuring cell being comparable in magnitude to the dispersion caused by the packed bed itself. This typically has not been considered in miscible displacement studies by petroleum engineers or in groundwater contamination studies by hydrologists, as they generally use quite large packed beds, but has been a topic of concern in chromatography (Wright *et al.*, 1982), where it is commonly referred to as "extra-column band-broadening", and in medical applications (Diffey *et al.*, 1976; Valentinuzzi *et al.*, 1975). The numerical technique to remove this effect from data is referred to as "deconvolution".

It can be shown (Wylie and Barret, 1982) that for an input function $f(t)$ to a system, the output response $y(t)$ of that system is obtained as the convolution integral:

$$y(t) = \int_0^t R'(\tau) f(t-\tau) d\tau \quad (3.2.1)$$

or

$$y(t) = \int_0^t R(t-\tau) f'(\tau) d\tau + R(t) f(0) \quad (3.2.2)$$

$R(t)$ is the characteristic response of the system to a unit step input and R' , or dR/dt , is the response of the system to an impulse input, often referred to as the impulse response function. In the Laplace domain, equation (3.2.1) is simply:

$$Y(s) = G(s) * f(s) \quad (3.2.3)$$

using G to replace R' for the general transfer function notation. If there are two non-loading systems in series (see Figure 5), the overall transfer function is the product of the two individual transfer functions (Ogata, 1970).

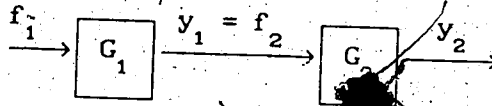


Figure 5: Non-loading Cascaded Elements

$$\frac{Y_2(s)}{f_1(s)} = G_1(s) * G_2(s) \quad (3.2.4)$$

The assumption that dispersion systems are non-loading (Wright et al., 1982; Valentinuzzi et al., 1975) for

incompressible flow has been supported experimentally by Niemann (1969), who obtained the same overall response on breakthrough curves for a system comprised of interchangeable packed bed sections no matter what order the beds were in. It was therefore assumed that our dispersion system could be written as three non-loading cascaded elements, comprised of the fittings and the lines before the packed bed (G_1), the packed bed itself (G_2) and the lines, fittings and measuring cell after the packed bed (G_3), as shown in the figure below.

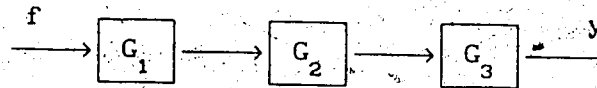


Figure 6: Block Diagram of System

$$\frac{y}{f} = G_1 G_2 G_3 \quad (s) \quad (3.2.5)$$

Since they are non-loading, G_1 and G_3 can be moved together to give a total fittings, line and measuring cell response, G_f , in line with the core or packed bed response, G_c , as shown in Figure 7.

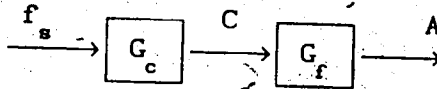


Figure 7: Block Diagram of Lumped System

The measured output absorbance, A , for a step input, f_s , to the above system is:

$$\frac{A}{f_s} = G_f(s) \cdot G_c(s) \quad (3.2.6)$$

The output concentration, C , from the core transfer function, G_c , is the input function to the fittings transfer function, G_f , and is the desired packed bed only step response data. i.e. It is the step response breakthrough of the core itself, with no contributions from the fittings, lines or measuring cell dynamics. The "blank" absorbance step response data is that obtained by taking the packed core offline. The blank, $A_b(s)$, is then the convolution of the step input, $f_s(s)$, with fittings transfer function, $G_f(s)$. It is used to characterize the fittings transfer function in a manner described in the next few paragraphs; since the characteristic parameters of this transfer function may change with flowrate, blank runs were obtained for every flowrate at which runs were done.

To obtain the $C(t)$ data it is necessary to solve equation

(3.2.6) for $f_b G_c$ or C . This can be done by using the convolution theorem written in discrete form (Valentinuzzi *et al.*, 1975; Diffey *et al.*, 1972) from the integral (3.2.1):

$$A(k) = \sum_{i=0}^k A_b'(i) C(k-i) \Delta t \quad (3.2.7)$$

This is not easy given experimental data that have noise; the impulse response function, A_b' , is found as the slope of the step response data for the blank runs, *i.e.* runs done at the same flowrate but without the packed core online. The initial slope $A_b'(0)$ appears at each time step K in the calculation of $A(k)$, thus making $A(k)$ very dependent on that one value. However, that value is rather poorly known because of the noise on the data. Taking the slope of noisy experimental data is always considered risky; the problem is compounded here as it is just the initial slope that is required. Deciding where the breakthrough begins is difficult enough and getting a reasonable estimate of the slope at that point becomes rather arbitrary; the reproducibility of these decisions is not that high. It should be pointed out that pulse responses would suffer this same limitation of finding the initial breakthrough point. Nevertheless, a straightforward discrete deconvolution based on equation (3.2.7) was attempted, and it did diverge. There the initial slope was taken as that experimentally obtained from the smoothed breakthrough data; no adjusting of its value was done as this would have been subjective and therefore

not reproducible. Fast Fourier transform techniques provide a popular means for solving such integrals (Chen *et al.*, 1987) but suffer from the same limitation in the dependence on the initial value of the impulse response function. The convolution integral must be solved in a manner that does not depend so strongly on one poorly identified experimental value.

The solution to this overdependence is straightforward using identification techniques from control theory. A similar application has been published recently (Van Zee *et al.*, 1987) for characterizing flow processes; the goal there was to obtain the longitudinal dispersion coefficient for a one dimensional problem. For this method, a discrete time model (z-plane) is assumed, for equation (3.2.6), containing several parameters whose values are obtained, *i.e.* identified, by least squares curve fitting to the experimental data. While there are several model forms used in the literature (Ljung, 1987), the following (ARX model) was found satisfactory for this study:

$$PA(z) y(t) = PB(z) f(t-nk) + e(t) \quad (3.2.8)$$

Here $e(t)$ is white noise, nk is the number of time step delays between input and output and PA and PB are polynomials in Z , given by:

$$PA(z) = 1 + PA_1 Z^{-1} + \dots + PA_{na} Z^{-na} \quad (3.2.9)$$

and

$$PB(z) = PB_1 + PB_2 Z^{-1} + \dots + PB_{nb} Z^{-nb+1} \quad (3.2.10)$$

Explicitly, equation (3.2.8) may be written as:

$$Y(t) + PA_1 Y(t-1) + \dots + PA_{na} Y(t-na) =$$

$$PB_1 f(t-nk) + PB_2 f(t-nk-1) + \dots + PB_{nb} f(t-nk-nb+1) + e(t) \quad (3.2.11)$$

The parameters of $PA(z)$ and $PB(z)$ are identified by least-squares comparison to experimental data, which were in this case the blank runs. For the flow system used in this study, the order of $PB(z)$ was taken as zero. i.e. Using $PB(z)$ equal to PB_1 , which was then given the value of unity, gave quite satisfactory results. Since the system data used was for a single step input, using a higher order on $PB(z)$ results in an ill-conditioned matrix. That is to be expected since most entries in the matrix would be the same; no new information about the system dynamics is obtained by differencing the input function data, but a great deal more computations have to be done in order to solve for the

significant parameters of $PA(z)$.

The equation solved by least squares for the parameters of $PA(Z)$ was:

$$PA_1 A_b(t) + PA_2 A_b(t-1) + \dots + PA_{na+1} A_b(t-na) = f_s(t-nk) \quad (3.2.12)$$

Note that PA was modified so that the coefficient of f_s is unity. i.e. The parameters for the transfer function G_f were identified for the form:

$$G_f(Z) = \frac{Z^{-nk}}{PA_1 + PA_2 Z^{-1} + \dots + PA_{na+1} Z^{-na}} \quad (3.2.13)$$

From equations (3.2.6) and (3.2.12), the concentration breakthrough curve $C(t)$ for a step input into only a packed core was found from:

$$PA_1 A(t) + PA_2 A(t-1) + \dots + PA_{na+1} A(t-na) = C(t-nk) \quad (3.2.14)$$

Solving this equation for $C(t-nk)$ is the actual deconvolution of the blank absorbance data from the run data to obtain the breakthrough response data. This blank-identification method may be used for any input $f(t)$, as long as exactly the same input is used for both the blank and the core runs. Its major advantage

over the integral deconvolution method is that the parameters of $PA(z)$ are obtained by least-squares using all of the data points of each blank run; it is not dependent on a single experimental value like the integral deconvolution method. However, if a reliable measurement of the initial slope of the step response can be obtained, then the integral deconvolution (e.g. Fast Fourier transform) method is faster and easier to do than the blank-identification method.

Before either method for deconvolution can be used, the initial point of the breakthrough must be determined. By smoothing the data with a cubic spline least squares routine from the I.M.S.L. library, the spline coefficients were used to numerically generate an integral (over multiple steps if desired) and derivatives for each point of the breakthrough curve. By inspection, the initial breakthrough point was chosen by coming back in time to the first point where the integral and slope both reached their minimum values. Results were consistent to within one or two time steps, and this variation is later shown to have virtually no effect on the deconvolved breakthrough curves.

In order to do the identification of the ARX parameters (of equation 3.2.12) for a particular blank, a program was written that read in the experimental data and the order of the polynomial $PA(Z)$ desired for the ARX-model, then solved by least squares for those parameters. The check on this identification was done by plotting together the experimental curve and the curve regenerated using the newly obtained parameters in equation (3.2.12); the more

coincident the two curves were, the better the identification. If the regenerated curve was exactly coincident with the experimental curve, then the parameters of $PA(z)$ were identified correctly. However, on the practical side, while increasing the number of parameters tended to give better fits, the relative magnitudes of the parameters of $PA(z)$ were examined in order to make sure that no insignificant parameters were obtained. i.e. If too many parameters were used, most would have values in the range of 5 to 30 but the "extra" ones would have values of 10^{-1} or less. If these relatively small and insignificant values were carried and used in the deconvolution step, the result was unpredictable and varied for different numbers of parameters. Those slightly distorted deconvolutions were not reliable, and this was especially the case when the run data had slight blips; the deconvolution would be distorted at the location of the anomalies. For the typical number of five hundred to two thousand data points for each blank, deconvolution results were almost exactly coincident within the range of six to eight parameters. Usually, the identification would be slightly off for the four or five parameter cases and some parameter values tended to be low or insignificant if seven or more parameters were calculated; in a few cases, three parameters gave a sufficiently accurate or stable solution for which increasing the number of parameters did not better, while in others the results only stabilized if eight parameters were used. In most cases, the order of $PA(z)$ was five.

Figure 8 shows the identification for blank #7, which is the

one used for deconvolving all runs done at a pump setting of 0.9 (see Table 3). It is quite evident from this figure that the parameters of $PA(Z)$ have been adequately identified, as the regenerated curves made using those parameters are virtually coincident with the original data. The order of $PA(Z)$ was taken as five in one case and as eight in another; there was little difference between their respective regenerated curves. The lower order identification was retained and used for the deconvolution step as it was the simpler form.

Figure 9 shows the reproducibility of the blanks and the deconvolutions; the best identifications were for six and eight parameters, respectively, for blank #7 and blank #6. The deconvolution of run #11 is shown for each blank. The deconvolved data become coincident with the run data at the point in time when the blank data reach their final value of unity. The reproducibility in the data and in the deconvolution, and in the identification shown in Figure 8, was typical for all runs. Note that this includes the effect of identifying the initial breakthrough point. It is important to realize that this blank identification method did not diverge at any time; an excellent identification and deconvolution could be made for any run. The effect of using too many parameters for $PA(Z)$, as mentioned previously, would introduce small oscillations or blips in the deconvolved data, but even then the data would not be excessively shifted. Table 3 gives the experimental run numbers and blanks paired for the deconvolution.

Figures 10 to 13 are the deconvolved results for the runs listed in Table 3. The pattern of the names in the legends is as follows: "GD"-number is from an accounting system for the deconvolution trials, and the trailer "R"-number refers to the run number. All plots have an upper time limit of 1500 seconds to facilitate comparisons; complete data are in the appendices.

PUMP SETTING	RUN #				BLANK #	TIME STEP (S)
	CORE					
	1	2	3	4		
2.4	1	11	20	23	6	3
	3			34	7	
	4					
1.7	-	12	-	25	12	5
		16		28	13	
1.3	6	-	-	-	14	6
1.1	-	13	-	27	16	6
		21			17	
		22				
0.9	8	-	31	-	18	7
					19	
0.6	7	-	32	-	21	9
					22	
0.32	10	-	33	-	23	20
					24	

Table 3: Deconvolution Pairs

N.B.: (1) Runs are deconvolved with blanks that are at the same pump setting.

(2) The flowrates set for the large diameter cores were offset to match the exit velocities for the small diameter ones.

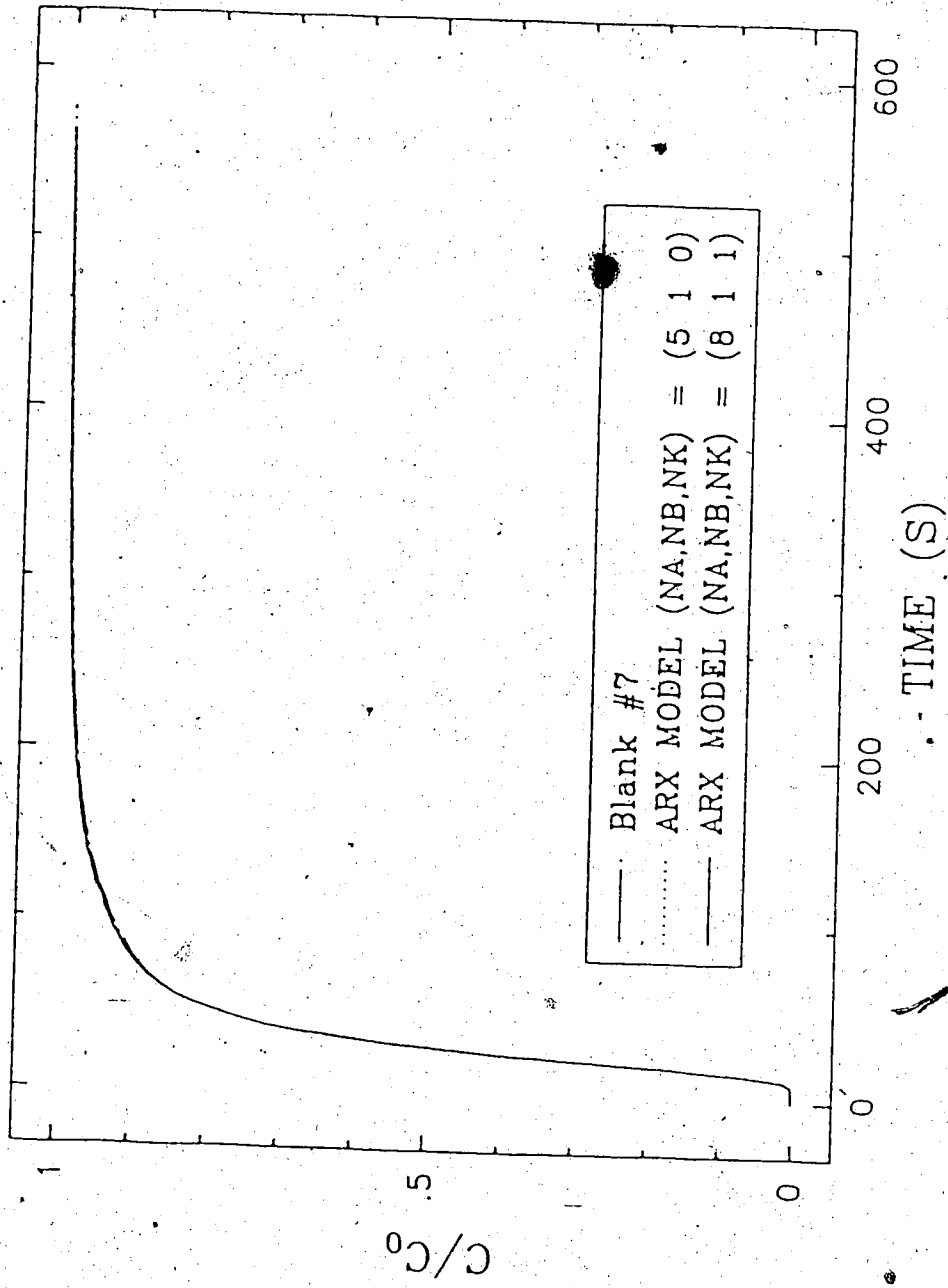


Figure 8: Identification Test

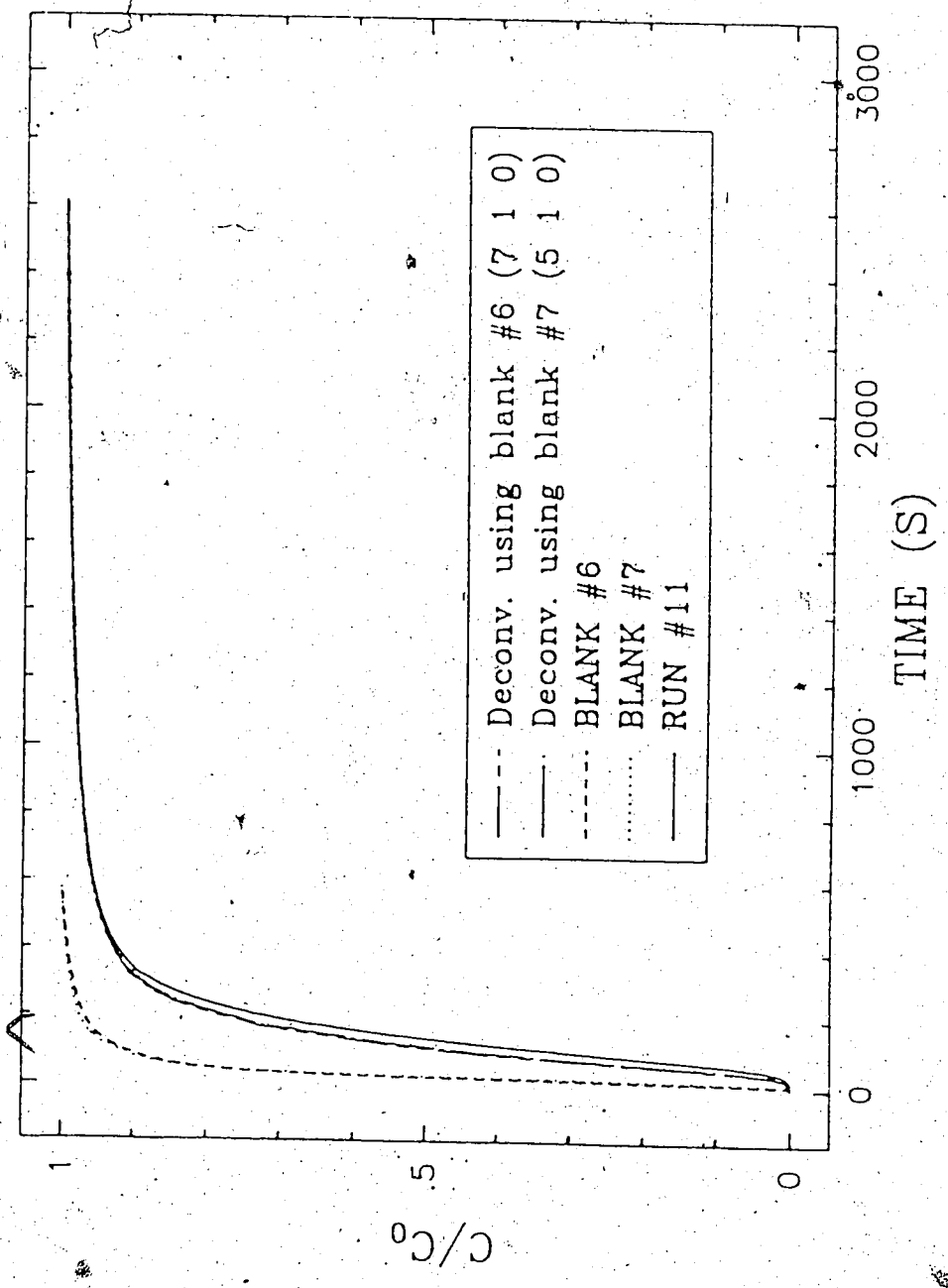


Figure 9: Reproducibility of Deconvolution

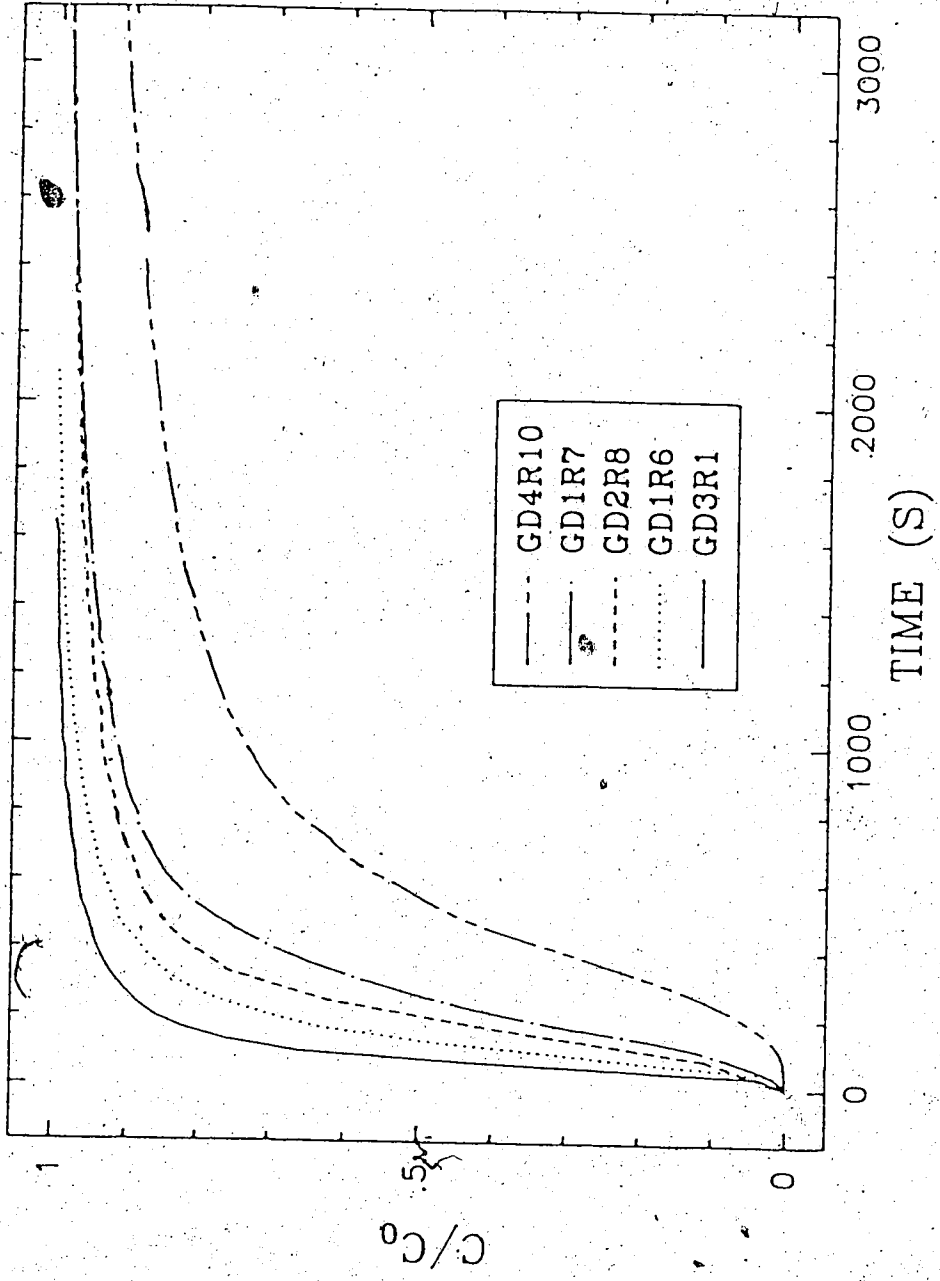


Figure 10: 3x1 Inch Core Runs

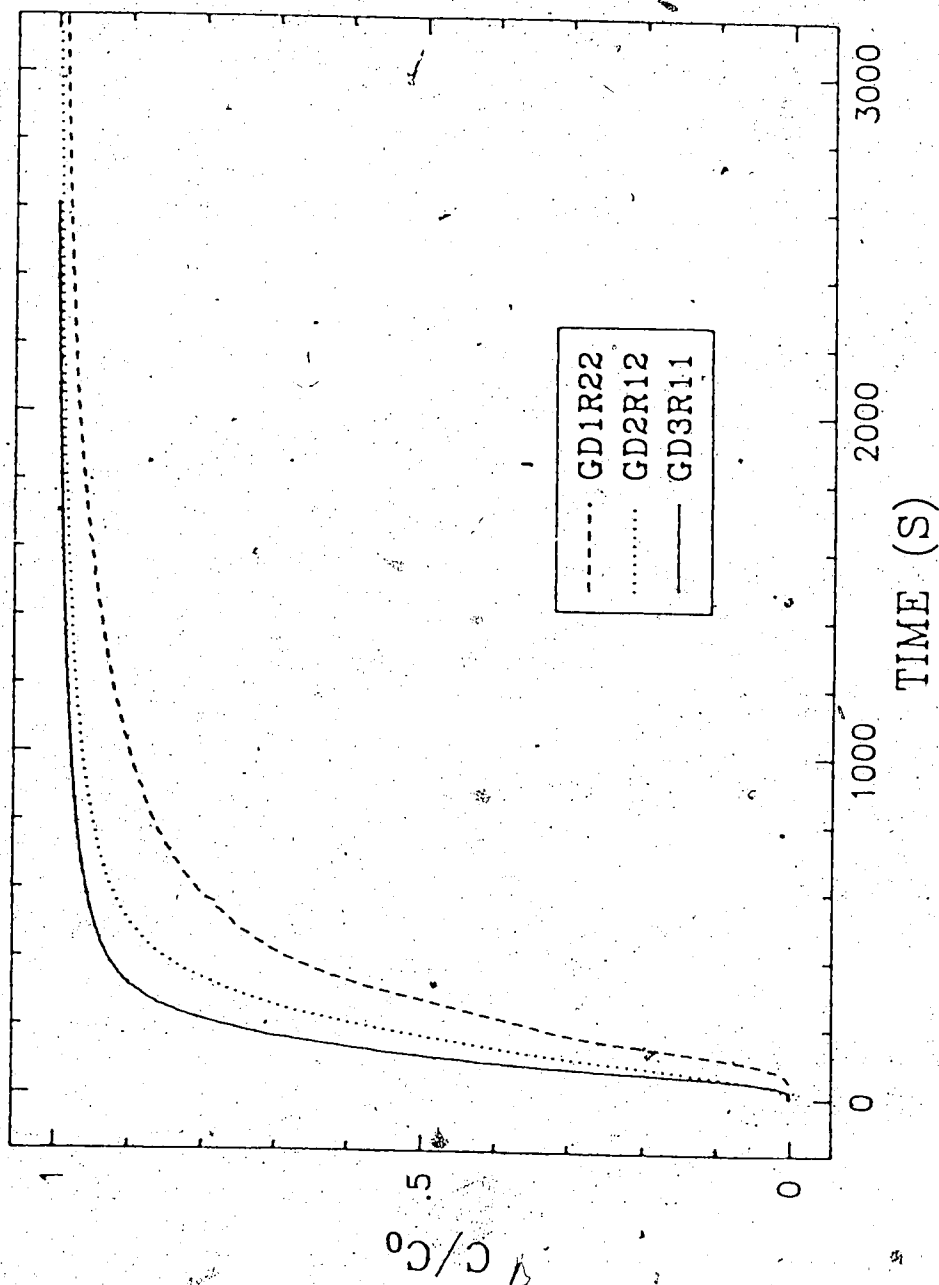


Figure 11: 3x1.5 Inch Core Runs

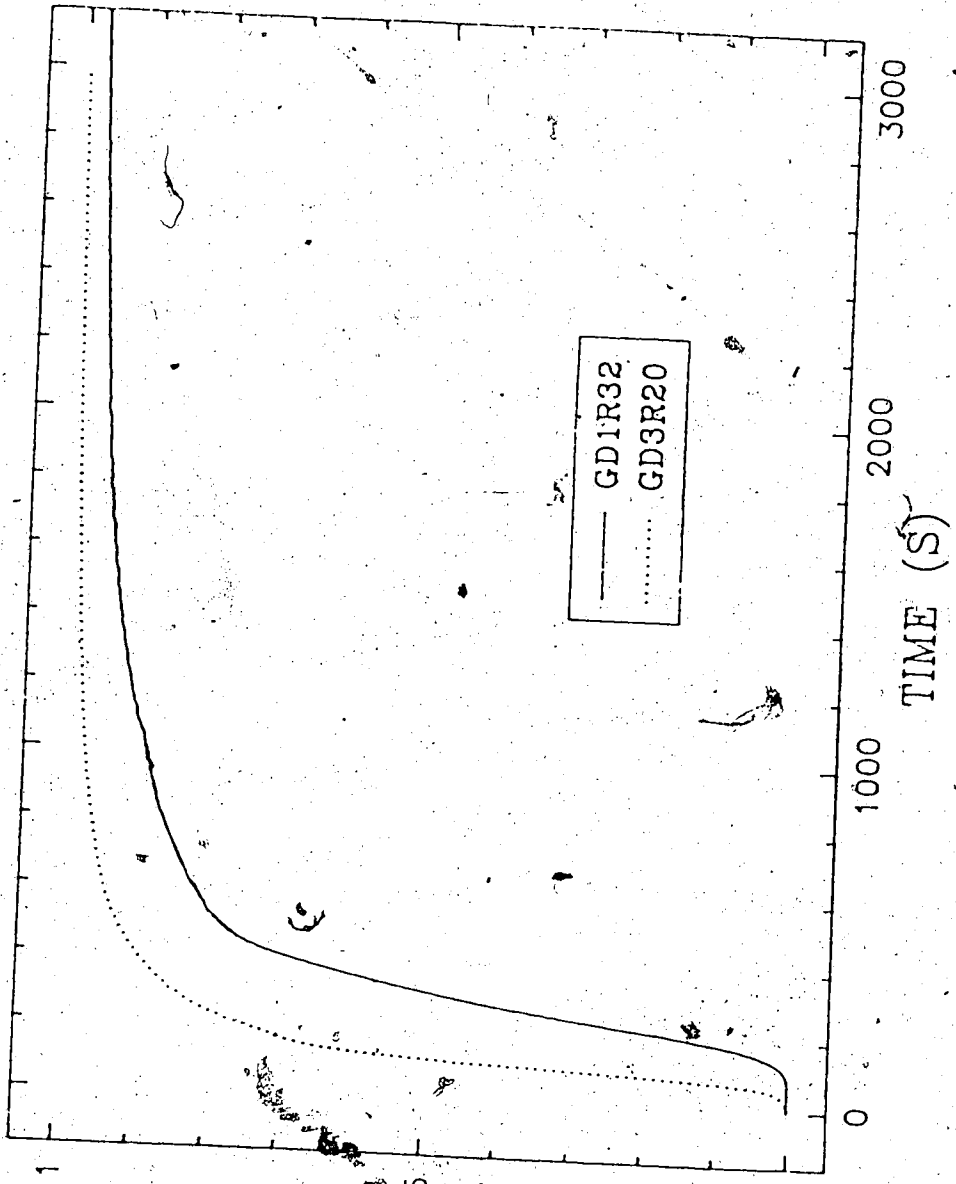


Figure 12: 6x1 Inch Core Runs

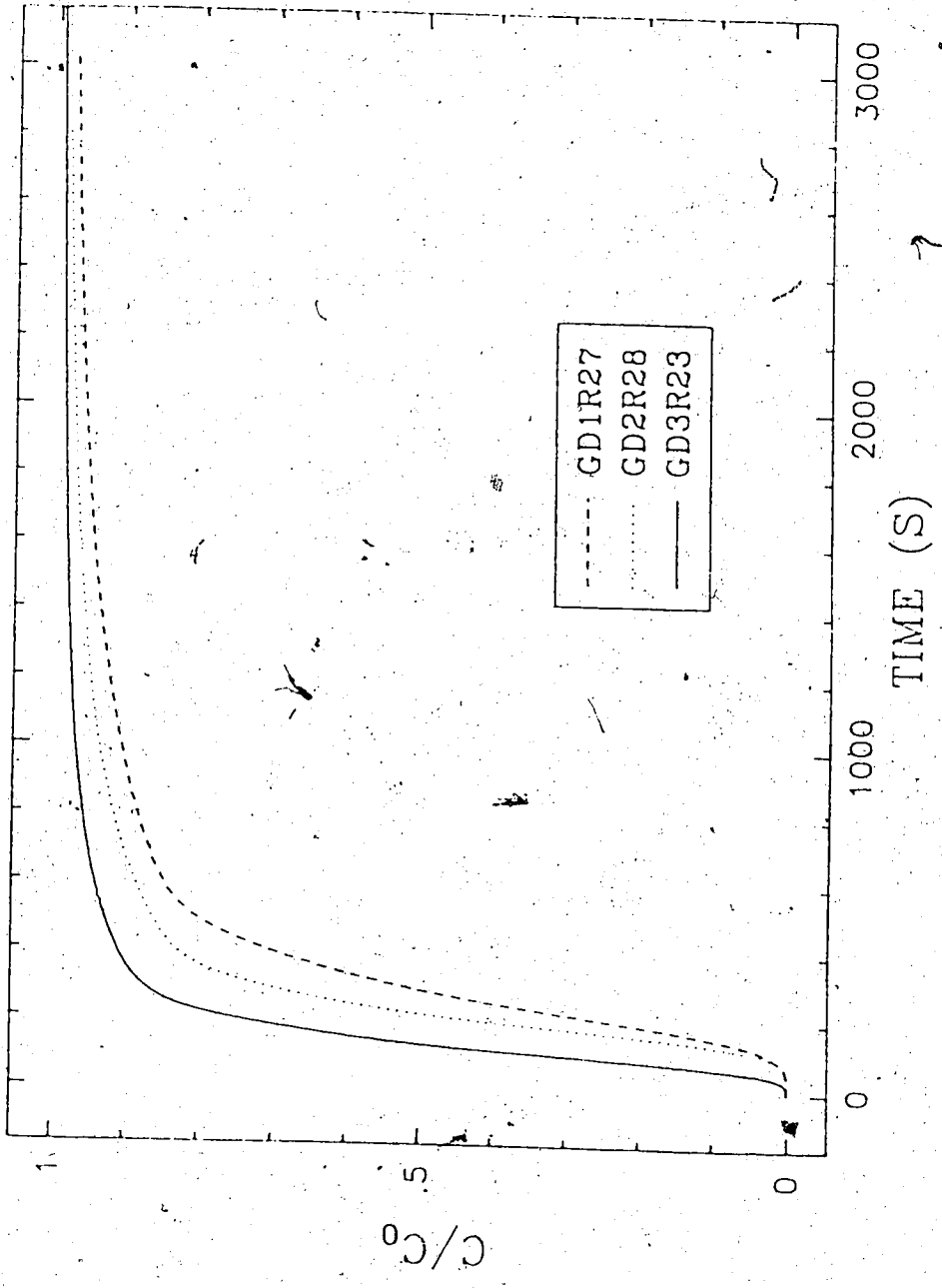


Figure 13: 6x1.5 Inch Core Runs

4. NUMERICAL SIMULATIONS

Numerical simulations based on the dispersion models listed in the second chapter are compared to their corresponding experimental runs. With the wide range of flow and dispersion conditions for the variety of core geometries associated with the experimental data for this study, the dispersion models are well tested. i.e. for a particular dispersion model to predict accurately the breakthrough data for all of the experimental runs, it would have to be robust and its adjustable parameters, if any, identified correctly.

A brief description of the numerical approach is given below, followed by simulation results, conclusions and recommendations.

4.1 FINITE ELEMENT METHOD

There does not exist at present an analytical solution to the convection dispersion equation (1.2.1). Numerical methods available for its integration include finite difference and finite element, with the latter favoured here due to its ease of handling boundary conditions (and irregular geometries) and its accuracy. The development of the particular approach for the dispersion problem is discussed in detail in Hayes and Tanguy (1988), and outlined below.

First, the continuity expression (equation 1.1.7) is used to generate a Darcy flow field corresponding to a specific

experimental run for the domain of the core Ω . This result is used in the solution of the convection dispersion equation. i.e. substituting Darcy's law into the continuity expression gives:

$$\nabla^2 P = 0 \quad \text{over } \Omega \quad (4.1.1)$$

for isothermal incompressible flow through the packed core. The above Laplace's equation over domain Ω is used with the following boundary conditions on Γ' and Γ (Hayes and Tanguy, 1988), where Γ' denotes the entrance and exit boundaries open to flow, and Γ is the core wall boundary:

$$P = P' \quad \text{on } \Gamma' \quad (4.1.2a)$$

and

$$\frac{\partial P}{\partial n} = 0 \quad \text{on } \Gamma \quad (4.1.2b)$$

Here "n" refers to the direction normal to the boundary. The value of P' is different for the exit and entrance boundaries. In practice, the pressure drop was not measured. The effective permeability, for the purpose of determining the velocity field only, was obtained by assigning P' the values of unity and zero for the entrance and exit boundaries, respectively, and using the calculated pressure drop for the one dimensional exit region and the experimentally obtained flowrate to calculate a hypothetical

value for k . That permeability was used, along with the normalized pressure drop across the bed, to calculate the Darcy flow field over the entire bed.

The convection dispersion equation (1.2.1) is solved using Danckwerts' boundary condition (equation 1.4.4) at the inlet or, more usually, the fixed inlet condition of:

$$C=C_f \quad \text{at injection} \quad (4.1.3)$$

and

$$\frac{\partial C}{\partial n} = 0 \quad (4.1.4)$$

on all other boundaries.

The weak variational form, for the Galerkin finite element method, of the pressure and dispersion equations is given as (Hayes and Tanguy, 1988),

$$(\nabla\psi, \nabla P) = 0 \quad (4.1.5)$$

and

$$\left[\psi, \frac{\partial C}{\partial t} \right] + (\psi, \bar{U} \cdot \bar{\nabla} C) + (\bar{\nabla} \psi, \bar{D} \cdot \bar{\nabla} C) = 0 \quad (4.1.6)$$

where ψ is the basis function and the inner product, $\int_{\Omega} \psi \phi \, d\Omega$, is

denoted as (x, y) . The respective solutions are approximated as:

$$P = \sum_i \psi_i P_i \quad (4.1.7)$$

and

$$C = \sum_i \psi_i C_i \quad (4.1.8)$$

for nodes i .

The time stepping was accomplished using the Gear scheme:

$$\left. \frac{\partial C}{\partial t} \right|_{t+\Delta t} = \frac{3C^{t+\Delta t} - 4C^t + C^{t-\Delta t}}{2\Delta t} \quad (4.1.9)$$

rather than the first order implicit Euler scheme (Hayes and Tanguy, 1988):

$$\left. \frac{\partial C}{\partial t} \right|_{t+\Delta t} = \frac{C^{t+\Delta t} - C^t}{\Delta t} \quad (4.1.10)$$

The advantage of this choice is less numerical dispersion for a given time step (Hayes and Tanguy, 1988), although it requires more storage.

4.2 SIMULATION RESULTS

Numerical testing of the dispersion models with the motive of obtaining a practical model for computational purposes led to an evaluation of two model types: Koch & Brady (1985) (KB) analytical and modified analytical results, and Fried & Combarous (1971) (FC) type correlations. An alternative dispersion model, based on the FC and KB results, is proposed that gives better agreement with the experimental data in simulations. Regarding other types of dispersion models and related effects, it was found that the transient and the (to be discussed shortly) path length dependence forms, particle diameter definition and type of boundary condition employed were not dominant in any situation, and they, along with numerical dispersion, are discussed briefly in the next few paragraphs. A discussion of the simulation testing of the dispersion models is presented following a review of the preliminary checks on boundary condition and particle diameter effects, numerical dispersion, etc. The simulation plots are grouped at the end of this section, along with tables detailing the simulation runs and a list of abbreviations used.

Typical particle diameter effects are shown in Figures 14 and 15; there is a slightly greater change for the higher flowrate run (#1, 6.7 ml/min) than for the low flowrate run (#6, 3.5 ml/min), but not a significant amount when compared to other effects such as choice of dispersion model. The definition of Han *et al.* (1985) was used systematically for the model comparison runs.

The choice of boundary condition is shown to be of little importance for these experimental conditions; in Figure 16, virtually no difference is seen between the two. Since the fixed condition ($C=C_f$ at $Z=0$) is simpler, it was used consistently in the comparison of the dispersion models.

To check numerical dispersion, both the time step(s) and the mesh size have to be considered. They are mutually dependent; a coarser mesh may be used when small time steps are taken, and relatively large time steps may be taken when fine meshes are employed. The critical part of the simulation is when the displacing front is in the narrow entrance region to the core; the Peclet number is very high, the gradients steep, and the velocity field is highly two dimensional. If the quantity Uh/D_1 is greater than one, where h is the local mesh size, numerical dispersion is a problem; low velocity areas then help meet this constraint. When the front has moved past this entrance section to the low velocity exit region, numerical dispersion is less of a problem. A larger time step may be used at that point in time; a small time step is only necessary for the time that the front is moving through the high velocity entrance region. As shown in Figure 17 for a high flow rate run, the time step to use for a particular flowrate is safely determined to within a factor of at least two; in that plot is shown the results for cases where both the initial and the final time steps are halved with no appreciable effect on the breakthrough. In Figure 18, for the larger core and moderate flowrate, changing both time steps by a factor of three (from

(1,3) to (0.33,1)) had no significant effect.

Figure 19 shows the minor effect of changing the number of elements in the axial direction from eighty to ninety. Figure 20 shows the slight change brought about by concentrating the grid in the entrance region compared to using a uniform mesh. For the purpose of calculation of the flow field (solving equation 4.1.1), an "injector region" was assumed. Using this numerical device alleviated the problem of numerical singularity in the pressure boundary condition at the corner of the entrance wall. The number of elements to concentrate radially in this area was specifically checked; too many would reduce the number available for the radial distance between the edge of the injector and the wall (hurting the solution there), and too few would not give a sufficiently accurate flow field for the very important entrance region. This injector region was not used in the solution of the convection dispersion equation (1.2.1). Figure 21 shows no impact from varying the injector region mesh size in the calculation of the Darcy flow field. Finally, the general dispersion effects that were avoided are shown in Figure 22. Dispersion model comparisons were typically done using a 20x100 mesh (radial by axial, 2x5 at the injector) with time steps of (0.5,3) seconds for the high velocity runs and (1.5,3) seconds for the low velocity runs.

Since the concentration profile is roughly parabolic by the time that the front has moved a third of the core length, it was expected that transverse dispersion would contribute significantly in the remaining portion of the bed. However, as shown in Figures

23 and 24, that was not the case. In Figure 23, the inlet α_1 and the outlet β_1 for the FC model were varied together to no effect. Figure 24 shows that ignoring transverse dispersion entirely is not unreasonable for the experimental conditions of this study.

While Koch & Brady (1985 & 1987) do not give time dependent equations suitable for use here, the effect of using transient dispersion coefficients was examined qualitatively. Longitudinal dispersion coefficients were calculated using the FC or KB model, but the result was then multiplied by a factor of the form

$$\text{factor} = 1 - \exp(-a \cdot t) \quad (4.2.1)$$

(or 0.1, whichever was greater, to avoid eliminating completely dispersion) where "t" denotes the time elapsed since the concentration at a node became non-zero, e.g. greater than 0.001. The parameter "a" was varied over two orders of magnitude; as shown in Figures 25 and 26, the primary result is simply decreased dispersion with very little change in the characteristic shape (tailing) of the breakthrough curve. Figure 25 shows the application to a moderate flowrate run for the various values of the transient factor, and Figure 26 shows the effect for varying flowrate.

A more straightforward attempt to accommodate transient dispersion coefficients was made by using the experimental result of Han *et al.* (1985). They show D_1 to increase in approximately the same form as that given by equation (4.2.1), using path length

instead of time as the independent variable. Following this approach, and multiplying the standard dispersion coefficients by this path length factor, gave once again a primary result of decreased dispersion rather than changing the characteristic shape of the breakthrough. A sample result is given in Figure 27. The correction factor used was taken as the maximum of 0.1 and

$$\text{factor} = 1 - \exp\{-10.25 * a_{ld} * (\text{path length}) / Pe_p\} \quad (4.2.2)$$

It is important to note that, for simulation purposes, it is relatively straightforward to curve fit a dispersion model to a particular set of breakthrough data given a sufficient number of adjustable parameters. In order to obtain a general or reliable set of dispersion parameters, it must also be shown that they predict as accurately the breakthrough curves for a variety of core dimensions and flowrates.

Many different dispersion model variations were run but only the most reasonably successful, plus a few included to illustrate certain trends, are shown in the figures to follow. The simulations are fully documented in tables, however.

A few general points should be made regarding the results. Since the Peclet number range is very large (in the thousands at the entrance, dropping to as low as thirty at the exit), it is not really expected that one dispersion model, or one set of parameters for a particular model, would suffice over the entire domain. As these results show, it is necessary to have different

models or model parameters for at least two flow regimes: high Peclet (greater than about 150) and low. For the FC model, there are four adjustable parameters (effectively two for our case, since transverse dispersion was not significant) while the KB longitudinal dispersion model allows for one significant adjustable factor on the (primary contributor) $\phi Pe_p \ln(\phi Pe_p)$ term. The standard dispersion models were tested for all runs to provide base case comparisons for subsequent simulations, and generally the most successful of the latter predict higher dispersion at Pe_p over 150 than has been previously presented in the literature. For the purpose of comparing results between cores, the exit Peclet number was listed in Table 2 (Chapter 3) for each run. The correspondence between cores of different diameters cannot be exact. *i.e.*, when the exit Pe_p are matched, the entrance Pe_p conditions in the thinner core have approximately twice the magnitude of those in the wider core.

Characteristic of all of the experimental breakthrough curves obtained here is a rapid climb followed by a very slow approach to the final value; this tailing was at first assumed to be the result of the boundary layer dispersion mechanism (transience) as described by Koch & Brady (1987 a & b) as it is claimed there to be the cause of similar tailing in other results. This was simulated in the transient and in the length dependent dispersion correction models, given as equations 4.2.2 and 4.2.3, and those results show very little increased tailing. It became apparent that the only source for the tailing was the initial

parabolic-type concentration profile that was always "matured" before the front left the entrance region, the first third of the core. Subsequent longitudinal dispersion can hide this effect if the core is long or the low Peclet dispersion rate assumed is very high, but usually only contributes to the leading edge of the breakthrough. Most of the tailing was the result of very high dispersion rates in the entrance region, and models that predict that type of high Peclet - high dispersion behaviour gave the best match to the experiments. Plots are shown where these high Peclet dispersion parameters are varied, along with the cutoff Peclet point. The FC-KB model was then seen as the natural one to try, because the FC(2) model that gave the best results had a $4.5 \cdot Pe_p$ dependence, which is approximately the same as $\ln(\phi Pe_p) \cdot Pe_p$ for Peclet numbers above 200 and below 8000. Koch & Brady provide the physical basis for the natural log term (boundary layer dispersion), validating the substitution for at least high Peclet.

The following general patterns may be observed: (1) better fits are obtained as flow rates are increased. (2) As the particle path length, or duration of the run spent at low Peclet number (front moving through the exit portion of the core), is increased the fit is better. A better fit may be generally described as one that better matches the tailing. In fact, very acceptable results were obtained for the high flowrate large (6x1.5 inch) core for the standard FC model, suggesting that entrance effects have been somewhat overshadowed by that point. It also implies that it is only the entrance region model that

requires adjusting, at least for the higher flowrates, and that the standard FC exit model works for low Peclet numbers (less than about 150). All of the low flowrate runs underpredicted tailing. As the core length increased for these runs the tailing was better matched, but not to the degree that was achieved in the higher flowrate runs.

For the following discussion, please refer to the list of abbreviations, tables and plots at the end of this section. For the sake of comparison, note that exit Peclet numbers were approximately matched at 235 for the 6x1 and 3x1 inch cores (runs 20 and 1, respectively), at 125 for the 3x1, 6x1.5 and 3x1.5 inch cores (runs 6, 23 and 11, respectively) and at 55 for the 6x1, 3x1, 6x1.5 and 3x1.5 inch cores (runs 32, 7, 27 and 22, respectively). The tables are in order of run number.

Figures 28 to 31 show the results for the small (3x1 inch) core (Run #1) at high flowrate, 6.73 ml. per minute. Figure 28 shows a comparison of the effect of changing the powers (β) on the FC models to changing the multipliers (α). The change in inlet α does well for the leading edge, but the trial with the very high inlet β does better on the tail. Various FC models are shown in Figure 29, which presents the testing for the best value of cutoff Peclet and for the best high Peclet dispersion model. The FC(2) with α_1 of 4.5 at the entrance with a cutoff Pe_p of 150 does as well as any there, but still does miss the tailing somewhat. Figure 30 shows that an enhanced high Peclet model does better than a standard FC, but neither is completely acceptable. Figure

31 shows some variations on the KB model, none of which are clearly superior, although the KB(2) does slightly better with respect to tailing.

The moderate flowrate (3.58 ml/min) 3x1 inch core (Run #6) simulations are given in Figures 32 and 33. No (FC) result shown in Figure 32 does well on the tail, but in Figure 33 the trend is that FC-KB does the best, slightly better than FC(2), and substantially better than KB. Compared to the higher flowrate results for run #1, these do not model the tail as well.

A complete round of plots for the low flowrate (1.56 ml/min) small (3x1 inch) core (Run #7) are shown next. Figure 34 shows that greatly increasing the FC dispersion does predict better, yet fails to produce tailing. Even a power of 1.6 on Pe_p for the entrance region does not have a strong enough effect; that power does when it is applied for all Peclet. Figure 35 shows that the Pe_p cutoff point chosen is not critical for the FC models. Figure 36 shows that FC(2) does better than FC-KB here, and both better than KB. The difference in the results for the variations on KB, shown in Figure 31, are not substantial. If the FC-KB model is given a boost on α_1 (up from one), it might be the best model for lower Peclet. *i.e.* though it seemed to diverge for Run #1 which has Peclet numbers roughly 4.5 times as large, this lower flow rate run has its dispersion underpredicted and an enhanced FC-KB might work.

Run #11, high flowrate (6.7 ml/min) 3x1.5 inch core, results are more encouraging. Figure 38 shows that a high power for a low

cutoff Peclet completely overestimates the dispersion, while an enhanced high Peclet region model with a slightly higher cutoff does not give significantly different results from a standard FC. Results better match tailing than for the small core. Figure 39 shows that varying the Peclet cutoff above 150 does not have a strong effect, and that greatly increasing the entrance α_1 still does completely capture the tailing. Figure 40 shows the FC-KB model to do slightly better than the FC(2) on the tailing, with KB still not achieving very much. Figure 41 shows that the choice of permeability for the KB models is not critical, while also showing that increasing KB dispersion does not help in the tailing but moves more to symmetry.

The moderate flowrate run, # 22, for the 3x1.5 inch core has its simulations given in Figures 42 and 43. They clearly show that, while the FC(2) enhanced high Pe_p model (Figure 43) does better than the KB variations, more dispersion is needed, especially in the entrance high Peclet region.

Figure 44, for the 6x1 inch high flowrate (6.7 ml/min) run, shows that either of a very high α or β for the entrance FC model strongly overestimates the dispersion. It also shows that a standard FC does well on the initial part of the breakthrough, as well as the FC(2) model having an entrance α_1 of 4.5, but does not cover the tailing like that FC(2). Results are significantly better for this core than for the 3x1 inch core. Figures 45 and 46 show the familiar pattern of the FC(2) model bettering the KB and KB MOD variations. The leading edge can be obtained

satisfactorily, but not the tailing.

The tailing for the low flowrate, 1.58 ml/min, run #32 for the same 6x1 inch core is more closely approached by the FC models shown in Figure 47; large variations in parameter values did not have much effect because of the relatively low Peclet numbers involved. The result is in line with others in that the longer cores tend to be better modelled by a standard FC equation. However, the tailing is still not completely matched. The FC-KB model, shown in Figure 48, does not do as well as the FC(2) models, but both once again do significantly better than KB or its modifications (Figure 49). The results are better than for the short core same flowrate run (#7), due to the relatively increased influence of the low Peclet exit model for the longer core.

The high flowrate large core (6.7 ml/min, 6x1.5 inch, #23) run was well reconstructed using the FC, the FC-KB and particularly the FC(2), with the high Peclet α_1 of 4.5, models. See Figure 50. The standard KB, in Figures 51 and 52, still does not capture the tailing, which by its presence indicates that the entrance effects have not been completely swamped. These results are the best of all of the simulations attempted. The initial climb is captured by all models, although more dispersion may be needed at the entrance to coincide exactly with the experimental data; the breakthrough is not as sensitive to entrance model effects for this run as it is for smaller cores and lower flowrates.

The large core moderate flowrate run (6x1.5 inch, 3.02

ml/min, #27) was not modelled quite as well as the high flowrate run; the tailing was given best by a high power on an entrance Pe_p , although a moderate value (4.5) for α_1 gives nearly the same result. The FC(2) variations (Figure 53) generally miss slightly on the tailing. Shown in Figure 54, the standard KB model still does not do as well as either of FC(2) or FC-KB. The KB variations in Figure 55 do not exhibit the necessary tailing.

Reviewing the runs whose exit Peclet's match, it can be seen that those runs which do not pick up the tailing, despite having the same Peclet number for most of the core, are those that have the shorter path length, i.e. those that have a relatively shorter duration at low Peclet number. Specifically, the 3 inch length core runs 7 and 22 have more tailing than predicted (at Pe_p of 55), while the corresponding 6 inch core runs, 32 and 27, were better modelled. The dispersion in the exit region for those longer cores, at the low Peclet number, tends to be modelled successfully by a standard FC and that overshadows the entrance effects. Comparing the thin core runs, 7 and 32, to the wide core ones shows that the results for the wider cores better match the tailing. With the relatively higher Pe_p in the entrance region, this is to be expected. There is also a somewhat longer path length for the dispersion in a wide core over which the amount of dispersion accumulates, masking the entrance effect on the breakthrough.

The higher Peclet number runs were consistently better modelled. This is due in part to the increased dispersion at the

exit tending to overshadow the entrance effects, but the best results were for those simulations that predicted enhanced dispersion, either through a KB type log term or through a FC(2) model containing a large value for α_1 , at high Peclet. This allowed the tailing to be matched without sacrificing the prediction for the leading edge. While the longer cores were generally better matched because of the relatively long time the front is moving at low Peclet number, it may be that even the low Peclet number models slightly underestimate dispersion. The dispersion in the high Peclet zone was significantly underestimated by the FC STD and KB models, in contrast.

While the KB runs did not do well for capturing the tailing, they did not do well in predicting the leading edge of the breakthrough, either. The conclusion is that they underpredict dispersion levels for high Peclet numbers, and overpredict for low. The transition point is around a Pe_p of 150.

For the following tables and plots, the abbreviations used are:

FC Fried & Combarous (1971), equations (2.1.2) and (2.1.3), applied for all Pe_p with parameters listed as $(\alpha_1, \alpha_t, \beta_1, \beta_t)$.

FC STD FC using (.5, .025, 1.2, 1.1) in the above notation.

FC(2) Using both the high (eqn. 2.1.4 & 2.1.5) and the low (FC STD) Peclet number models, with the cutoff Pe_p given in

parenthesis. e.g. FC(2) (260) was the default case.

FC(2) STD (1.8, .025; 1, 1) for high Pe_p and FC STD for the low Pe_p flow, from equations (2.1.2) to (2.1.5).

FC(2) STD Matching (1.52, .0436, 1, 1) for high Pe_p and FC STD for low. The parameters were set by matching the predicted value of the dispersion coefficient at the cutoff Pe_p . i.e. As per Fried & Combarous (1971), the transition from the low Pe_p model to the high Pe_p one occurs at Pe_p approximately equal to 260; for a matching FC model, the two are set so that they produce the same number for the dispersion coefficient at that common boundary.

KB Standard Koch & Brady (1985) model, equations (2.1.29) and (2.1.31). Note that either a dilute bed permeability (eqn. 2.1.16, assumed in the standard KB model) or a more realistic value (eqn. 1.1.15) produced using the Ergun equation may be used; the choice is usually taken to be the dilute one, but if the Ergun one is applied it is noted in parenthesis after the model name. e.g. KB (Ergun).

KB MOD KB modified to give a $AKB \cdot \phi Pe_p \cdot \ln(\phi Pe_p)$ term, where AKB is a constant subject to change for various microstructures. AKB has a value of $\pi^2 \phi_s / 6$ in the original KB model, equation (2.1.29). This adjustable parameter was given by Koch & Brady (1985), as a qualification on their model.

KB(2) KB MOD with different values for AKB for the high and low Pe_p domains. They are 1.5 and 1, respectively, with the cutoff Pe_p given in parenthesis after the model name. e.g. KB(2); (150).

KB U_1 KB based on interstitial velocity for Pe_p . i.e. Pe_p is used everywhere in place of ϕPe_p . Only a few runs of a speculative nature were tried on this model, as it produced far too much dispersion.

FC-KB For low Pe_p , FC STD is used. For high Pe_p (over 150),

$$D_1 = Pe_p * \ln(\phi Pe_p) \quad (4.2.3)$$

This form was inspired by the KB model.

LD Length dependence, equation (4.2.2)

FH Fair & Hatch d_p , equation (1.1:2)

F Fixed $C=C_f$ boundary condition. (BC), eqn. (1.4.1)

D Danckwerts boundary condition, eqn. (1.4.4)

For the following tables, the mesh used will be specified as the number of elements in the core (radial x axial) plus the number used for the injector area in the flow field calculation. The time steps used are specified as (t_1, t_2) which refer to the step used until the concentration front is out of the entrance region (t_1), and the step used thereafter (t_2). Except where noted, the mesh was uniform (quadrilateral elements). For the FC(2) models, the parameters for the high Pe_p are given first, with those for the low Pe_p region are given in parenthesis in the line below, in the format $(\alpha_1, \beta_1, \beta_t)$.

#	Mesh	Time Steps	BC	d _p	Model
60	10x100 2x5	4,3	D	Han	FC STD
61	"	"	"	"	FC (.5, .025, 1.6, 1.5)
62	"	"	"	"	FC (.5, .025, 1.8, 1.6)
63	"	"	"	"	FC (.5, .025, 1.6, 1.2)
64	"	"	"	FH	FC (.5, .025, 1.6, 1.5)
65	"	"	"	Han	FC (.6, .03, 1.2, 1.4)
66	"	"	"	"	FC (.5, .025, 1.2, 1.4)
67	"	"	"	"	FC (.5, .025, 1.1, 1.3)
77	"	"	"	"	FC(2) (260) (1.8, .025, 1, 1) (.5, .025, 1.1, 1.3)
89	20x80 8x10	"	"	"	FC(2) STD
95	20x80 4x10	1,3	"	"	FC(2) STD
97	20x90 5x10	"	"	"	"
113	20x80 5x10	.5,3	"	"	"
185	"	"	"	"	KB MOD $AKB = \pi \phi_s / 6$

Table 4: Run #1 Simulations (continued)

#	Mesh	Time Steps	BC	d _p	Model
246	20x80 5x10	.5, .5	D	Han	FC(2) MATCH (14.06, .0436, 1, 1) (.5, .025, 1.2, 1.1)
313	20x100 2x5	.5, 3	F	"	FC(2) STD MATCH
314	"	"	"	"	FC(2) STD MATCH Transient, a=.01
320	"	"	"	"	FC(2) (1.52, .0436, 1.6, 1.1) Low Peclet FC STD
329	"	"	"	"	FC(2) (1.52, .0436, .8, .8) Low Peclet FC STD
333	"	"	"	"	FC(2) (45, .0436, 1, 1) Low Peclet FC STD
334	"	"	"	"	FC(2) (4.5, .0436, 1, 1) Low Peclet FC STD
346	"	"	"	"	FC(2) (150) (4.5, .0436, 1, 1) Low Peclet FC STD
347	20x100 2x5	.5, 3	F	Han	FC(2) (200) (4.5, .0436, 1, 1) Low Peclet FC STD
360	"	"	"	"	FC(2) (150) (4.5, .0436, 1.2, 1.1) Low Peclet FC STD
365	"	"	"	"	KB (Ergun)
376	"	"	"	"	KB U ₁ (Ergun)
387	"	"	"	"	KB

Table 4: Run #1 Simulations (continued)

#	Mesh	Time Steps	BC	d _p	Model
399	20x100 2x5	.5, 3	F	Han	KB MOD AKB=1.65*2
400	"	"	"	"	KB MOD AKB=1.65*3
407	"	"	"	"	KB(2) (150) (dilute)
424	"	"	D	"	FC(2) (150) (4.5, .0436, 1, 1) Low Peclet FC STD
425	"	1, 3	F	"	"
426	"	.5, 3	"	"	"

Table 4: Run #1 Simulations

#	Mesh	Time Steps	BC	d _p	Model
39	10x60 2x5	4, 3	D	FH	FC STD
40	10x100 2x5	4, 3	"	"	"
42	10x60 2x5	"	"	"	KB MOD $AKB = \pi \phi_s / 6$
43	"	"	"	Allen	"
44	"	"	"	Han	"
45	"	"	"	"	FC (.6, .03, 1.2, 1.1)
46	"	"	"	"	FC (.5, .025, 1.25, 1.15)
47	"	"	"	"	FC (.6, .03, 1.25, 1.15)
48	"	"	"	"	FC (.5, .025, 1.3, 1.2)
49	"	"	"	"	FC STD
50	"	"	"	FH	FC (.6, .03, 1.2, 1.1)
51	"	"	"	"	FC (.5, .025, 1.25, 1.15)
52	"	"	"	"	FC (.6, .03, 1.25, 1.15)
53	"	"	"	"	FC (.5, .025, 1.3, 1.2)
54	10x100 2x5	"	"	Han	FC (.5, .025, 1.6, 1.5)

Table 5: Run #6 Simulations (continued)

#	Mesh	Time Steps	BC	d _p	Model
55	10x100 2x5	4,3	D	Han	FC (.5, .025, 1.6, 1.2)
68	"	"	"	"	FC (.6, .03, 1.2, 1.4)
69	"	"	"	"	FC (.5, .025, 1.2, 1.4)
70	"	"	"	"	FC (.5, .025, 1.1, 1.3)
79	"	"	"	"	FC(2) STD
81	"	"	"	"	FC(2) (1.8, .025, 1, 1) (.5, .025, 1.3, 1.1)
114	20x80 5x10	1,3	"	"	FC(2) STD
130	"	"	"	"	FC (.5, .025, 1.22, 1.12)
131	"	"	"	"	FC (.04, .02, 1.15, 1.05)
140	"	"	"	"	FC (.5, .025, 1.1, 1.05)
152	"	"	"	"	FC (.5, .01, 1.2, 1.1)
153	"	"	"	"	FC (.3, .025, 1.2, 1.1)
154	"	"	"	"	FC (.5, .025, 1.2, .8)
155	"	"	"	"	FC (.5, .025, 1.1, 1.1)
162	"	"	"	"	FC(2) STD Match.

Table 5: Run #6 Simulations (continued)

#	Mesh	Time Steps	BC	d _p	Model
163	20x80 2x5	1,3	1,3	Han	FC(2) Match. (2.2, .0436, 1, 1) (.723, .025, 1.2, 1.1)
164	"	"	"	"	FC(2) Match. (1.4, .0436, 1, 1) (.46, .025, 1.2, 1.1)
165	"	"	"	"	FC(2) Match (1.8, .0436, 1, 1) (.592, .025, 1.2, 1.1)
166	"	"	"	"	FC(2) Match (1.8, .025, 1, 1) (.592, .0143, 1.2, 1.1)
167	"	"	"	"	FC(2) Match (1.52, .01, 1, 1) (.5, .00573, 1.2, 1.1)
168	"	"	"	"	FC(2) Match (1.52, .06, 1, 1) (.5, .0344, 1.2, 1.1)
184	"	"	"	"	KB MOD $AKB = \pi \phi_s / 6$
192	"	"	"	"	FC(2) Match (1.8, .025, 1, 1) (.5, .025, 1.23, 1.1)
193	"	"	"	"	FC(2) Match (1.4, .025, 1, 1) (.5, .025, 1.185, 1.1)
194	"	"	"	"	FC(2) Match (2.2, .025, 1, 1) (.5, .025, 1.266, 1)
195	"	"	"	"	FC(2) Match (2.2, .01, 1, 1) (.5, .025, 1.266, .835)

Table 5: Run #6 Simulations (continued)

#	Mesh	Time Steps	BC	d _p	Model
196	20x80 5x10	1,3	D	Han	FC(2) Match (2.2, .06, 1, 1) (.5, .025, 1.266, 1.157)
197	"	"	"	"	FC(2) Match (1.4, .06, 1, 1) (.5, .025, 1.185, 1.157)
198	"	"	"	"	FC(2) Match (1.4, .01, 1, 1) (.5, .025, 1.185, .835)
231	"	"	"	"	FC(2) Match (1.52, .15, 1, 1) (.5, .086, 1.2, 1.1)
232	"	"	"	"	FC(2) Match (4, .0436, 1, 1) (1.374, .025, 1.2, 1.1)
233	"	"	"	"	FC(2) Match (1.52, .403, 1, 1) (.5, .025, 1.2, 1.5)
234	"	"	"	"	FC(2) Match (14.06, .0436, 1, 1) (.5, .025, 1.6, 1.1)
241	"	"	"	"	FC(2) Match (130, .0436, 1, 1) (.5, .025, 2, 1.1)
242	"	"	"	"	FC(2) Match (.025, .01, 1, 1) (.025, .01, 1, 1)
243	"	"	"	"	FC(2) Match (14.06, .231, 1, 1) (.5, .025, 1.6, 1.4)
244	"	"	"	"	FC(2) Match (14.06, .00822, 1, 1) (.5, .025, 1.6, .8)

Table 5: Run #6 Simulations (continued)

#	Mesh	Time Steps	BC	d _p	Model
304	20x100 2x5-	1,3	F	Han	FC(2) STD Match. Transient, a=1
305	"	"	"	"	FC(2) Match. (14.06, .0436, 1, 1) (.5, .025, 1.6, 1.1) Transient, a=20
306	"	"	"	"	FC(2) Match. (14.06, .0436, 1, 1) (.5, .025, 1.6, 1.1) Transient, a=1
307	"	"	"	"	FC(2) Match. (14.06, .0436, 1, 1) (.5, .025, 1.6, 1.1) Transient, a=.1
308	"	"	"	"	FC(2) Match. (14.06, .0436, 1, 1) (.5, .025, 1.6, 1.1) Transient, a=.01
366	"	"	"	"	KB (Ergun)
377	"	"	"	"	KB U (Ergun)
408	"	"	"	"	KB MOD AKB=1.65*2

Table 5: Run #6 Simulations

#	Mesh	Time Steps	BC	d _p	Model
56	10x100 2x5	4,3	D	Han	FC (.5,.025,1.6,1.5)
57	"	"	"	"	FC (.5,.025,1.6,1.2)
58	"	"	"	"	FC STD
59	"	"	"	"	FC (.5,.025,1.8,1.6)
117	20x80 2x5	1,3	"	"	FC(2) STD
186	"	"	"	"	KB MOD $AKB = \pi \phi_s / 6$
247	20x80 5x10	"	"	"	FC(2) Match. (14.06,.0436,1,1) (.5,.025,1.6,1.1)
315	20x100 5x10	1.5,3	P	"	FC(2) Match. (14.06,.231,1,1) (.5,.025,1.6,1.4)
316	"	"	"	"	FC(2) STD Match.
319	"	"	"	"	FC(2) (1.52,.0436,1,1) Low Peclet FC STD
328	"	"	"	"	FC(2) (1.52,.0436,.8,.8) Low Peclet FC STD
337	"	"	"	"	FC(2) (15,.0436,1,1) Low Peclet FC STD
338	"	"	"	"	FC(2) (4.5,.0436,1,1) Low Peclet FC STD

Table 6: Run #7 Simulations (continued)

#	Mesh	Time Steps	BC	d _p	Model
339	20x100 2x5	1.5, 3	F	Han	FC(2) (45, .0436, 1, 1) Low Peclet FC STD
342	"	"	"	"	FC(2) (150) (4.5, .0436, 1, 1) Low Peclet FC STD
343	"	"	"	"	FC(2) (200) (4.5, .0436, 1, 1) Low Peclet FC STD
344	"	"	"	"	FC(2) (150) (15, .0436, 1, 1) Low Peclet FC STD
345	"	"	"	"	FC(2) (200) (15, .0436, 1, 1) Low Peclet FC STD
359	"	"	"	"	FC(2) (150) (4.5, .0436, 1.2, 1) Low Peclet FC STD
367	"	"	"	"	KB (Ergun)
378	"	"	"	"	KB U ₁ (Ergun)
389	"	"	"	"	KB (Dilute)
398	"	"	"	"	KB (Dilute) Mesh concentrated as 30% in 20% of core
409	"	"	"	"	KB(2) (Dilute)
418	"	"	"	"	FC-KB

Table 6: Run #7 Simulations

#	Mesh	Time Steps	BC	d p	Model
121	25x80 5x10	.5, 3	D	Han	FC(2) STD
176	"	"	"	"	FC(2) STD Match.
177	"	"	"	"	FC(2) Match. (1.8, .0436, 1, 1) (.592, .025, 1.2, 1.1)
178	"	"	"	"	FC(2) Match. (1.8, .025, 1, 1) (.592, .0143, 1.2, 1.1)
179	"	"	"	"	FC(2) Match. (1.8, .01, 1, 1) (.592, .00573, 1.2, 1.1)
187	"	"	"	"	KB MOD $AKB = \pi \phi_s / 6$
255	"	.5, 1.5	"	"	FC(2) Match. (14.06, .0822, 1, 1) (.5, .025, 1.6, .8)
260	"	"	"	"	FC(2) Match. (9.12, .0436, 1, 1) (3, .025, 1.2, 1.1)
261	"	"	"	"	FC(2) Match. (14.06, 0, 1, 1) (.5, 0, 1.6, 0)
285	25x100 5x10	"	"	"	FC STD
311	25x100 2x5	.5, 3	F	"	FC(2) STD Match.
323	"	"	"	"	FC(2) Match. (100) (1.52, .0436, 1, 1) Low Peclet FC STD

Table 7: Run #11 Simulations (continued)

#	Mesh	Time Steps	BC	d _p	Model
331	25x100 2x5	5,3	F	Han	FC(2) (1.52,.0436,.8,.8) Low Peclet FC STD
335	"	"	"	"	FC(2) (4.5,.0436,1,1) Low Peclet FC STD
336	"	"	"	"	FC(2) (15,.0436,1,1) Low Peclet FC STD
348	"	"	"	"	FC(2) (150) (4.5,.0436,1,1) Low Peclet FC STD
349	"	"	"	"	FC(2) (200) (4.5,.0436,1,1) Low Peclet FC STD
371	"	"	"	"	KB (Ergun)
382	"	"	"	"	KB U ₁ (Ergun)
393	"	"	"	"	KB (Dilute)
413	"	"	"	"	KB MOD AKB=1.65*2
421	"	"	"	"	FC-KB

Table 7: Run #11 Simulations

#	Mesh	Time Steps	BC	d _p	Model
312	20x100 2x5	3	F	Han	FC(2) Match.
324	"	"	"	"	FC(2) (100) (1.52, .0436, 1.6, 1.1) Low Peclet FC STD.
355	"	"	"	"	FC(2) (150) (4.5, .0436, 1, 1) Low Peclet FC STD
356	"	"	"	"	FC(2) (150) (15, .0436, 1, 1) Low Peclet FC STD
368	"	"	"	"	KB (Ergun)
379	"	"	"	"	KB U ₁ (Ergun)
390	"	"	"	"	KB (Dilute)
410	"	"	"	"	KB MOD AKB=1.65*2

Table 8: Run #20 Simulations

#	Mesh	Time Steps	BC	d _p	Model
258	20x80 5x10	1,3	D	Han	FC(2) Match. (14.06, .00822, 1, 1) (.5, .025, 1.6, .8)
301	20x100. 2x5	.5, 3	F	"	FC(2) Match (14.06, .0436, 1, 1) (.5, .025, 1.6, 1.1) LD, a _{ld} =15
302	"	"	"	"	FC(2) Match. (14.06, .0436, 1, 1) (.5, .025, 1.6, 1.1) LD, a _{ld} =20
303	"	"	"	"	FC(2) STD Match. LD, a _{ld} =20
302	25x100. 2x5	"	"	"	FC(2) (150) (4.5, .0436, 1, 1) Low Peclet FC STD
372	"	"	"	"	KB (Ergun)
383	"	"	"	"	KB U ₁ (Ergun)
394	"	"	"	"	KB (Dilute)

Table 9: Run #22 Simulations

#	Mesh	Time Steps	BC	d _p	Model
259	20x80 5x10	1,3	D	Han	FC(2) Match. (14.06, .0436, 1, 1) (.5, .025, 1.6, 1.1)
310	25x100 2	.5, 3	F	"	FC(2) STD Match.
325	"	"	"	"	FC(2) (100) (1.52, .0436, 1.6, 1.1) Low Peclet FC STD
327	"	"	"	"	FC(2) (100) (1.52, .0436, .8, .8) Low Peclet FC STD
340	"	"	"	"	FC(2) (260) (15, .0436, 1, 1) Low Peclet FC STD
341	"	"	"	"	FC(2) (260) (4.5, .0436, 1, 1) Low Peclet FC STD
350	"	"	"	"	FC(2) (150) (4.5, .0436, 1, 1) Low Peclet FC STD
351	"	"	"	"	FC(2) (200) (4.5, .0436, 1, 1) Low Peclet FC STD
374	"	"	"	"	KB (Ergun)
385	"	"	"	"	KB U ₁ (Ergun)
396	"	"	"	"	KB (Dilute)
403	"	"	"	"	KB MOD (Dilute) AKB=1.65*2
404	"	"	"	"	KB MOD (Dilute) AKB=1.65*3
422	"	"	"	"	FC-KB

Table 10: Run #23 Simulations

#	Mesh	Time Steps	BC	d_p	Model
293	20x100 2x5	1, 3	F	Han	FC(2) STD Match.
294	"	"	"	"	KB MOD $AKB = \pi \phi_s / 6$
295	"	.33, 1	"	"	FC(2) STD Match.
297	"	.5, 3	"	"	FC(2) STD Match. LD, $a_{ld} = 15$
298	"	"	"	"	FC(2) STD Match. LD, $a_{ld} = 20$
299	"	"	"	"	FC(2) Match. (14.06, .0436, 1, 1) (.5, .025, 1.6, 1.1) LD, $a_{ld} = 15$
300	"	"	"	"	FC(2) Match. (14.06, .0436, 1, 1) (.5, .025, 1.6, 1.1) LD, $a_{ld} = 20$
309	"	"	"	"	FC(2) Match. (14.06, .0436, 1, 1) (.5, .025, 1.6, 1.1) Transient, $a = 0.01$
326	25x100 2x5	"	"	"	FC(2) (1.52, .0436, 1.6, 1.1) Low Peclet FC STD
362	"	"	"	"	FC(2) (150) (1.52, .0436, 1.6, 1.1) Low Peclet FC STD

Table 11: Run #27 Simulations (continued)

#	Mesh	Time Steps	BC	d _p	Model
375	25x100 2x5	5,3	F	Han	KB (Ergun)
386	"	"	"	"	KB U ₁ (Ergun)
397	"	"	"	"	KB (Dilute)
405	"	"	"	"	KB MOD (Dilute) AKB=1.65*2
406	"	"	"	"	KB-MOD (Dilute) AKB=1.65*3
416	"	"	"	"	KB(2) (Dilute)
423	"	"	"	"	FC-KB

Table 11: Run #27 Simulations

#	Mesh	Time Steps	BC	d _p	Model
318	20x100 2x5	1.5, 3	F	Han	FC(2) STD Match.
321	"	"	"	"	FC(2) (1.52, .0436, 1.6, 1.1) Low Peclet FC STD
357	"	"	"	"	FC(2) (150) (4.5, .0436, 1, 1) Low Peclet FC STD
358	"	"	"	"	FC(2) (150) (15, .0436, 1, 1) Low Peclet FC STD
370	"	"	"	"	KB (Ergun)
381	"	"	"	"	KB U ₁ (Ergun)
392	"	"	"	"	KB (Dilute)
412	"	"	"	"	KB MOD (Dilute) AKB=1.65*2
420	"	"	"	"	FC-KB

Table 12: Run #32 Simulations

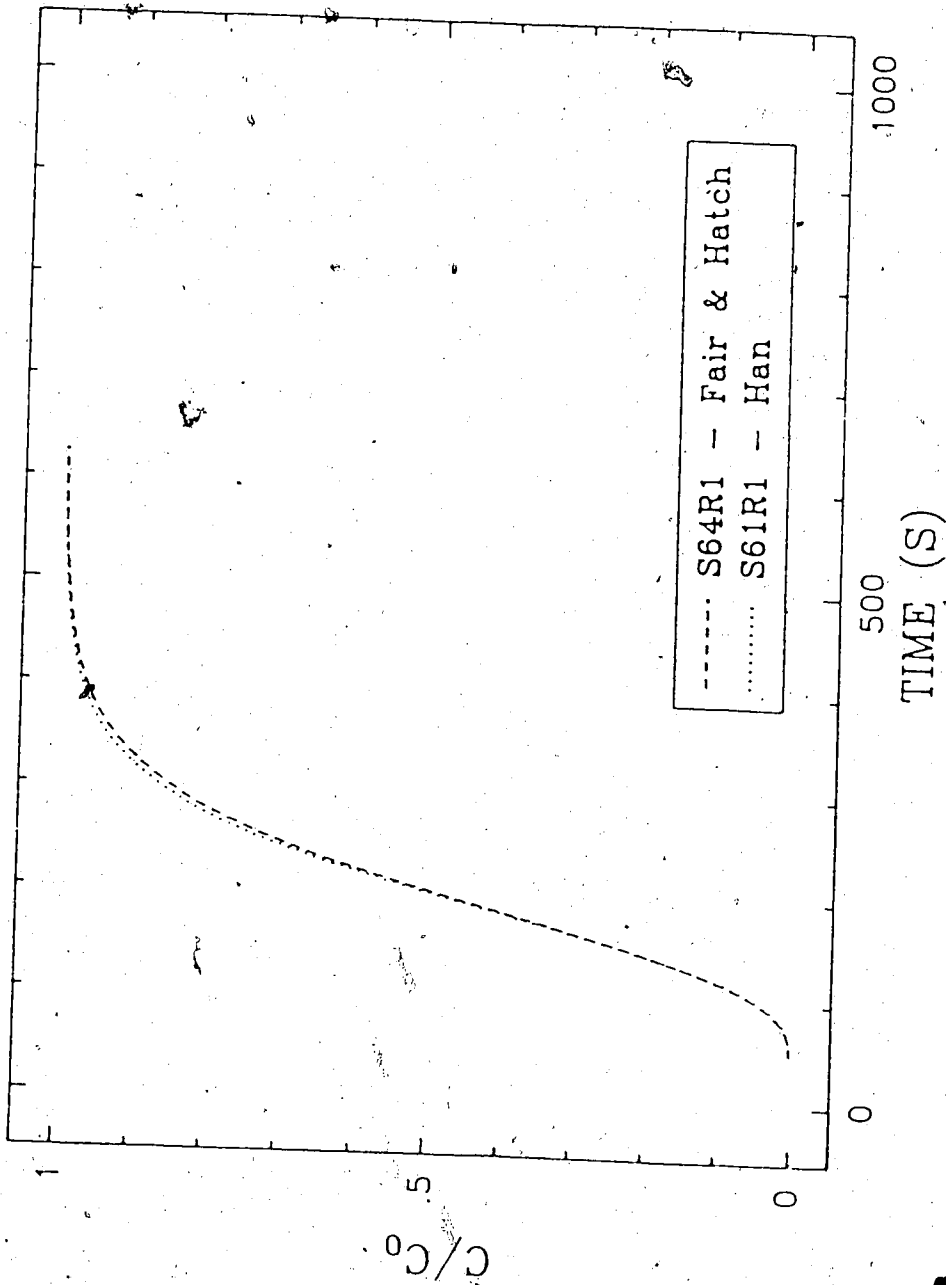


Figure 14: Run #1 d_p Variation

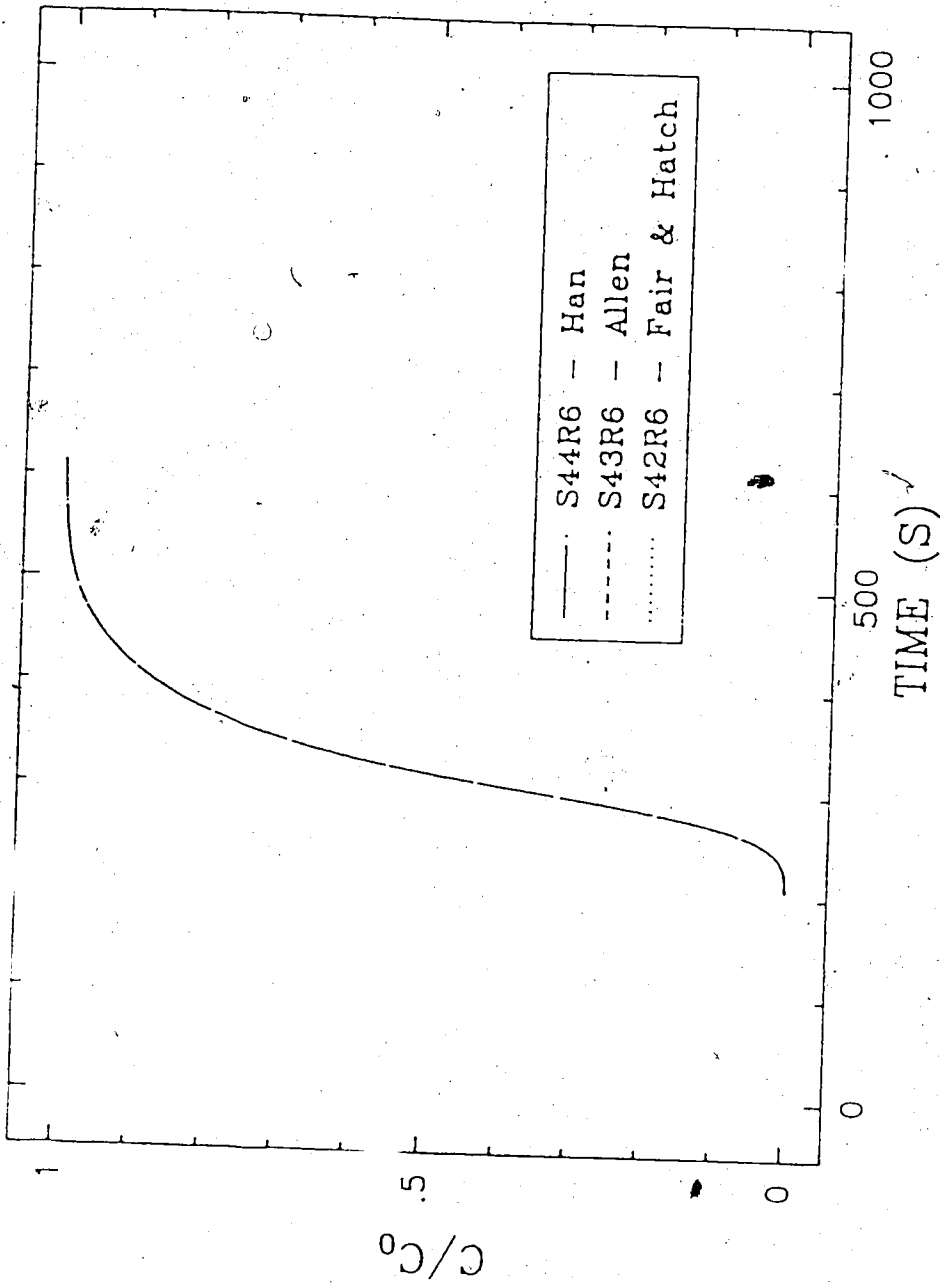


Figure 15: Run #6 d_p Variation

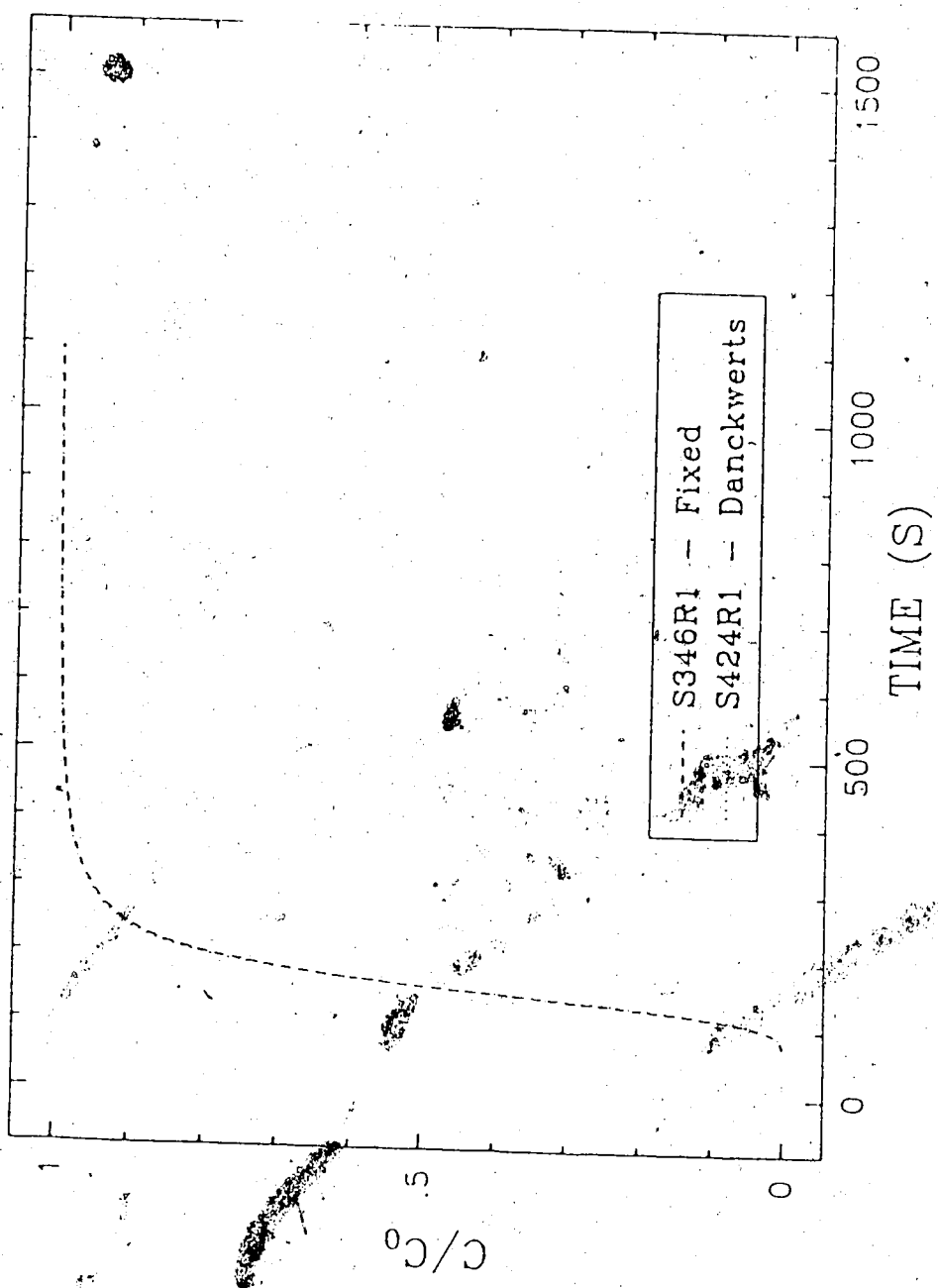


Figure 16: Boundary Condition Effect

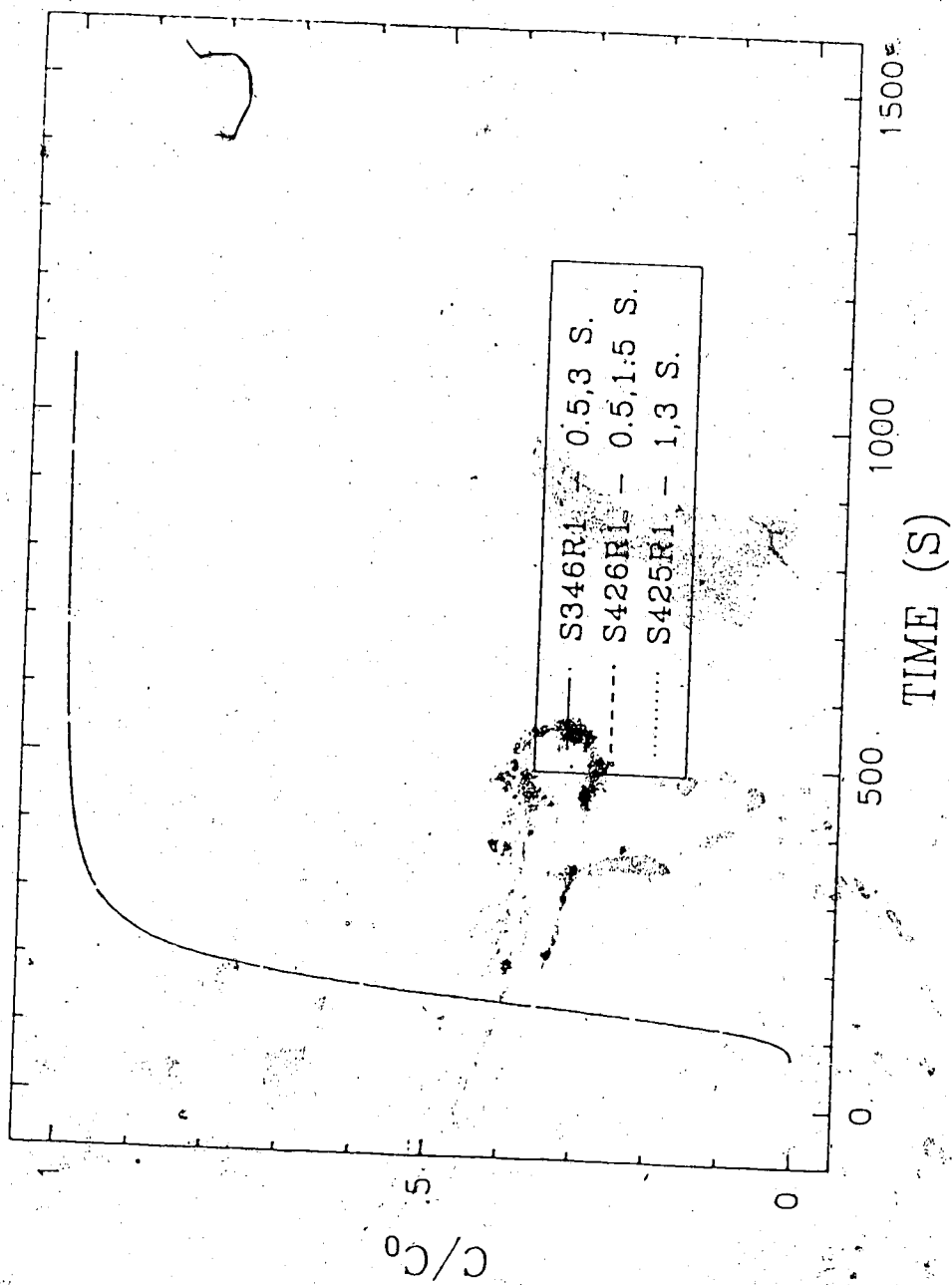


Figure 17: Time Step Small Core

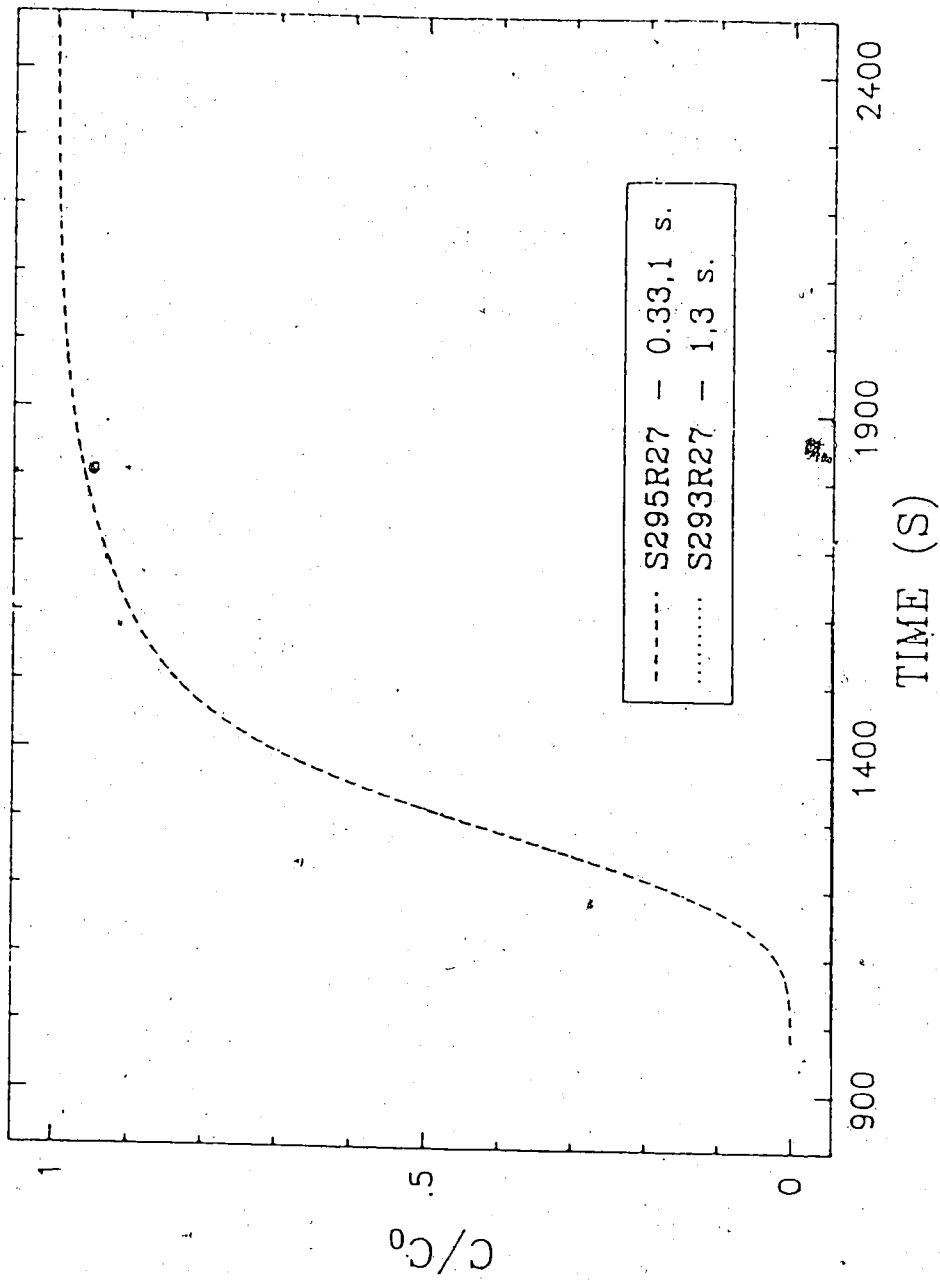


Figure 18: Time Step Large Core

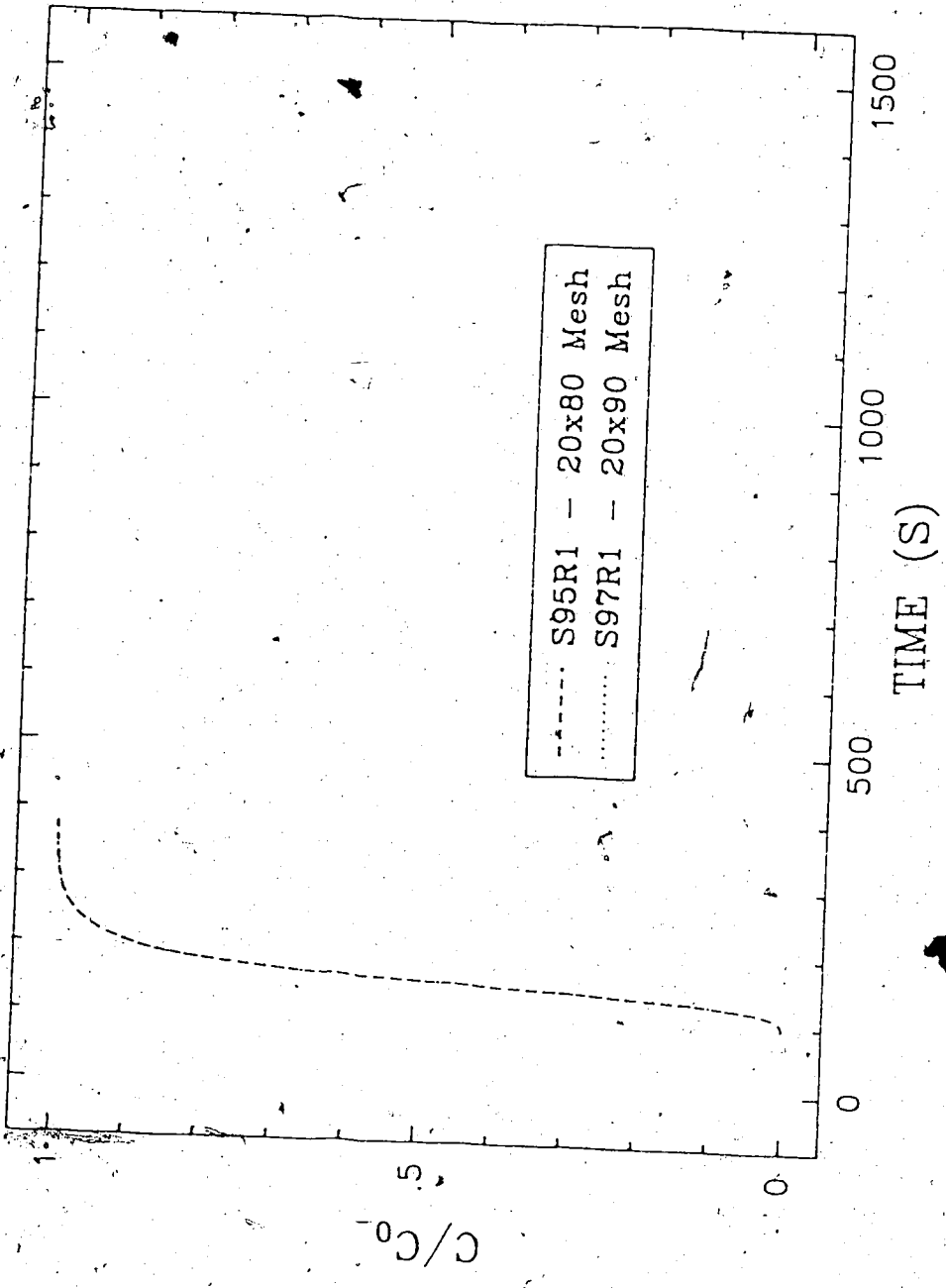


Figure 19: Mesh Effects.

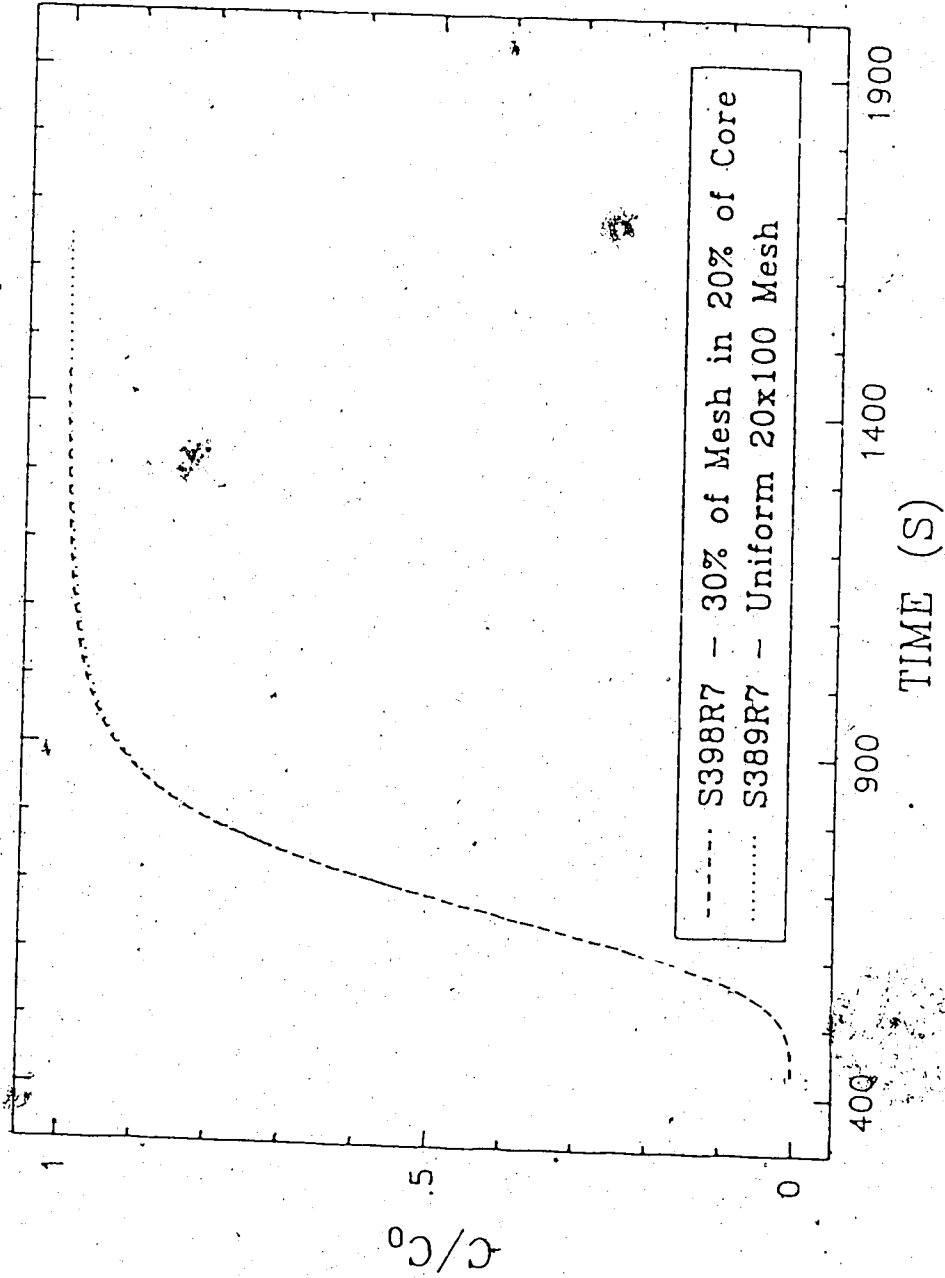


Figure 20: Mesh Uniformity Effects

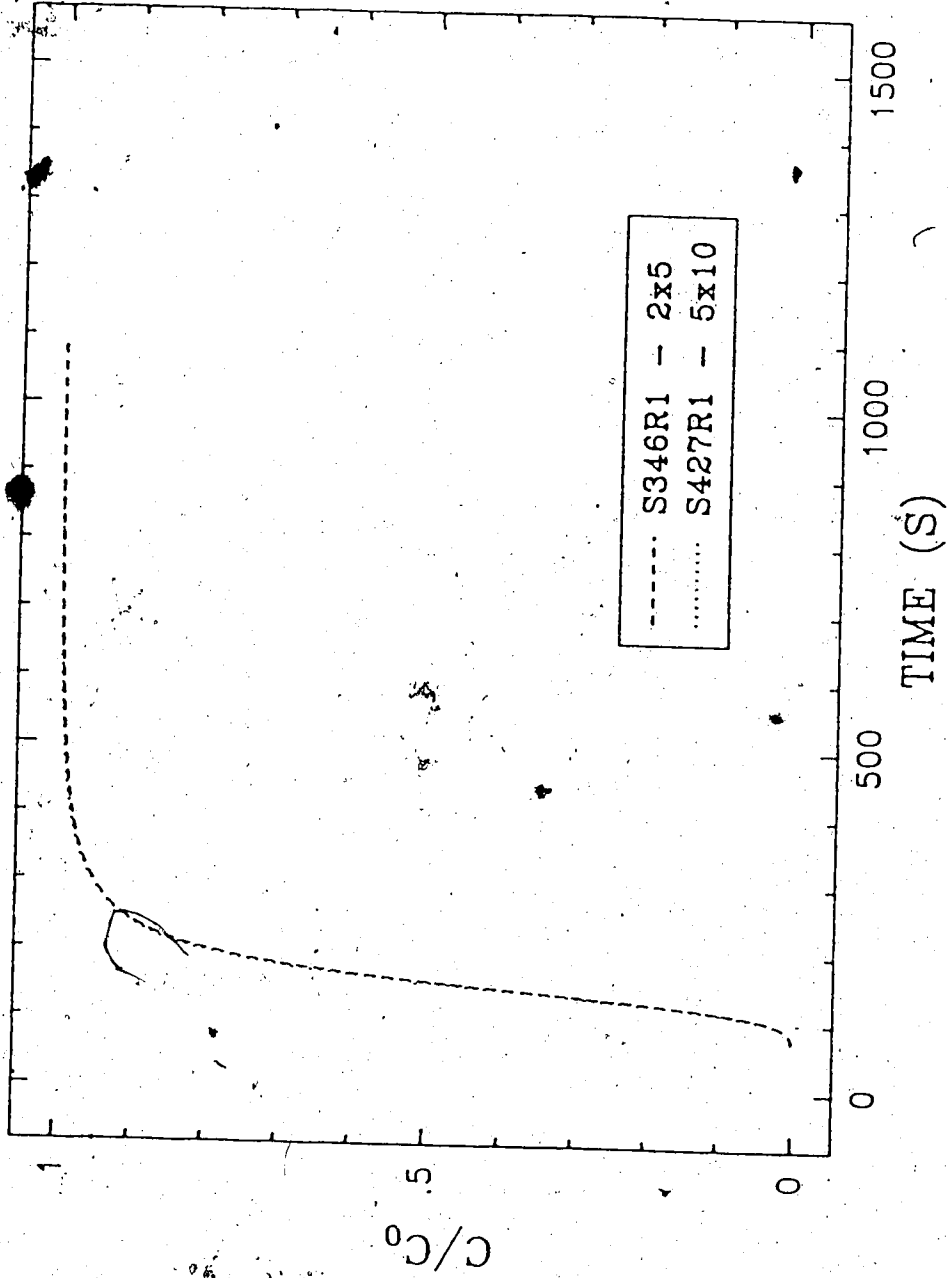


Figure 21: Injector Mesh Effects

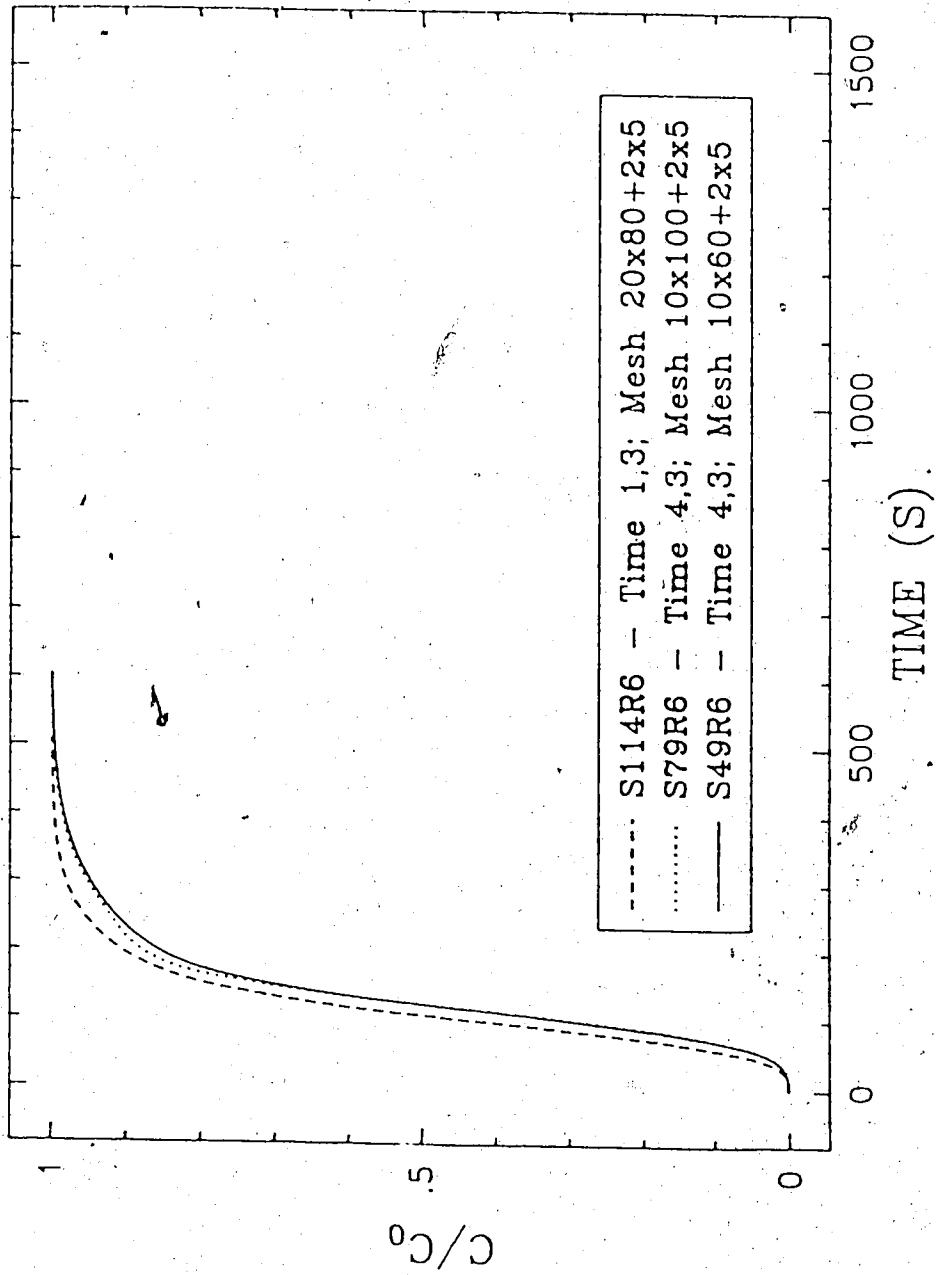


Figure 22: Numerical Dispersion Effects

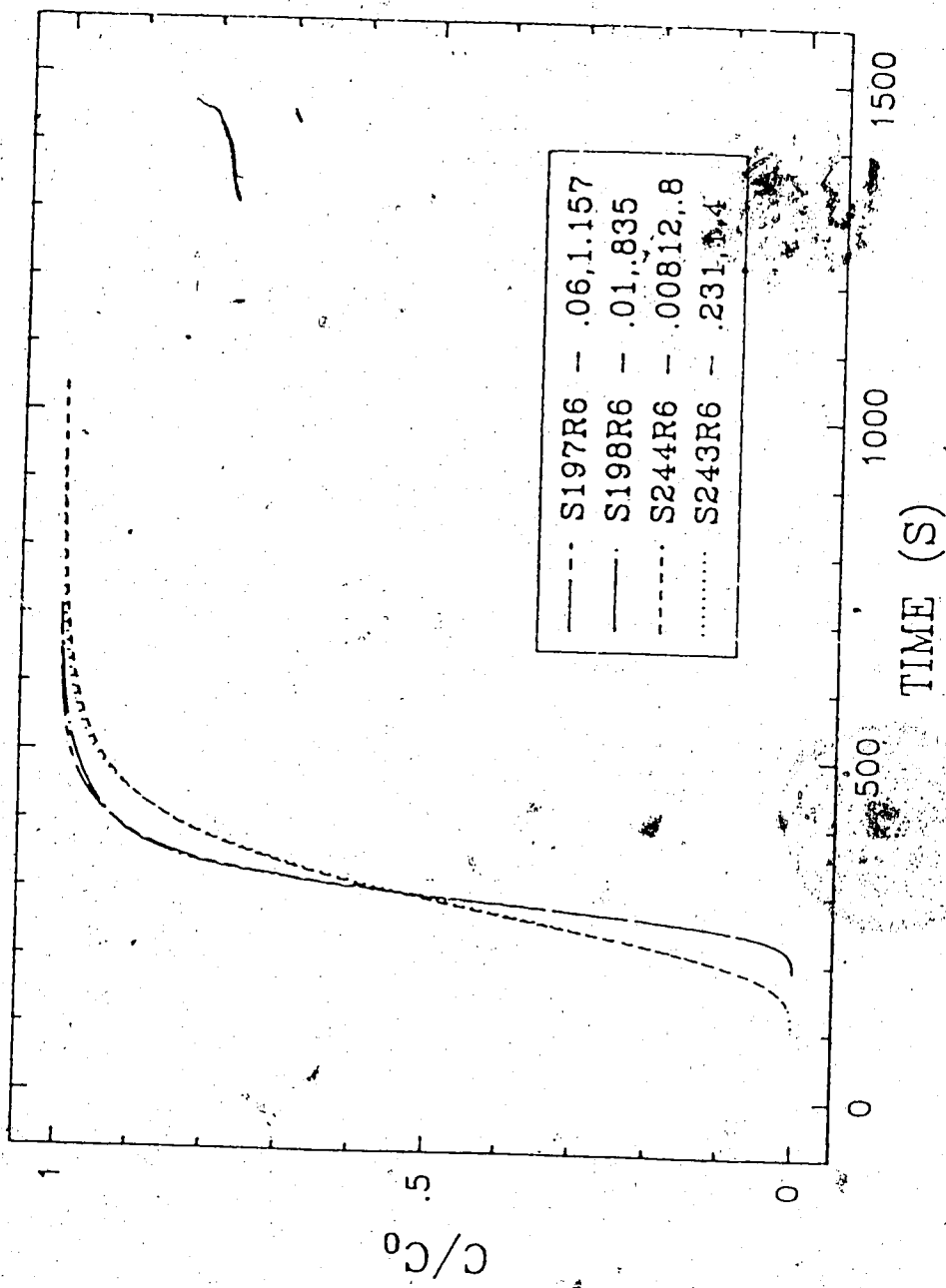


Figure 23: Transverse Dispersion Effects

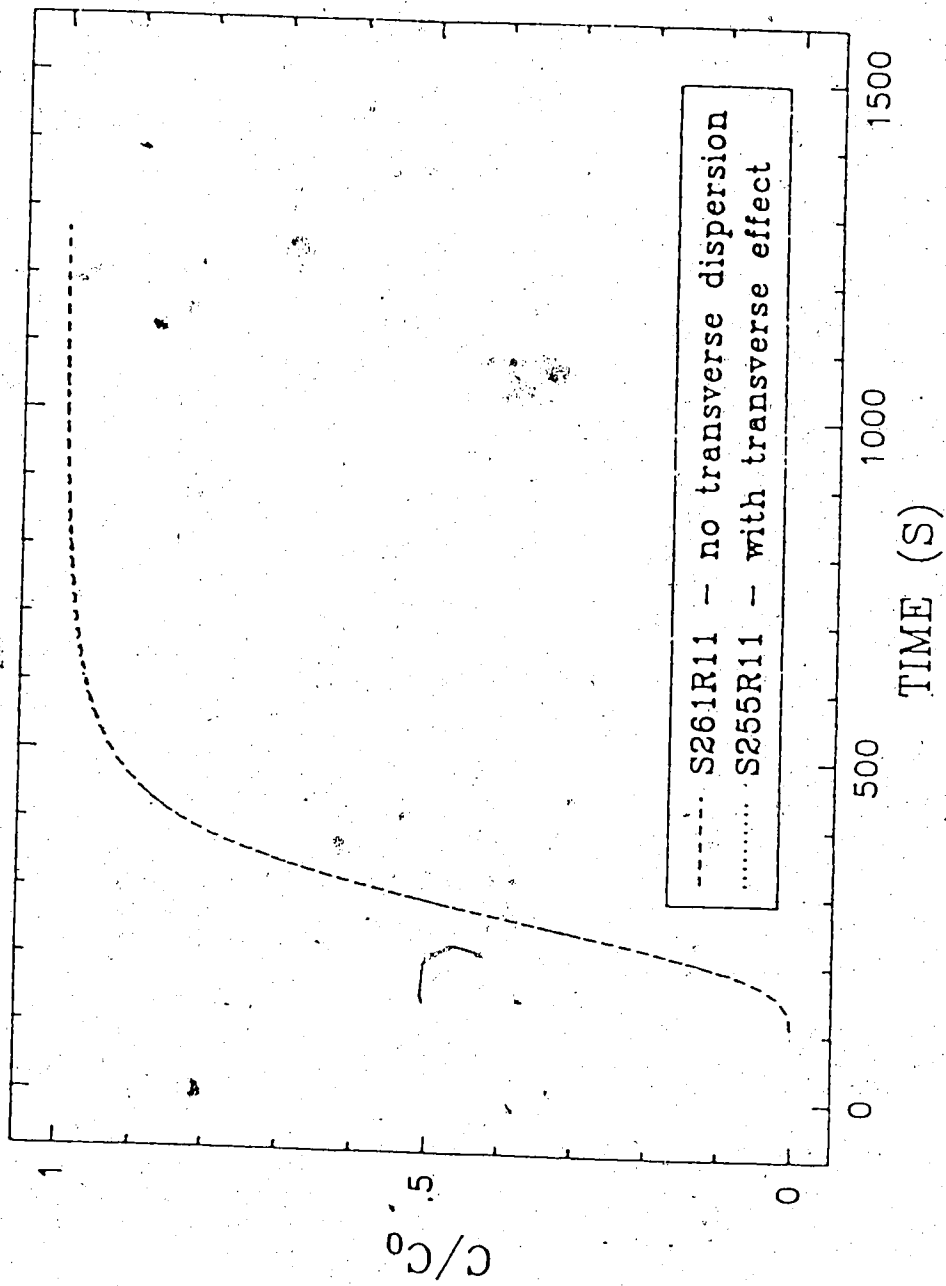


Figure 24: Limit of Transverse Effects

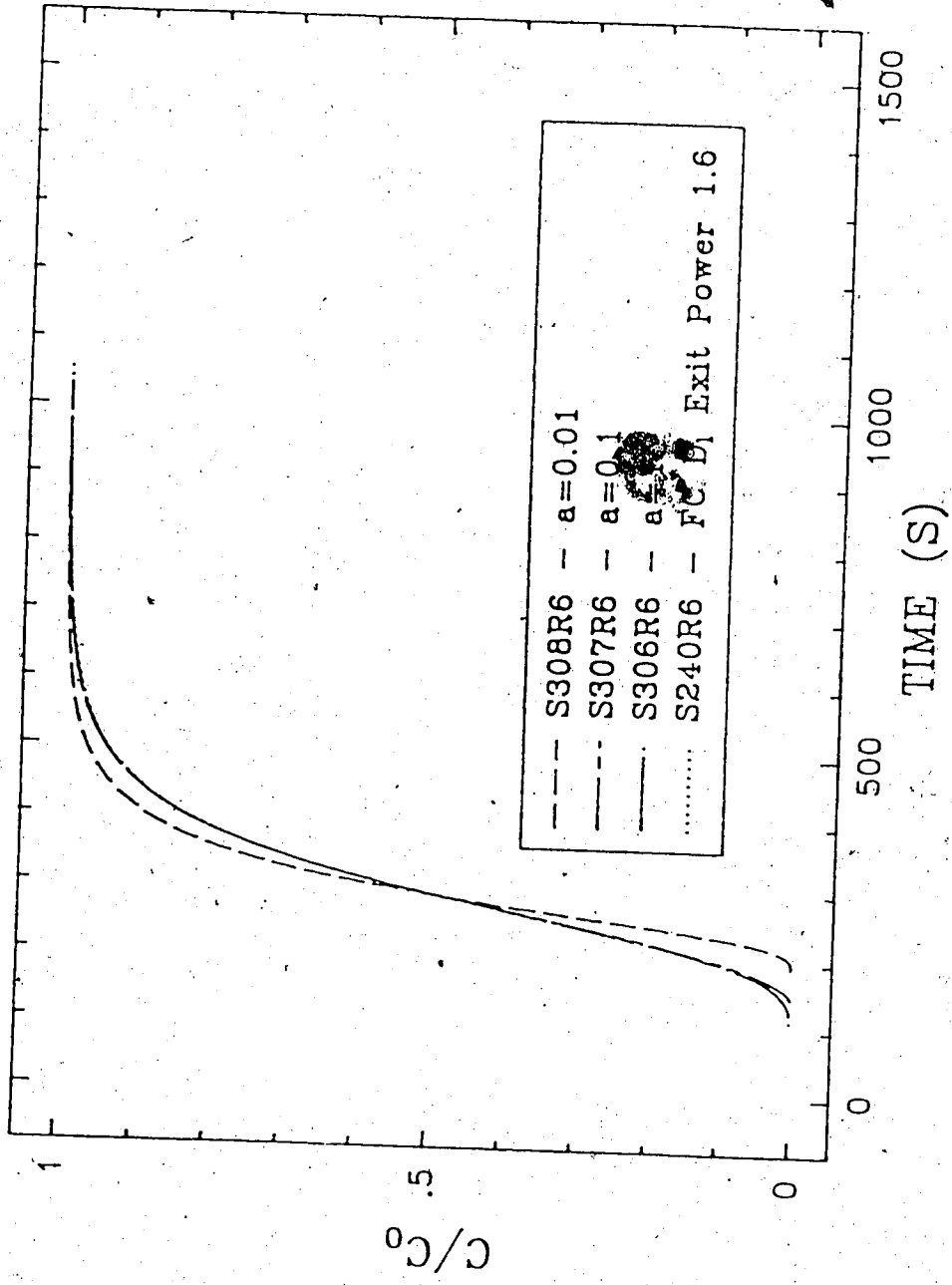


Figure 25: Transient Variations

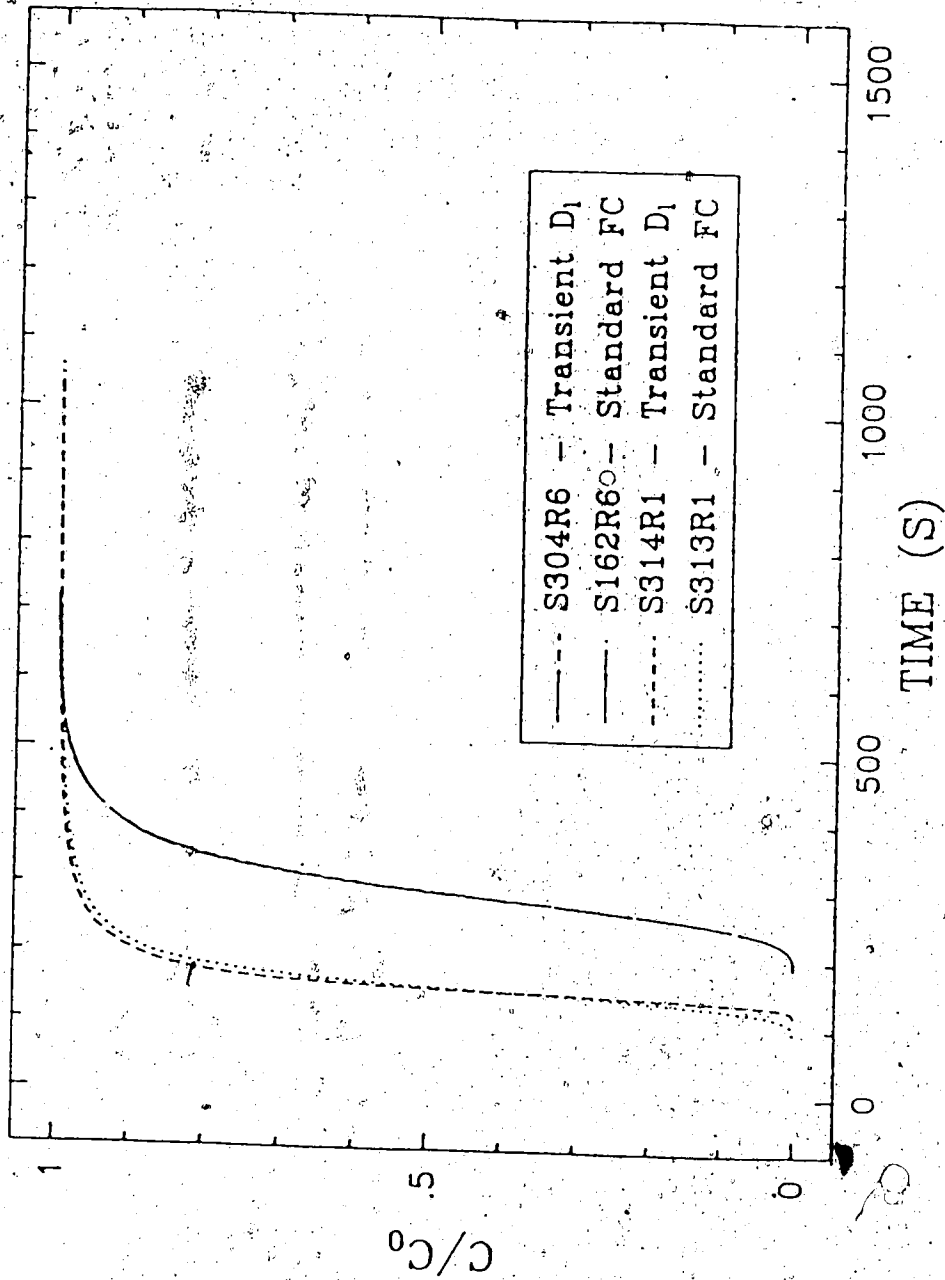


Figure 26: Transient Effects

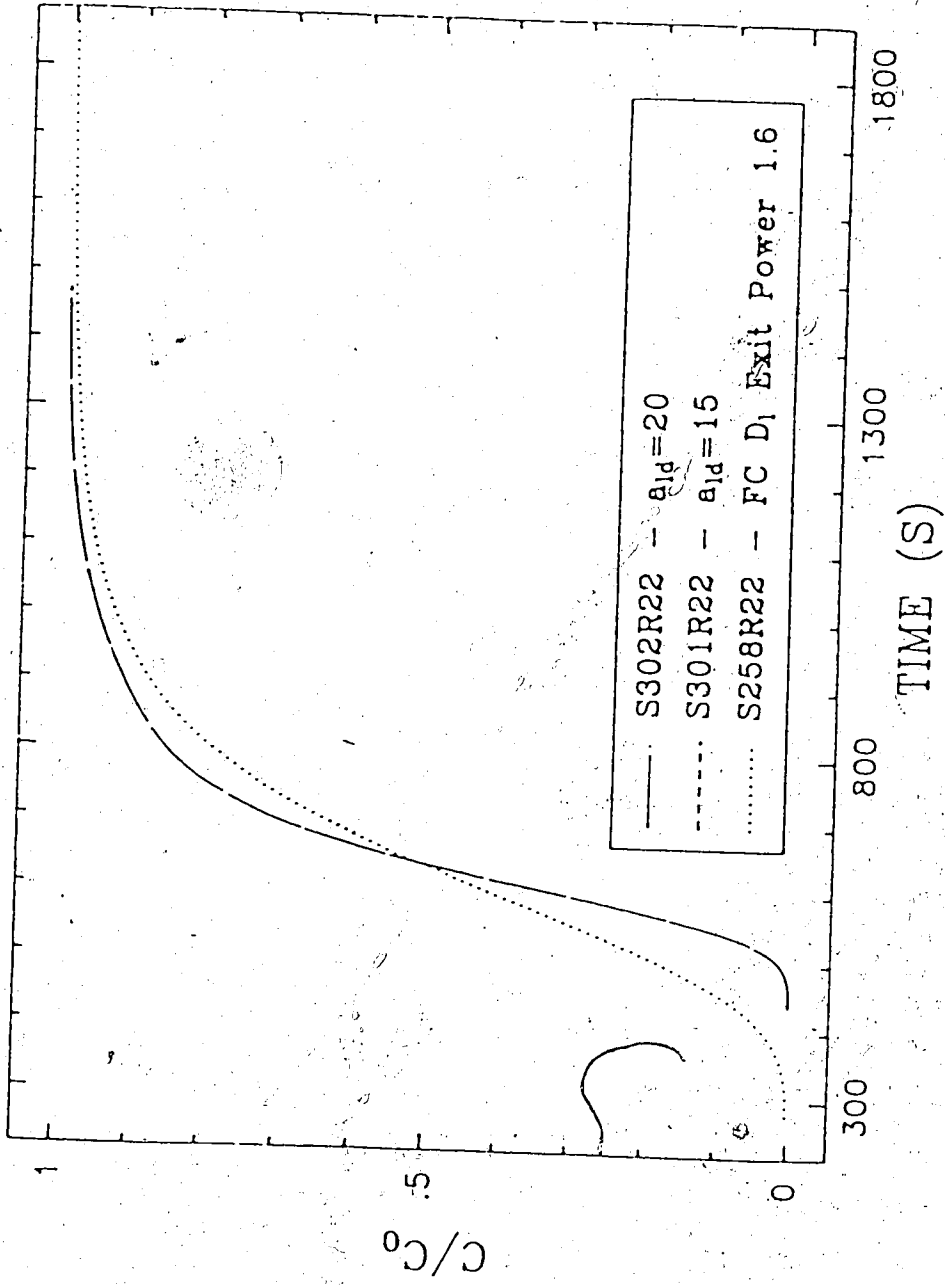


Figure 27: Length Dependence Effects

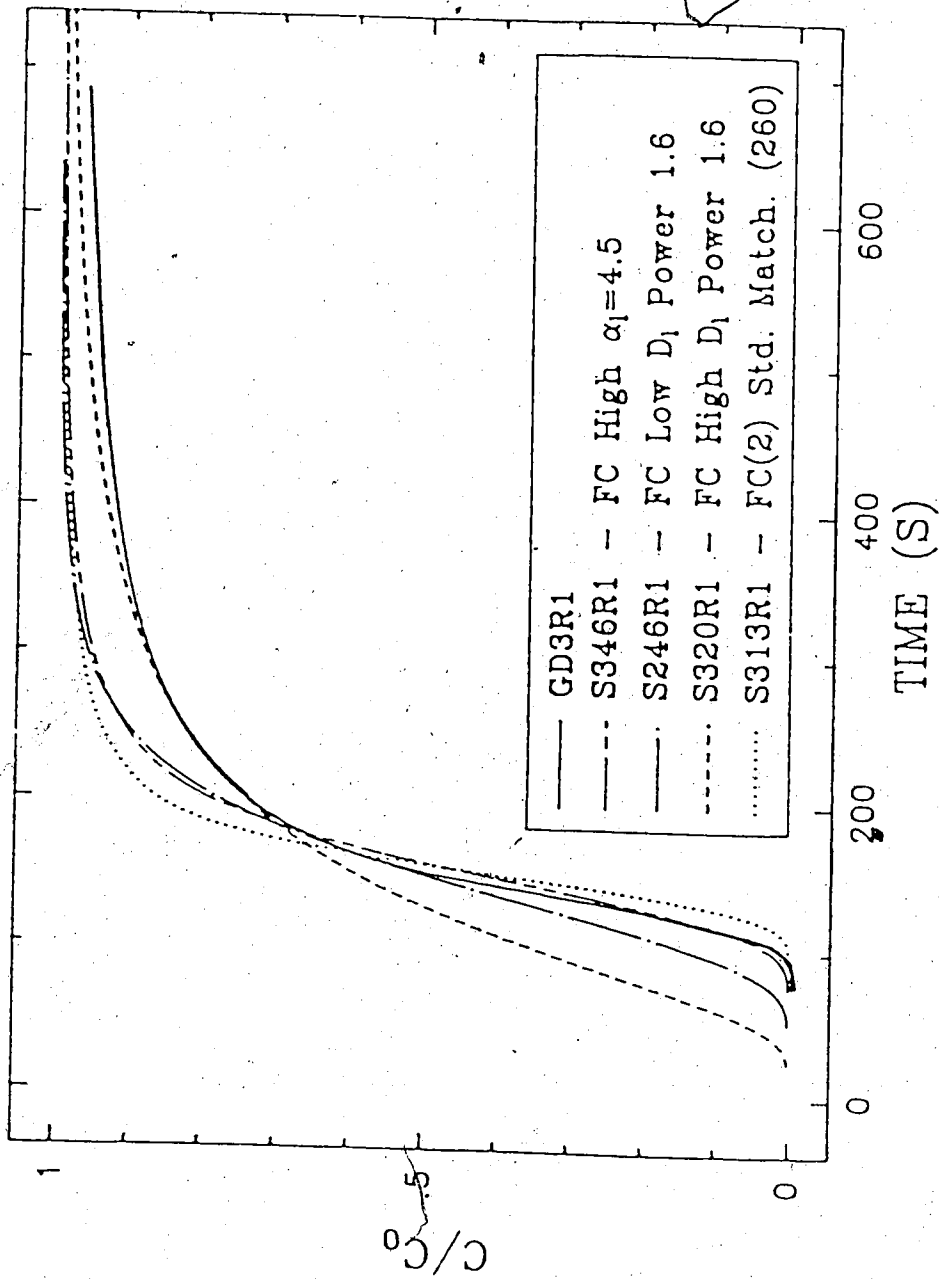


Figure 28: FC Variations

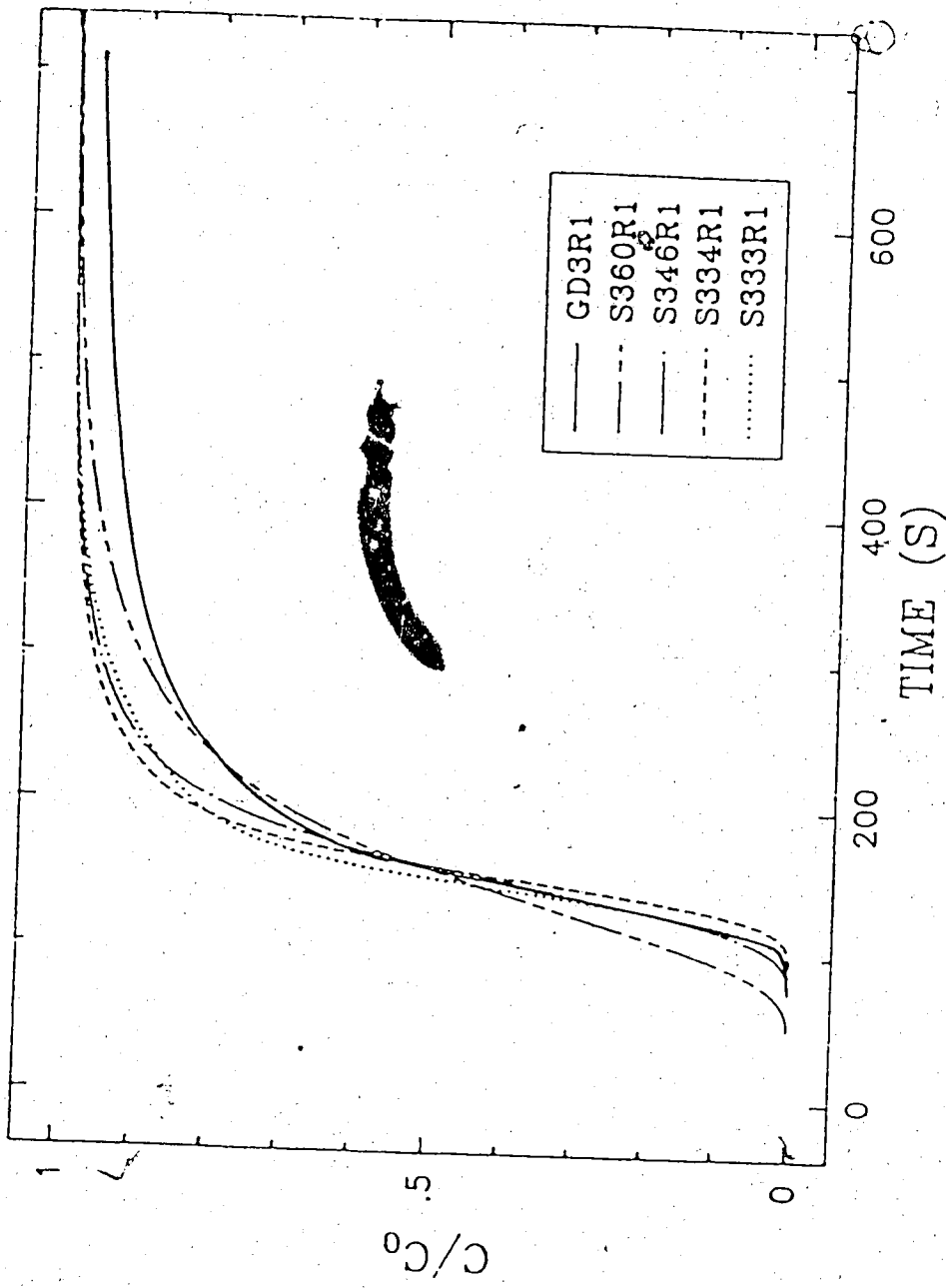


Figure 29: Cutoff Effects on FC(2)

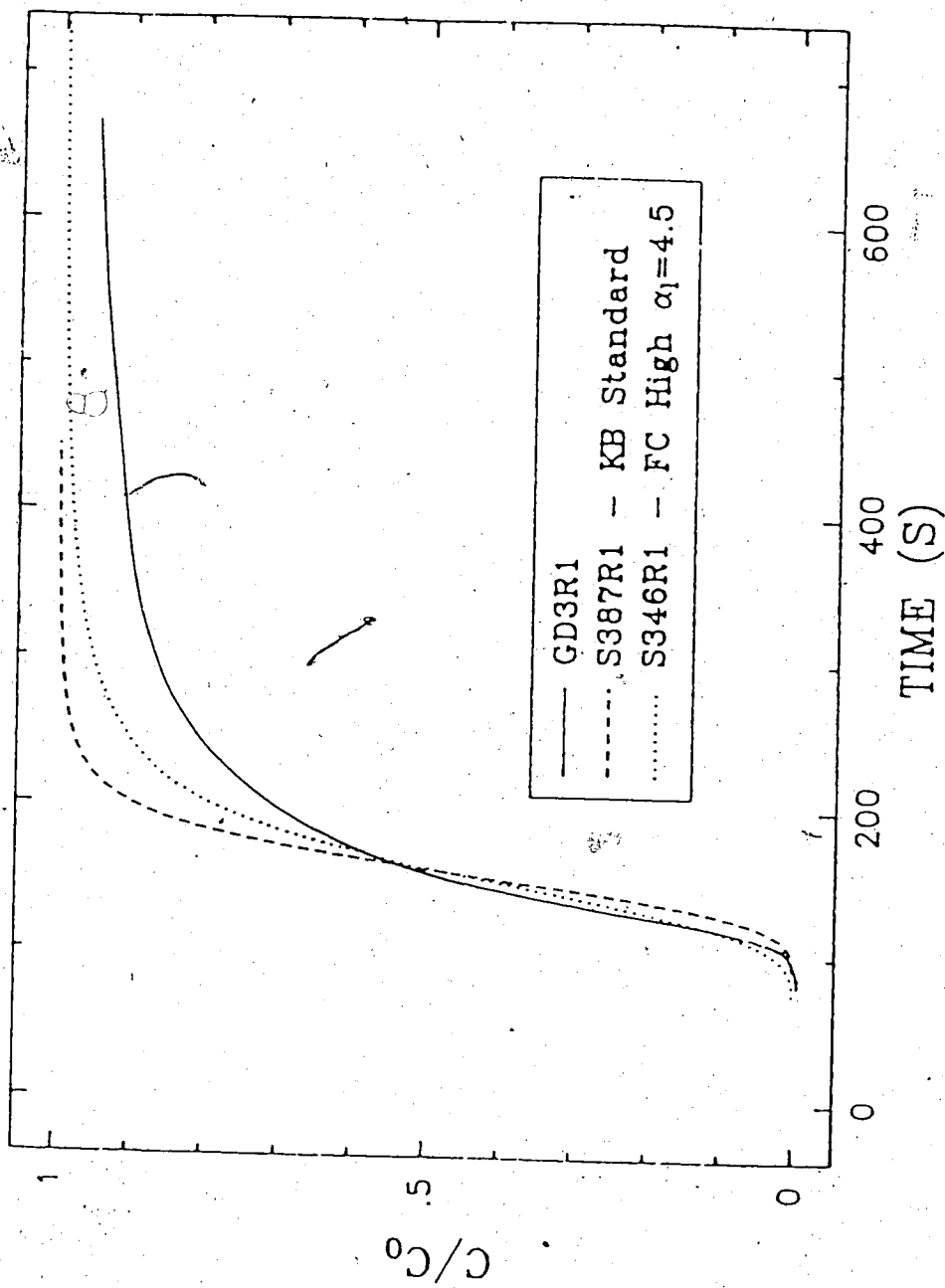


Figure 30: Model Type Comparison Run #1

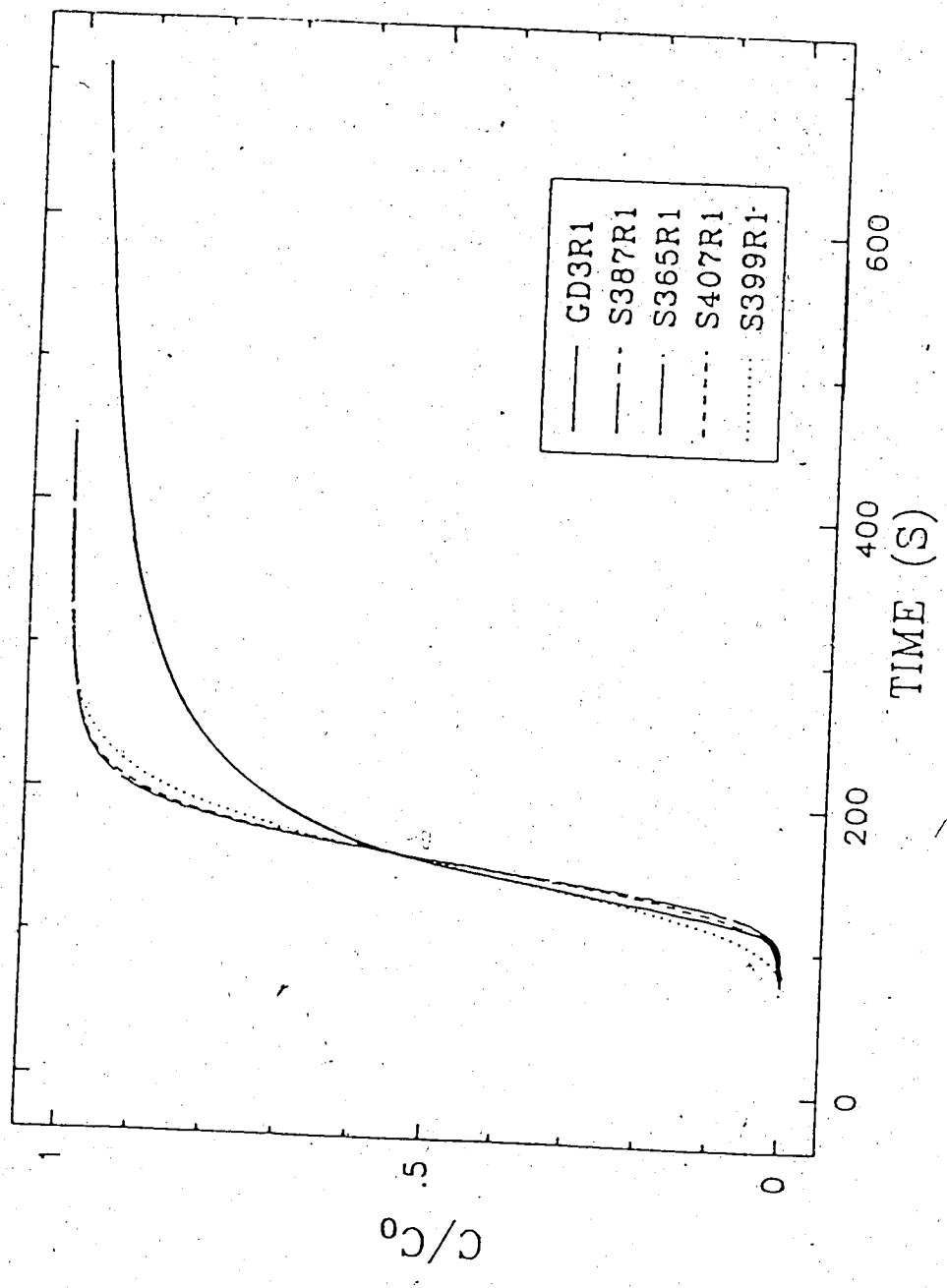


Figure 31: KB Variations

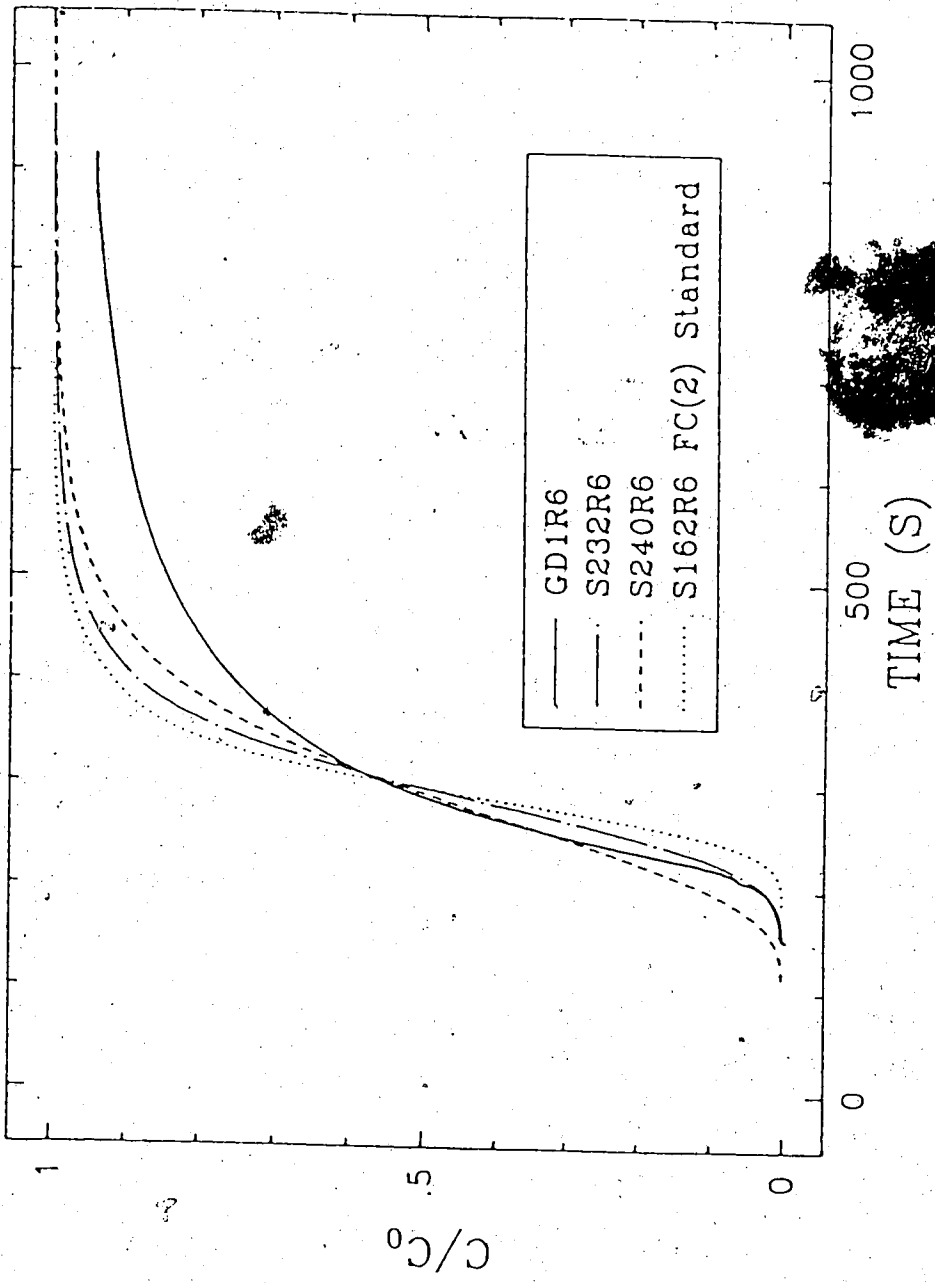


Figure 32: FC Variations

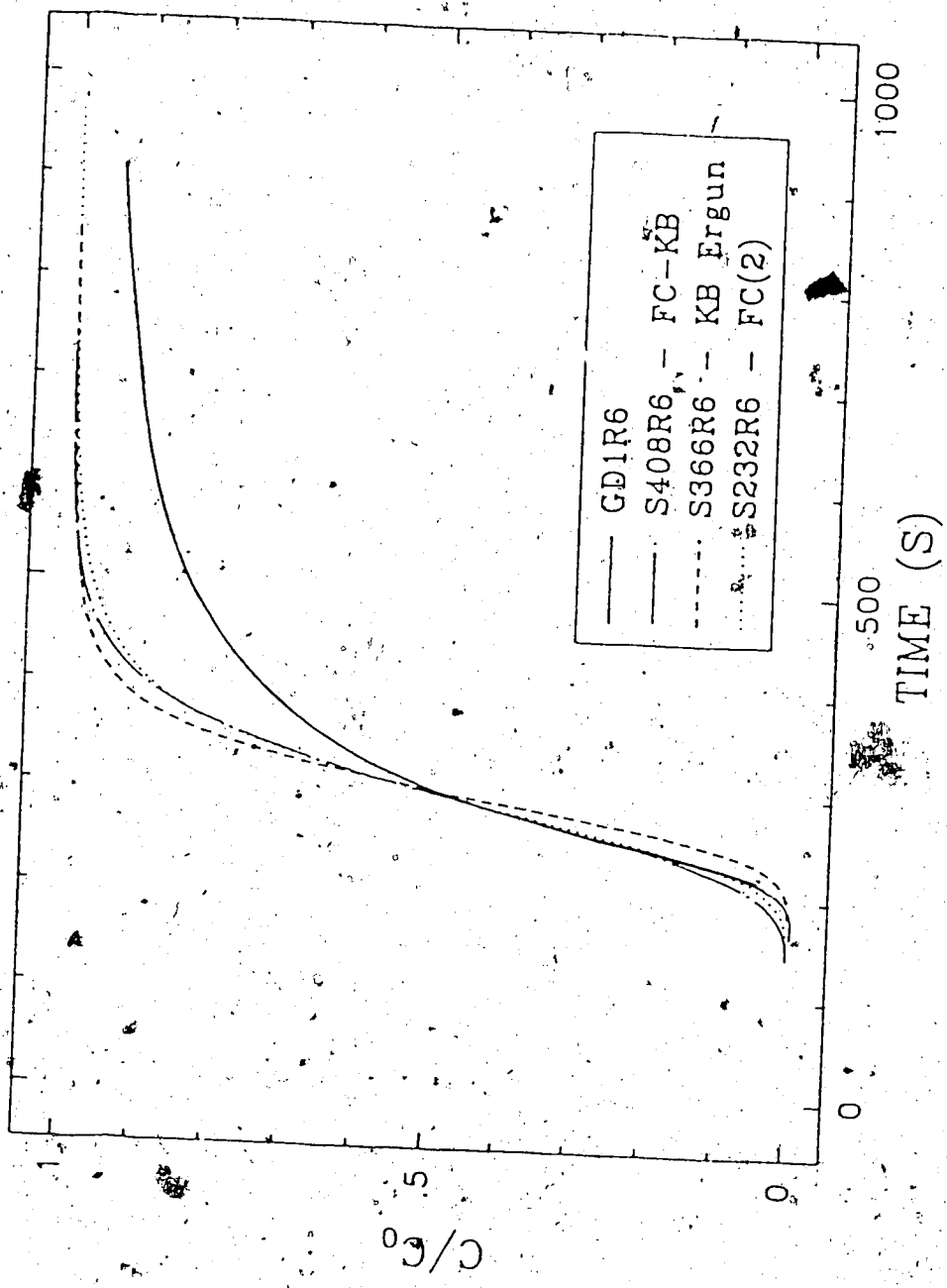


Figure 33: Model Type Effects

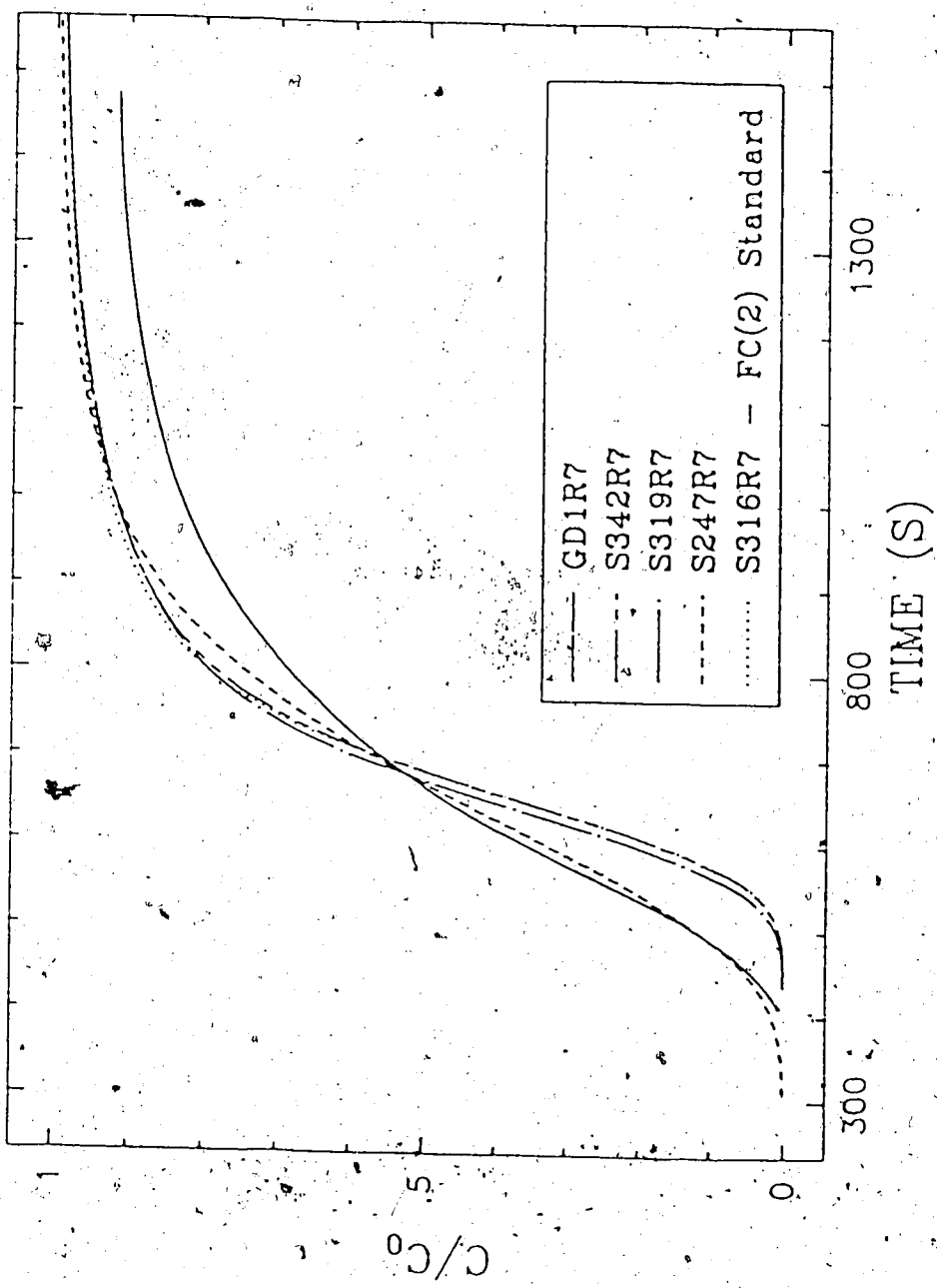


Figure 34: FC Variations

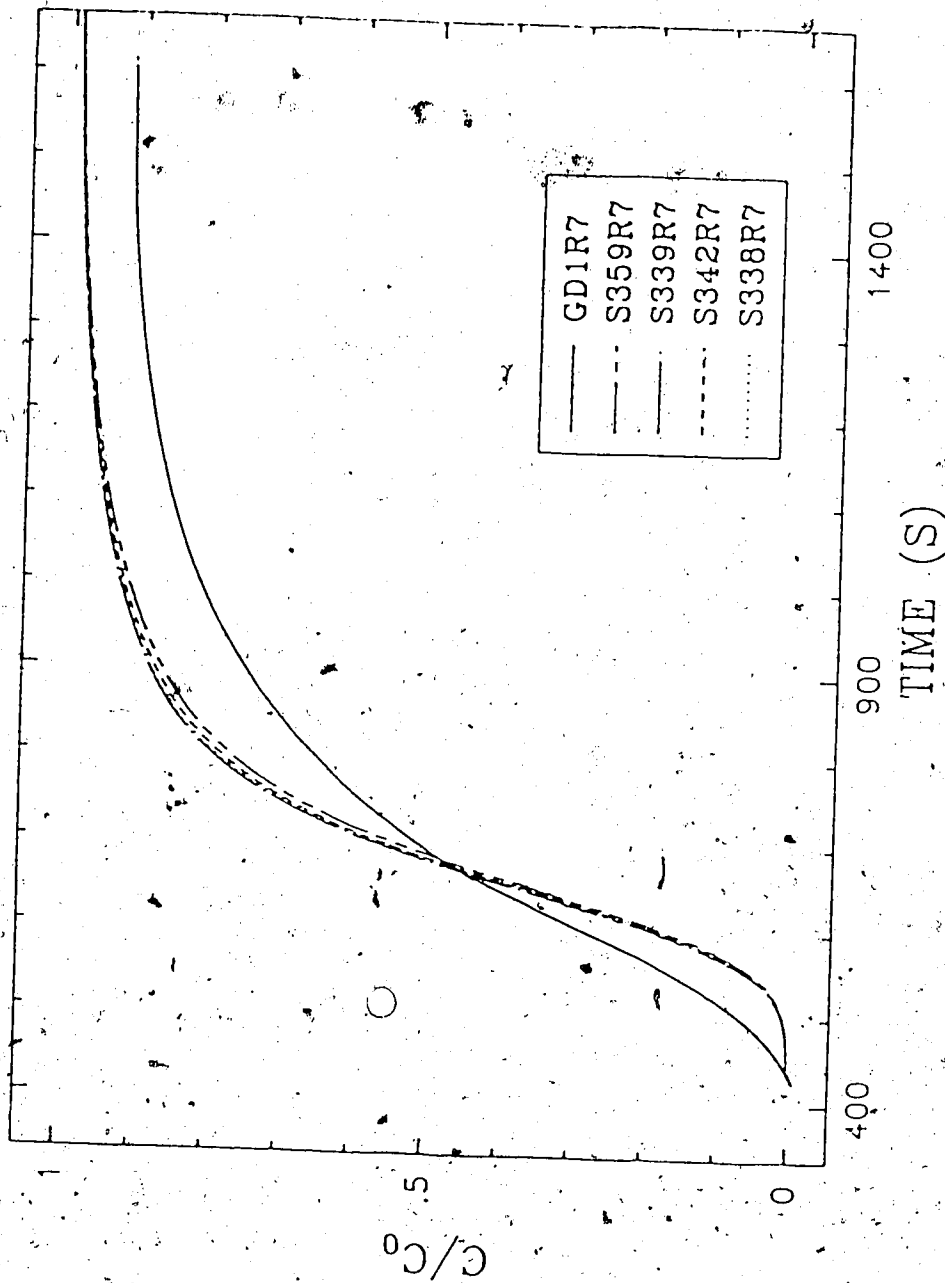


Figure 35: Cutoff Effects on FC(2)

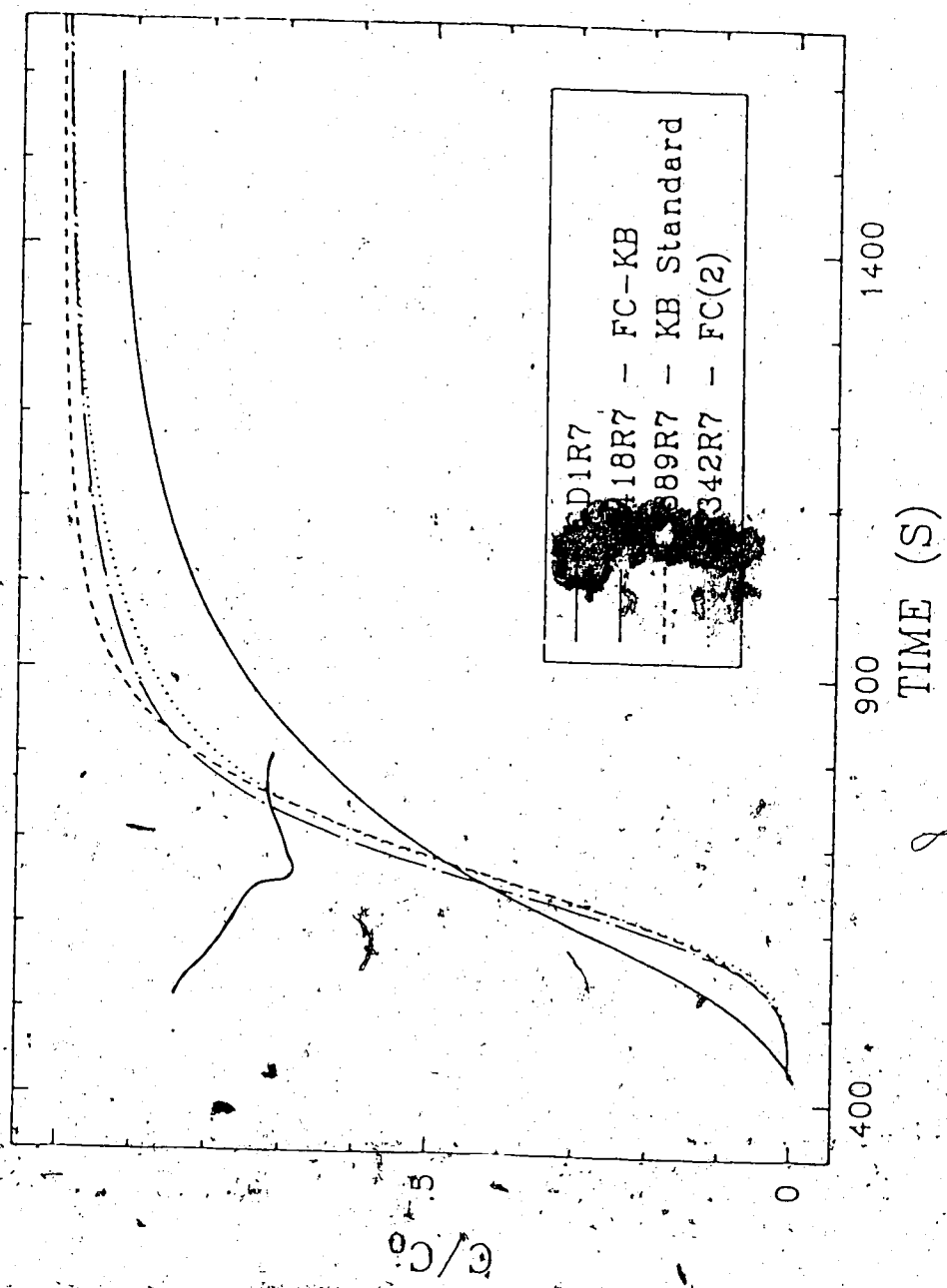


Figure 36: Model Type Effects

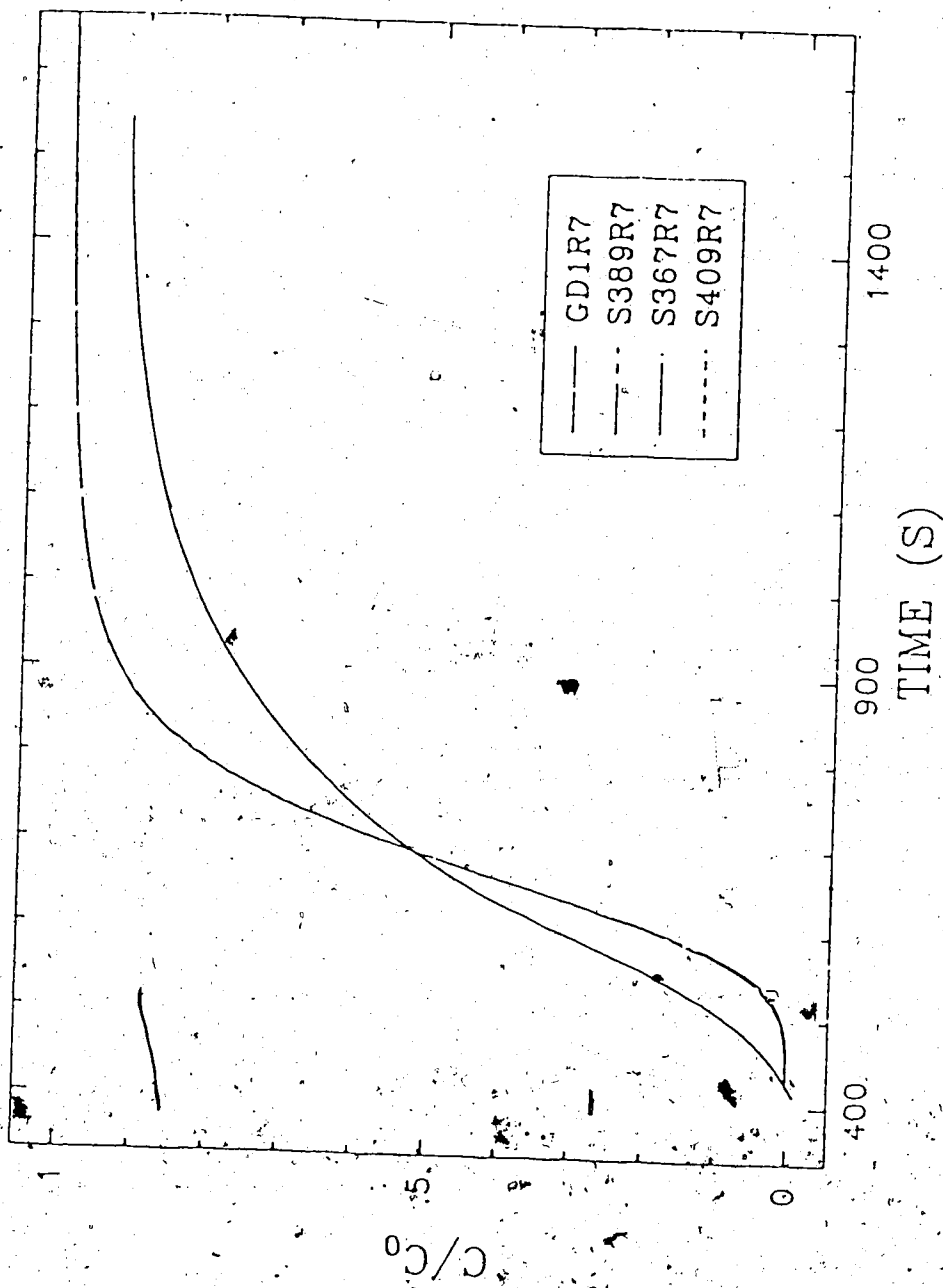


Figure 37: KB Variations

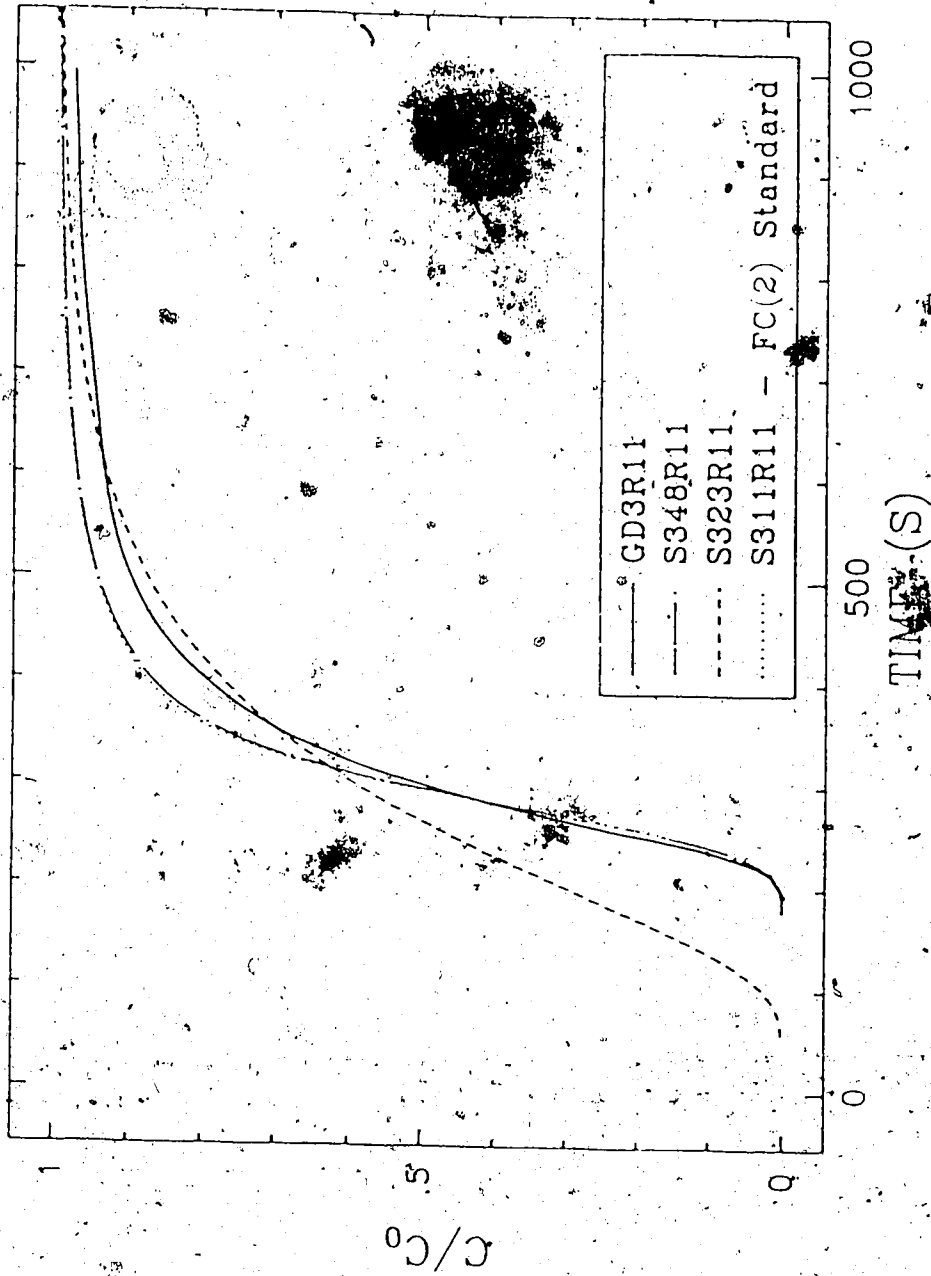


Figure 38: FC Variations

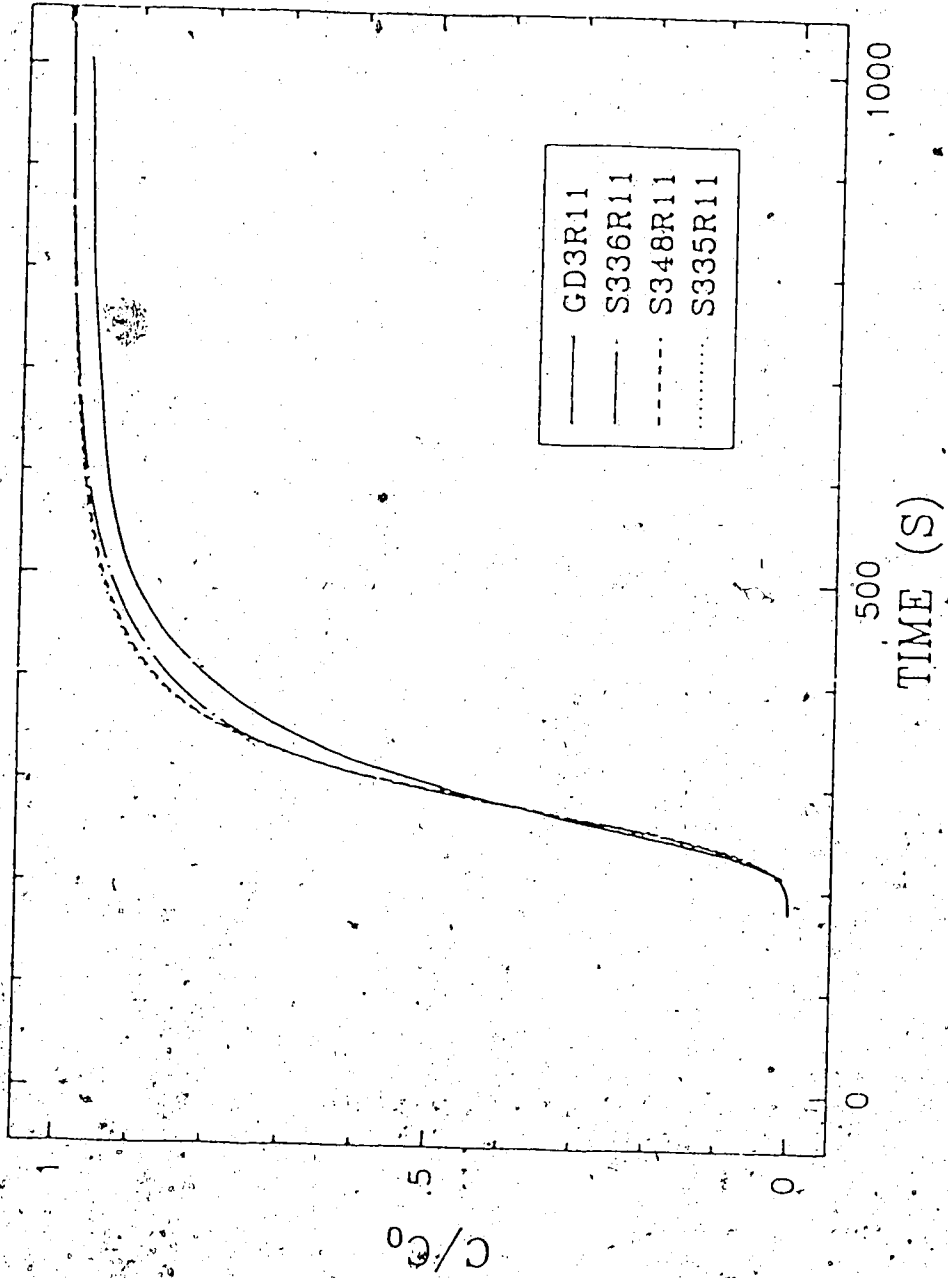


Figure 39: Cutoff Effect on FC(2)

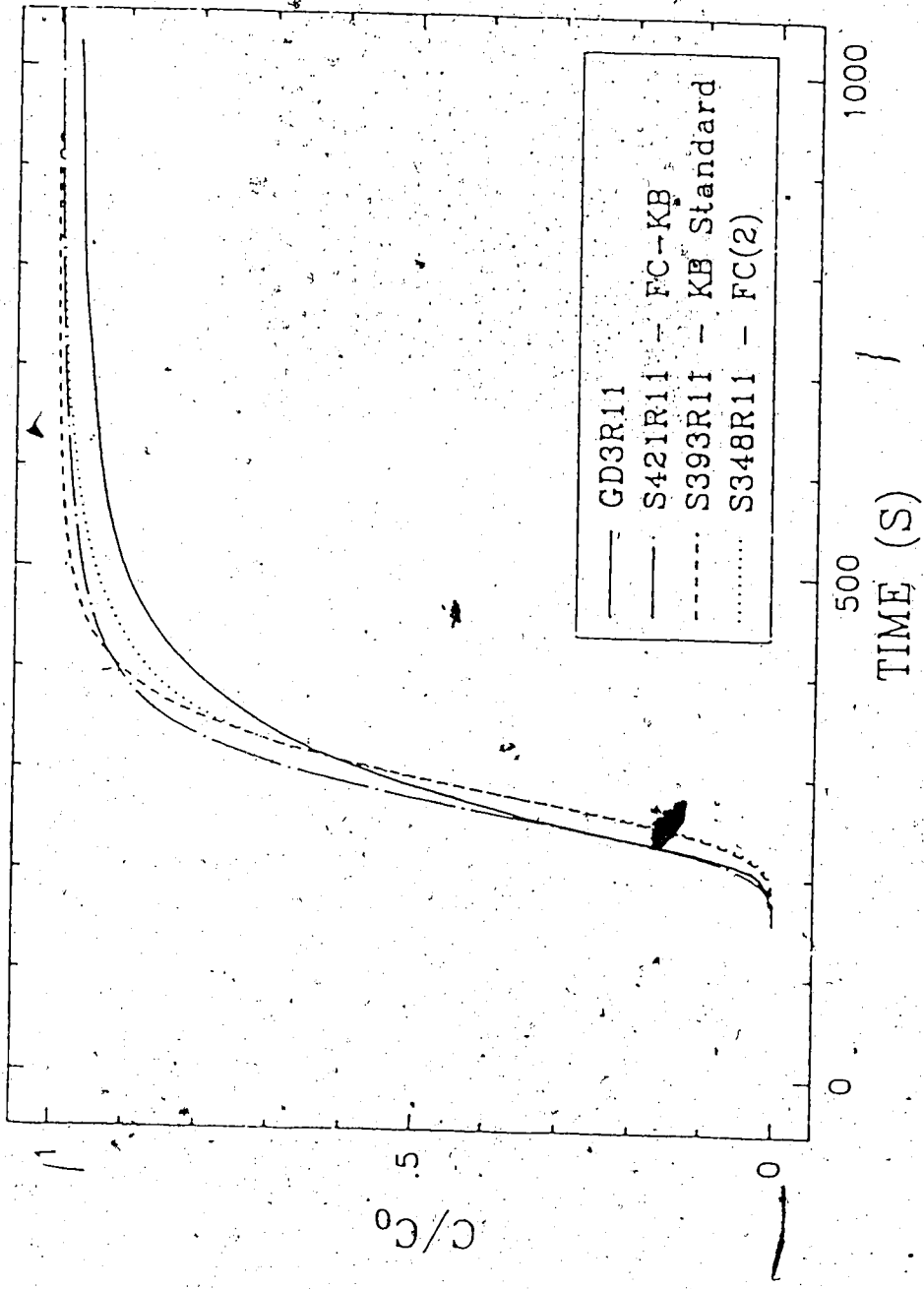


Figure 40: Model Type Effect

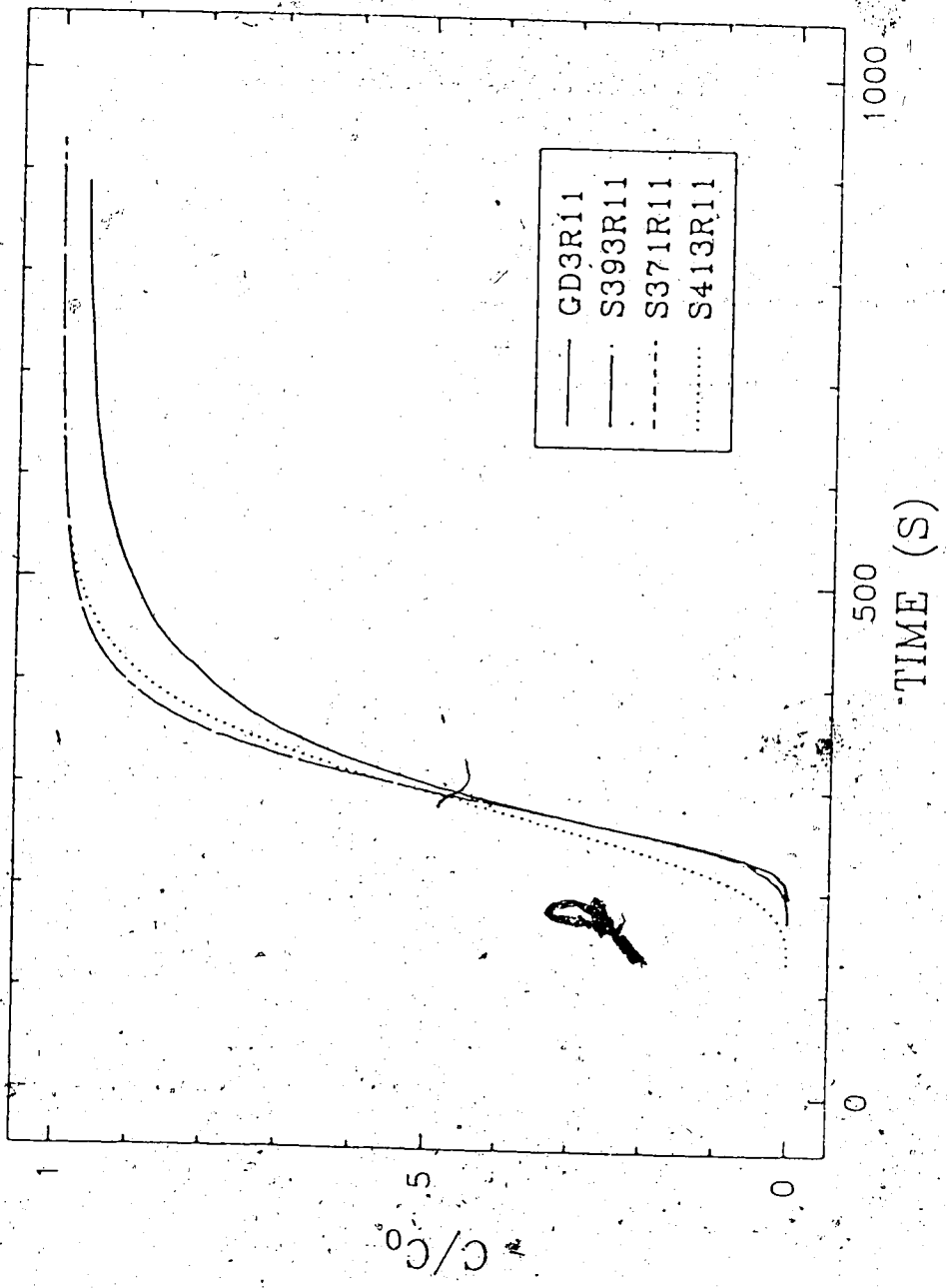


Figure 41: KB Variations

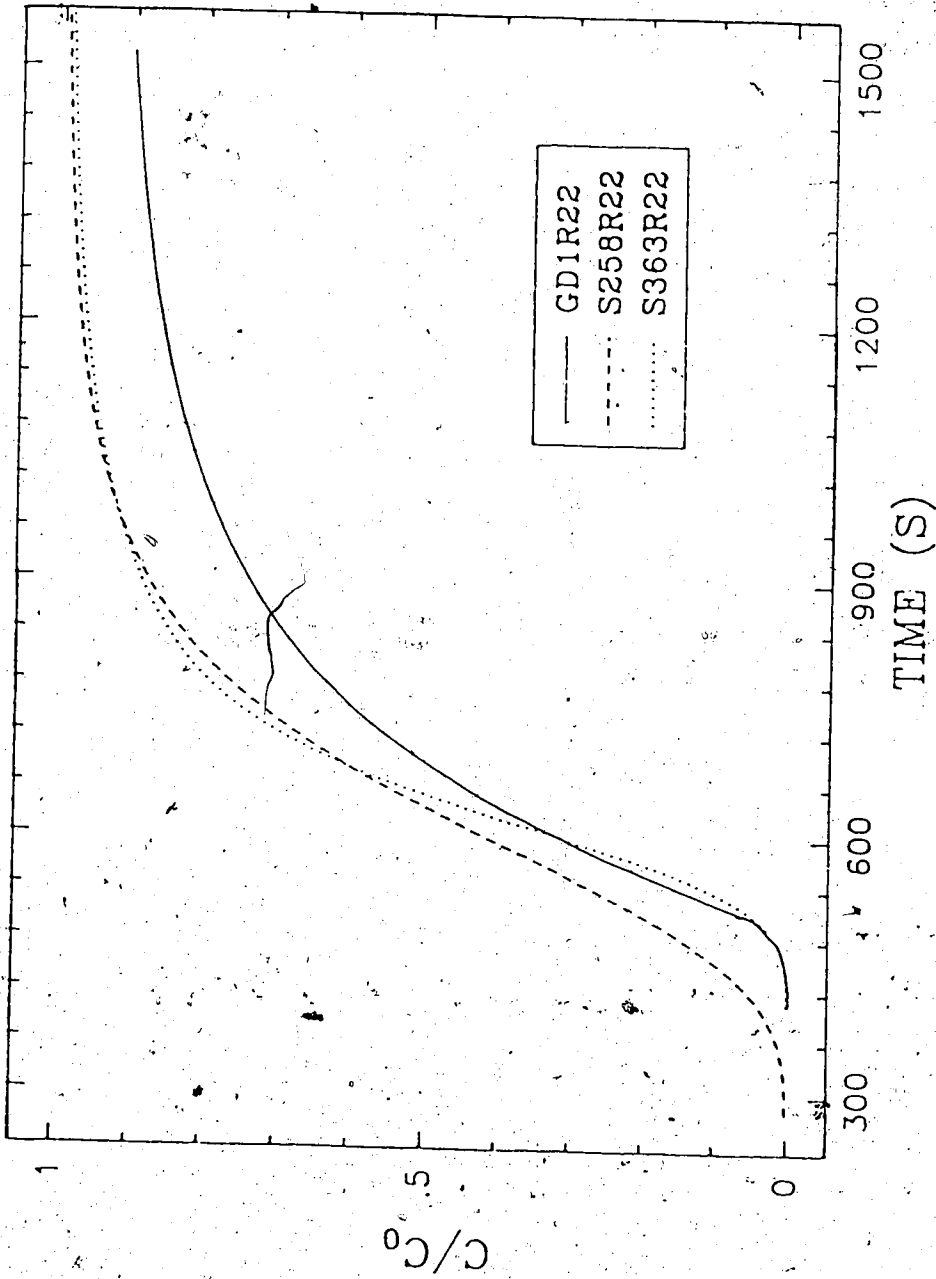


Figure 42: FC Variations Run #22

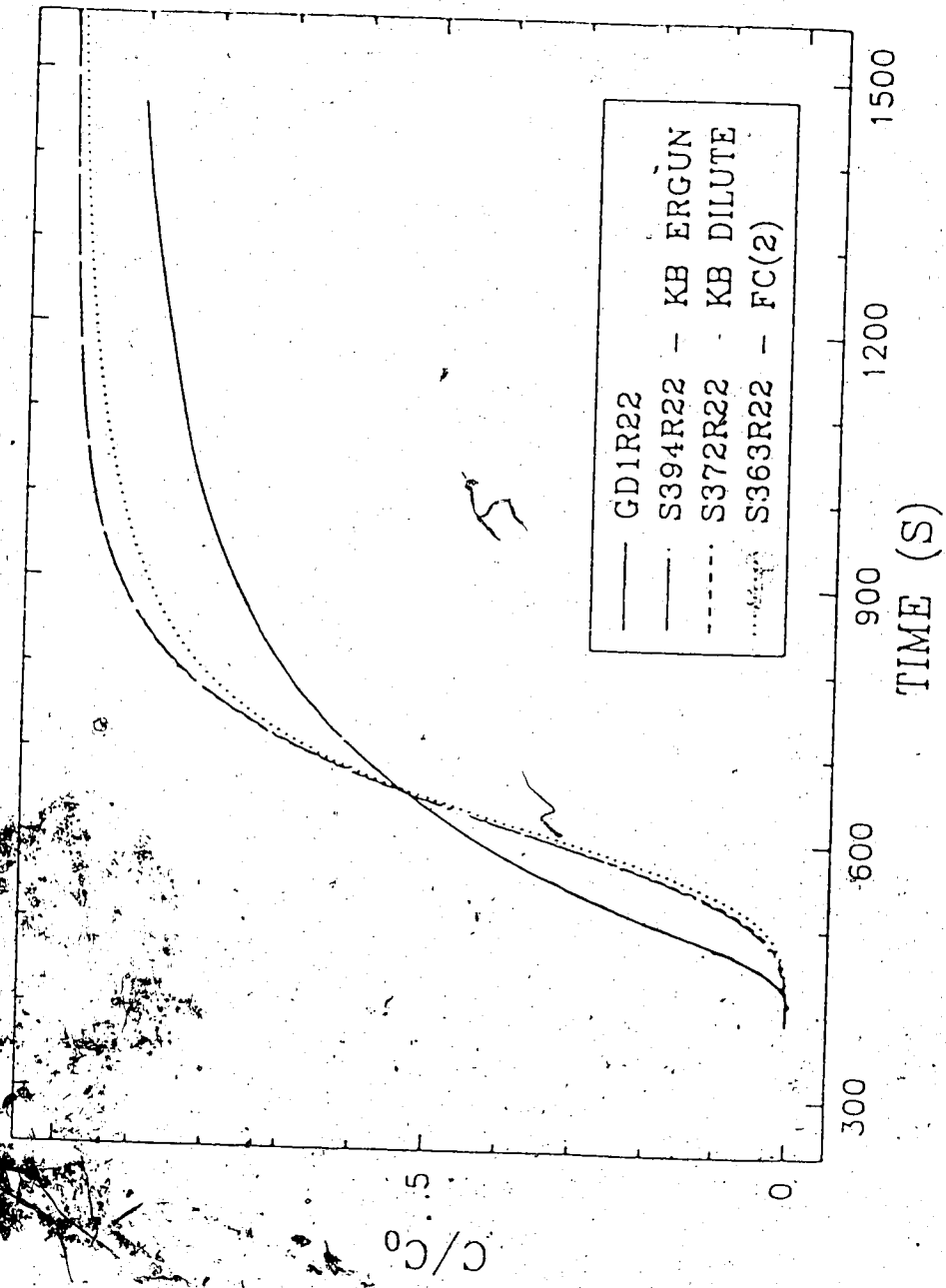


Figure 43: Model Type Effects

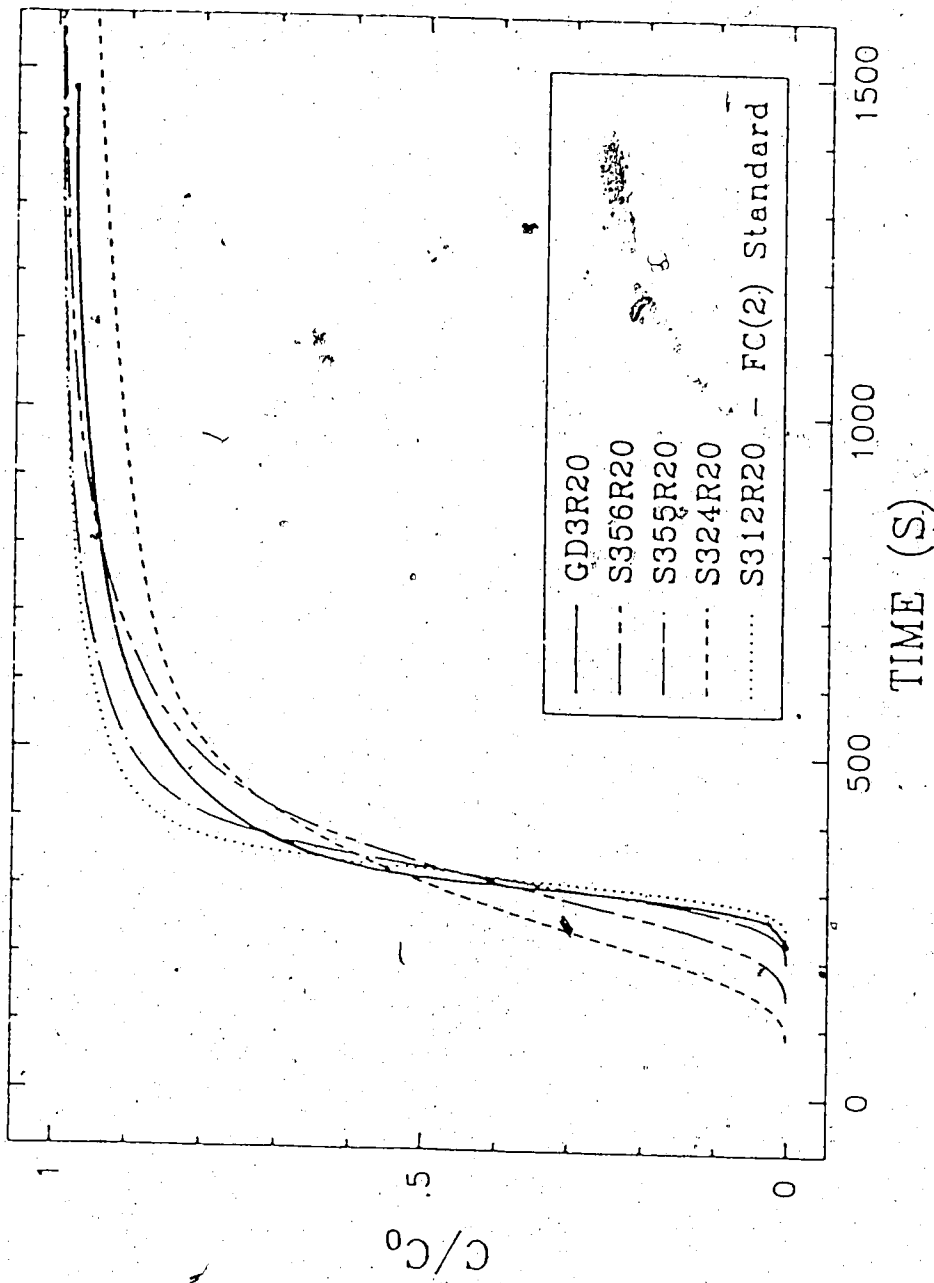


Figure 44: FC Variations

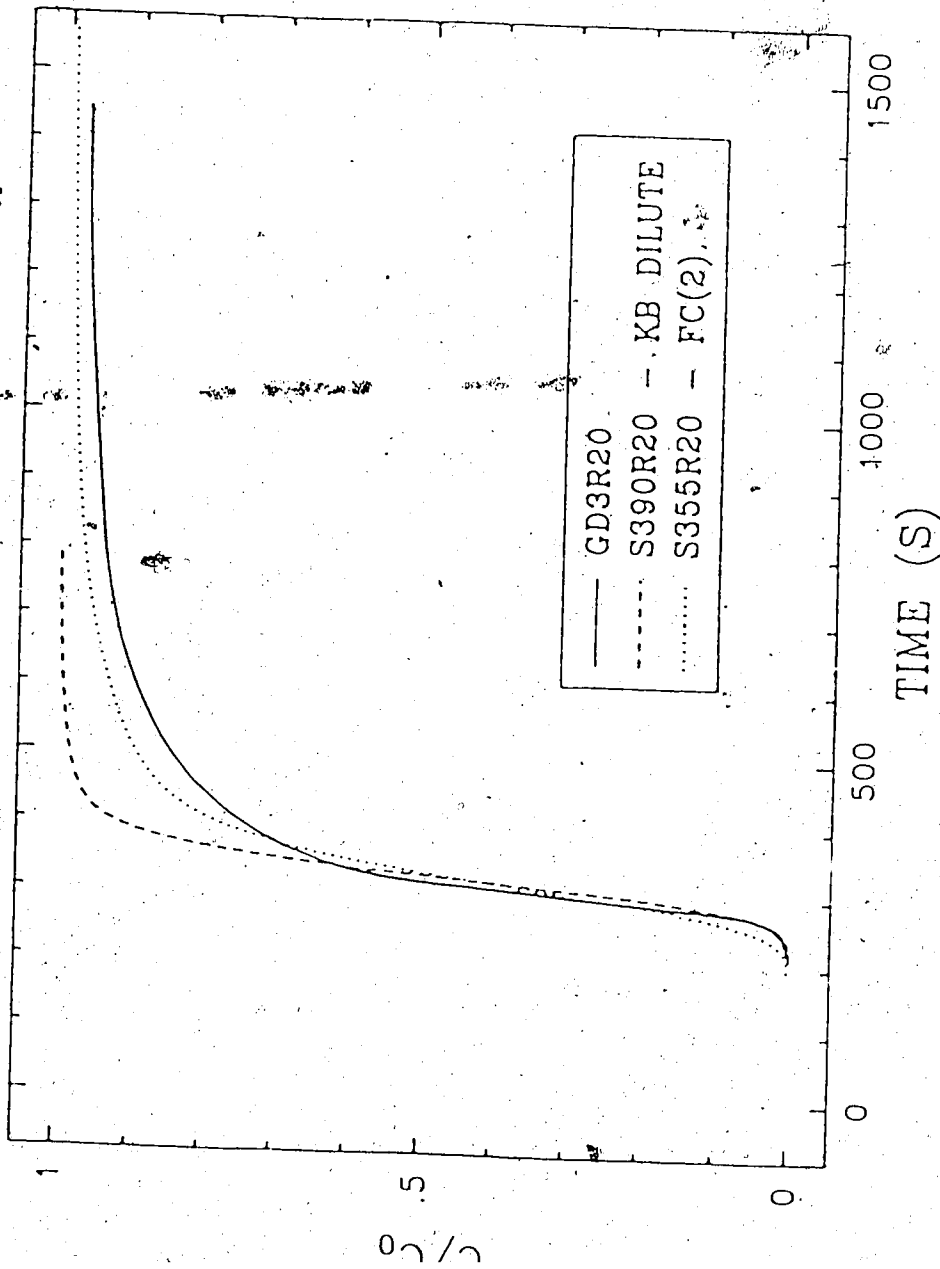


Figure 45: Model Type Variations

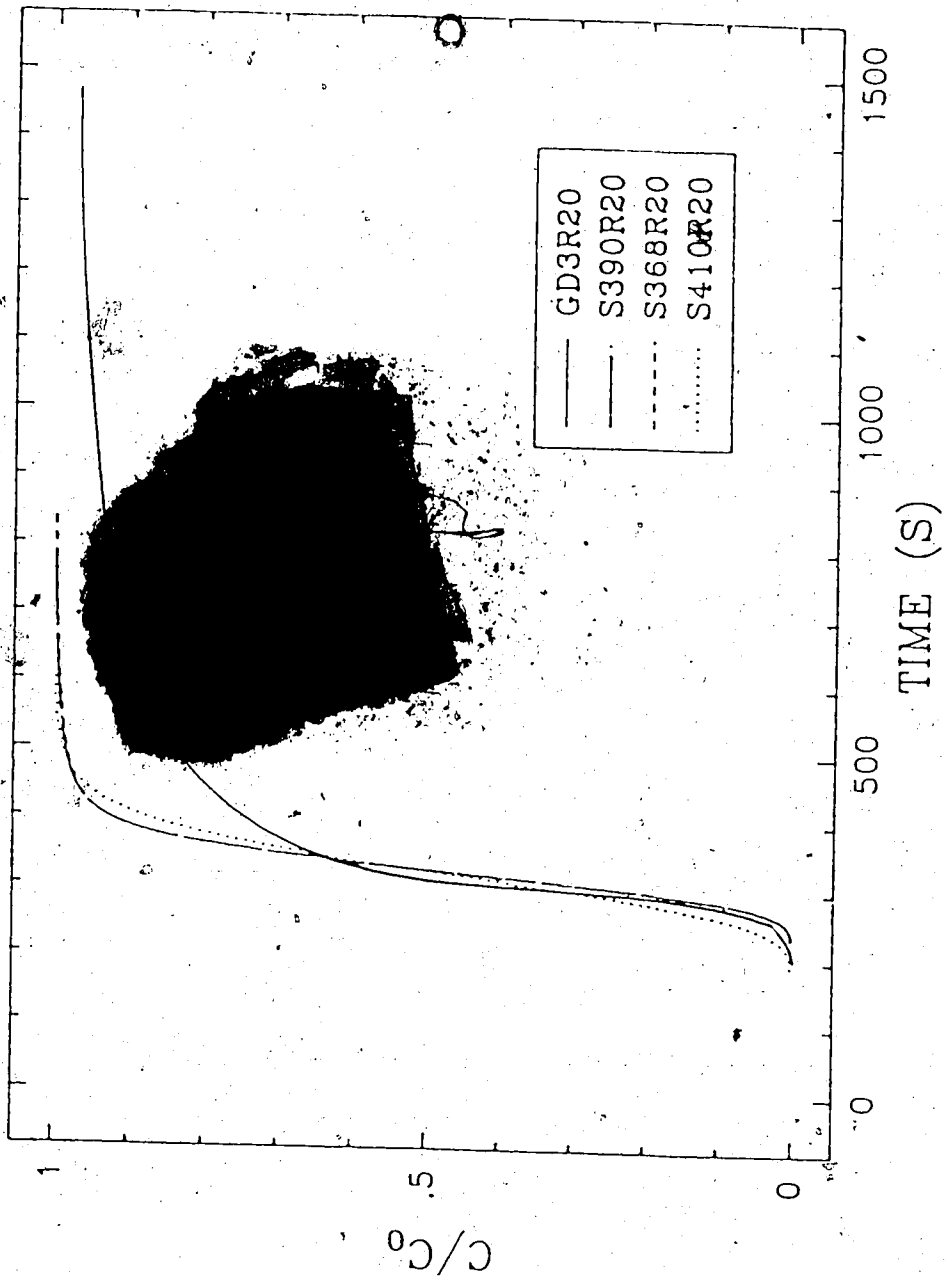


Figure 46: KB Variations

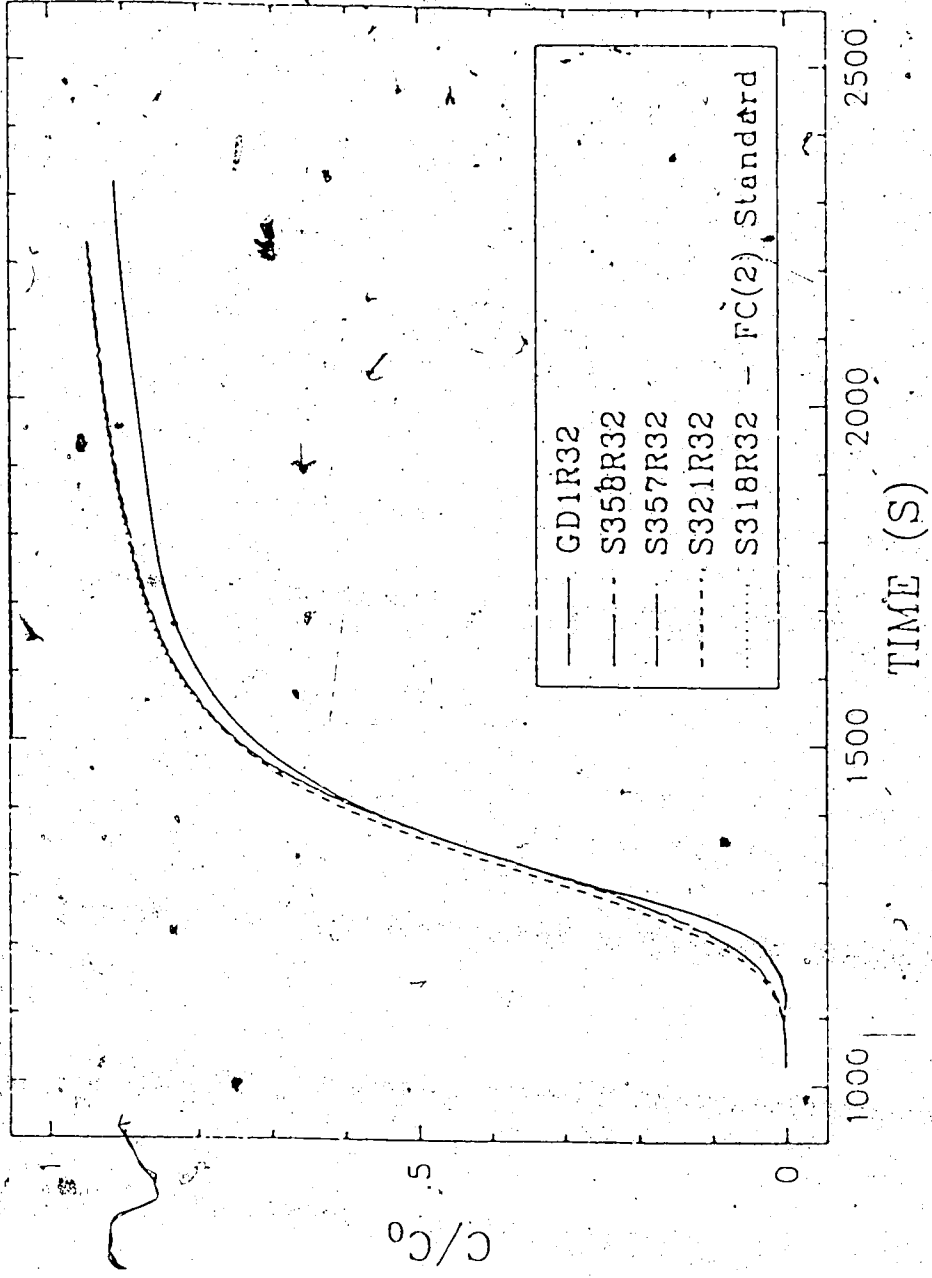


Figure 47: FC Variations

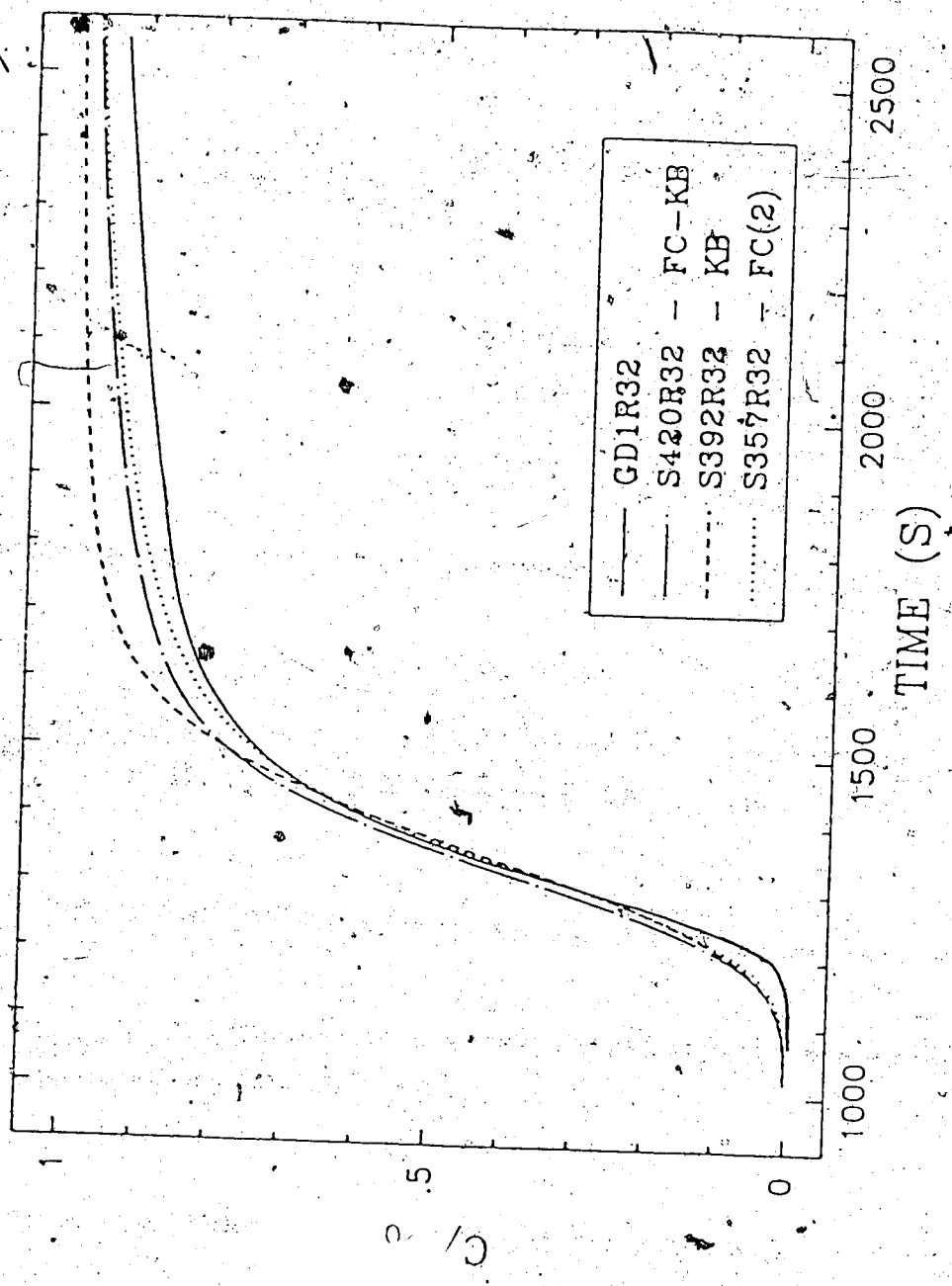


Figure 48: Model Type Variations

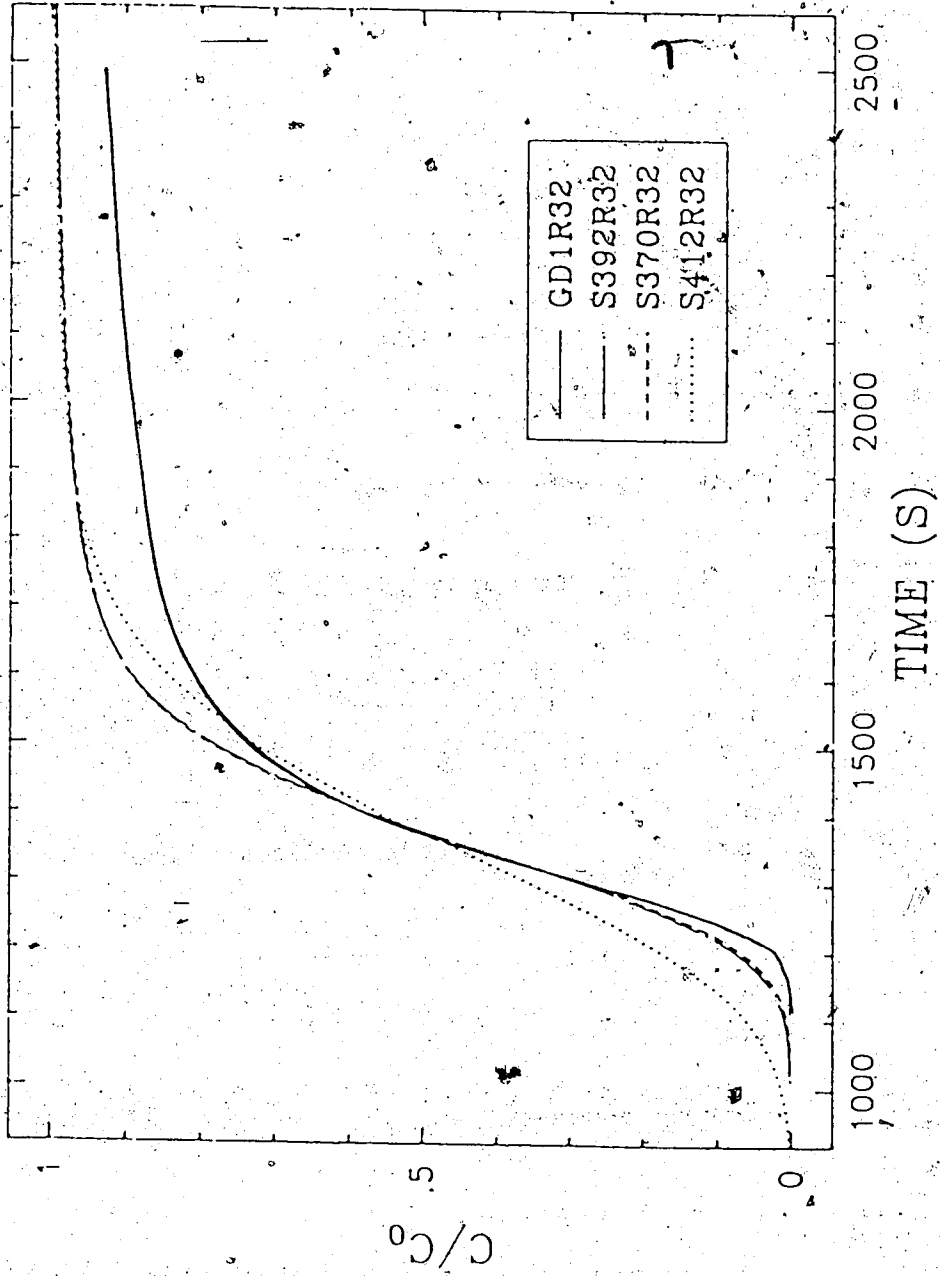


Figure 49: KB Variations

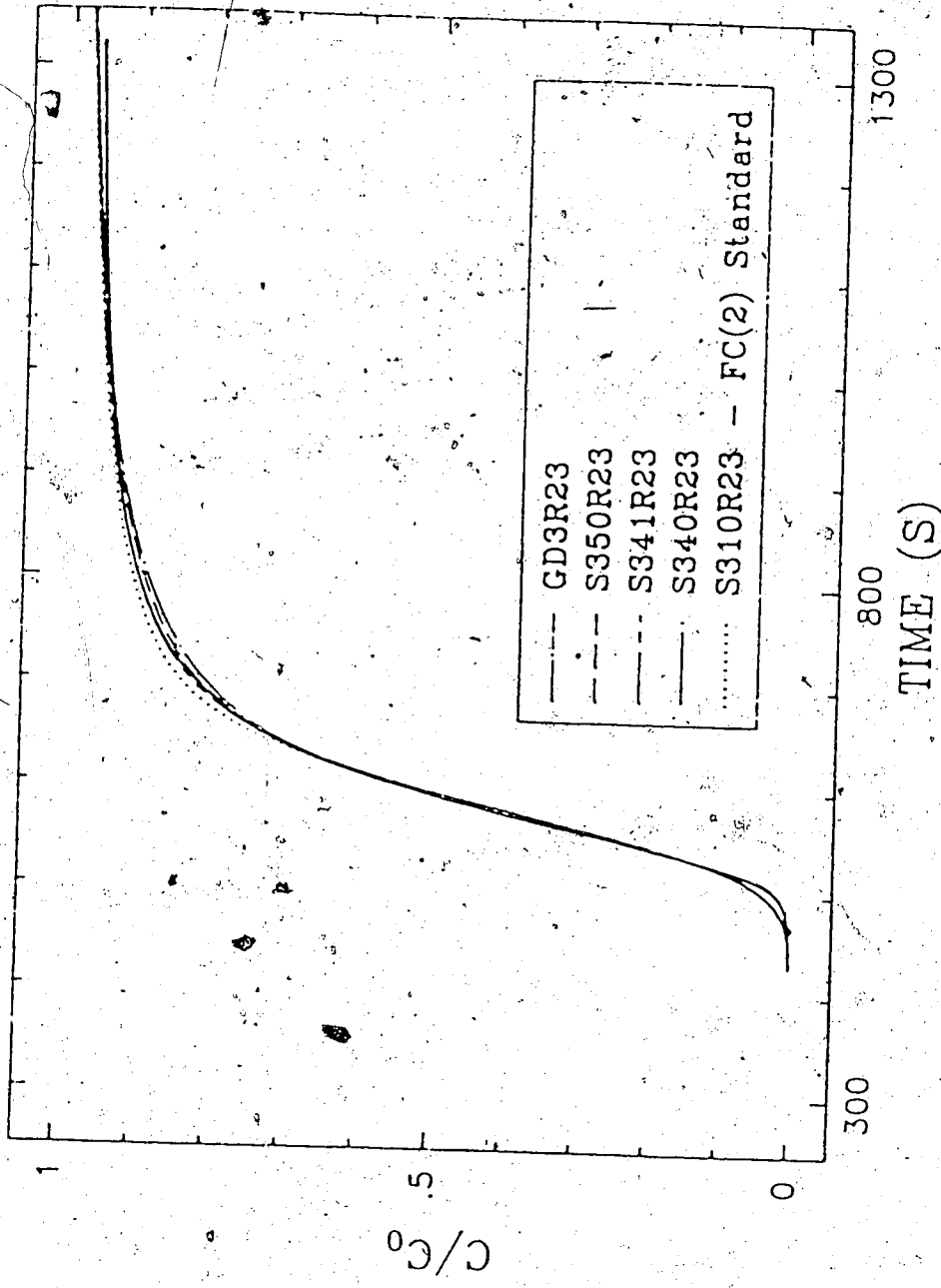


Figure 50: FC Variations

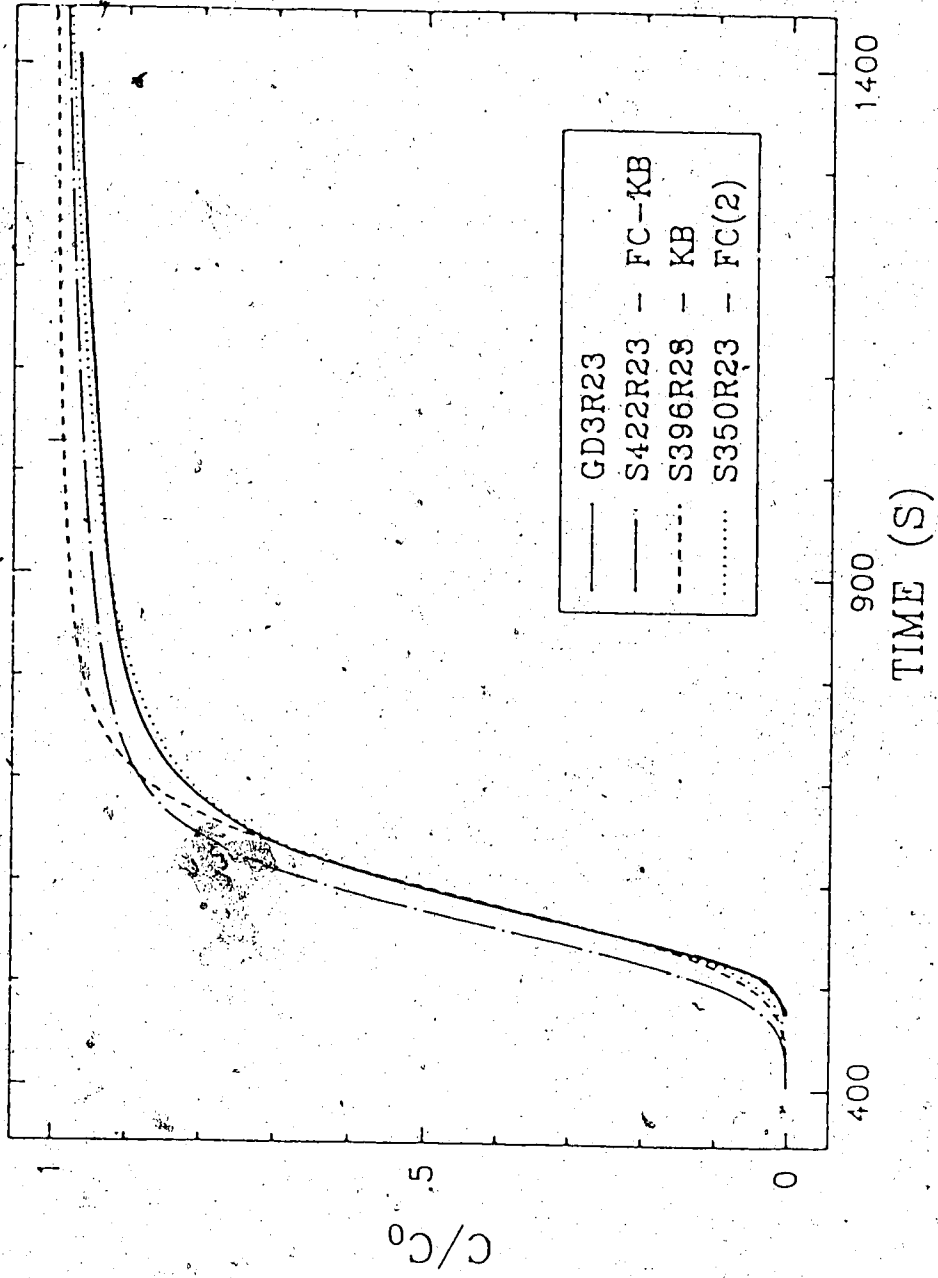


Figure 51: Model Type Variations

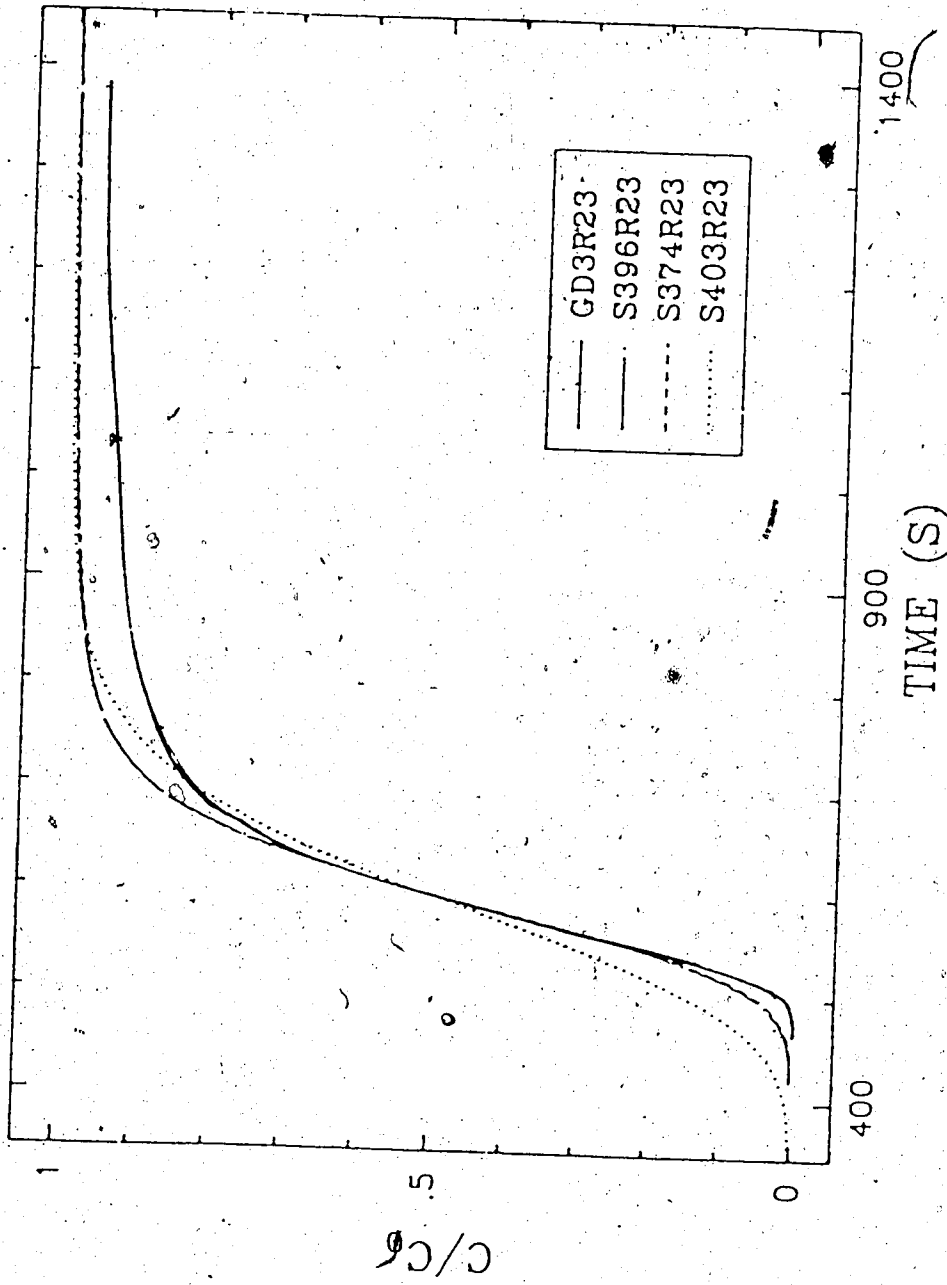


Figure 52: KB Variations

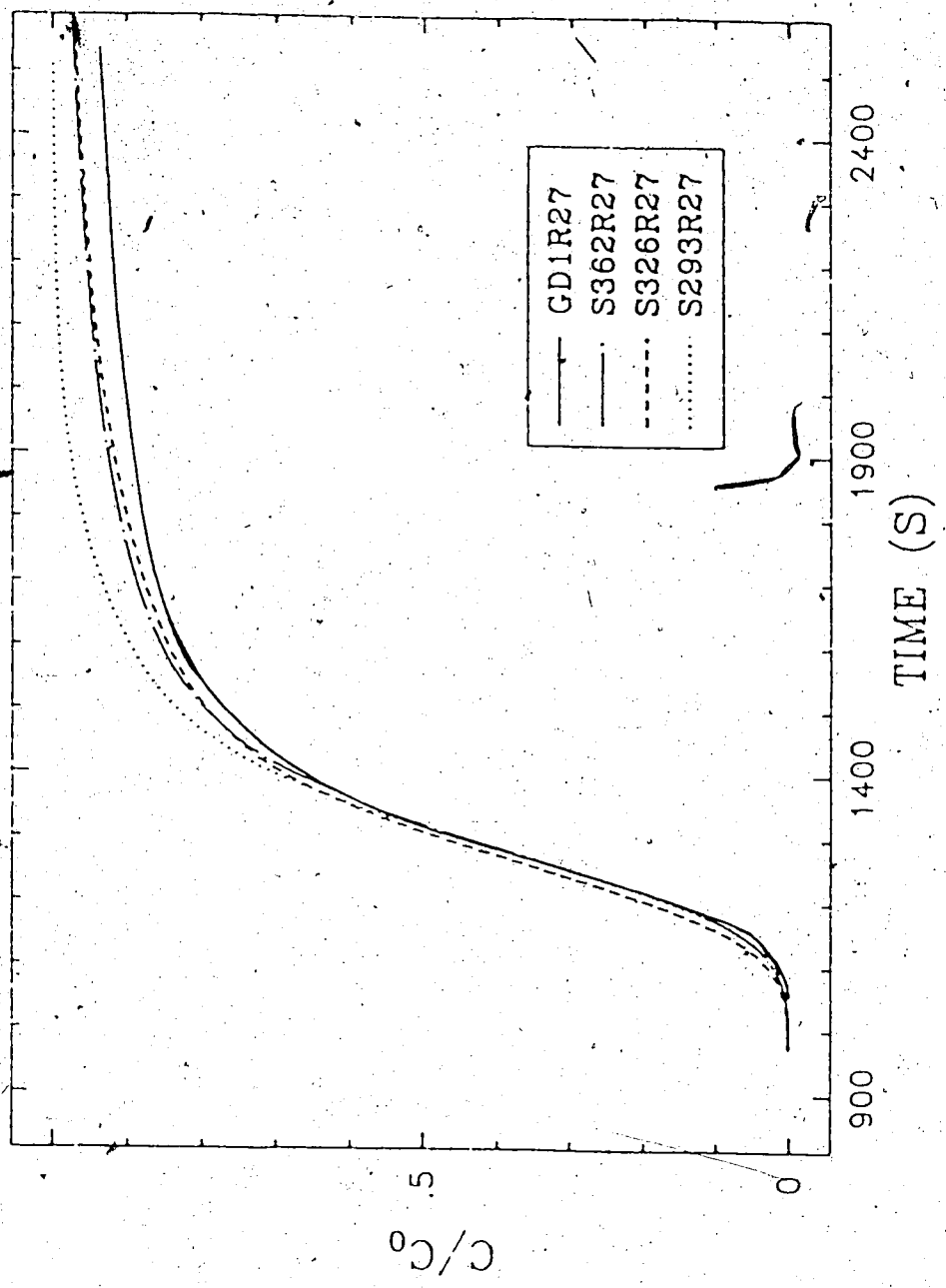


Figure 53: FC Variations



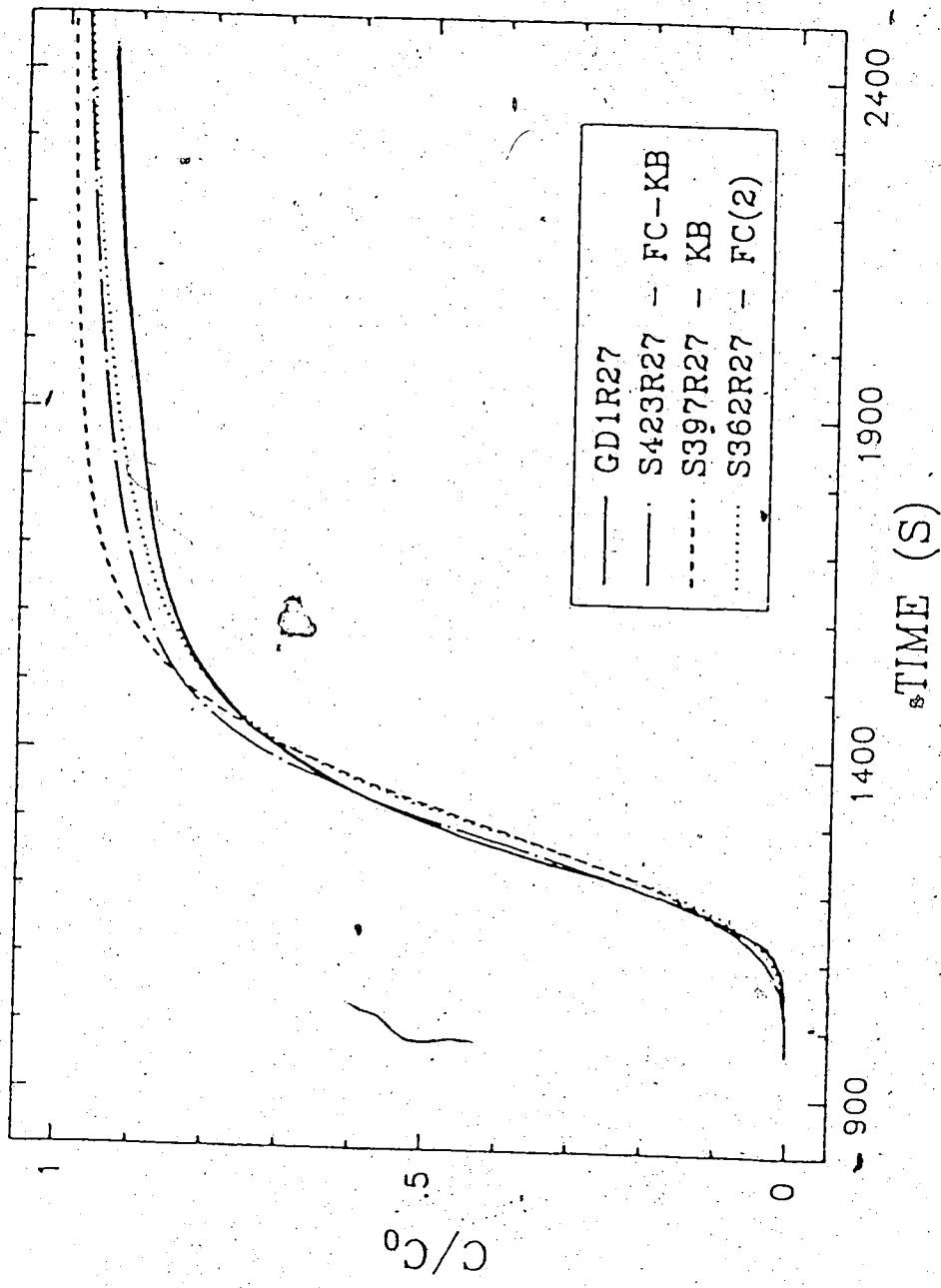


Figure 54: Model Type Variation

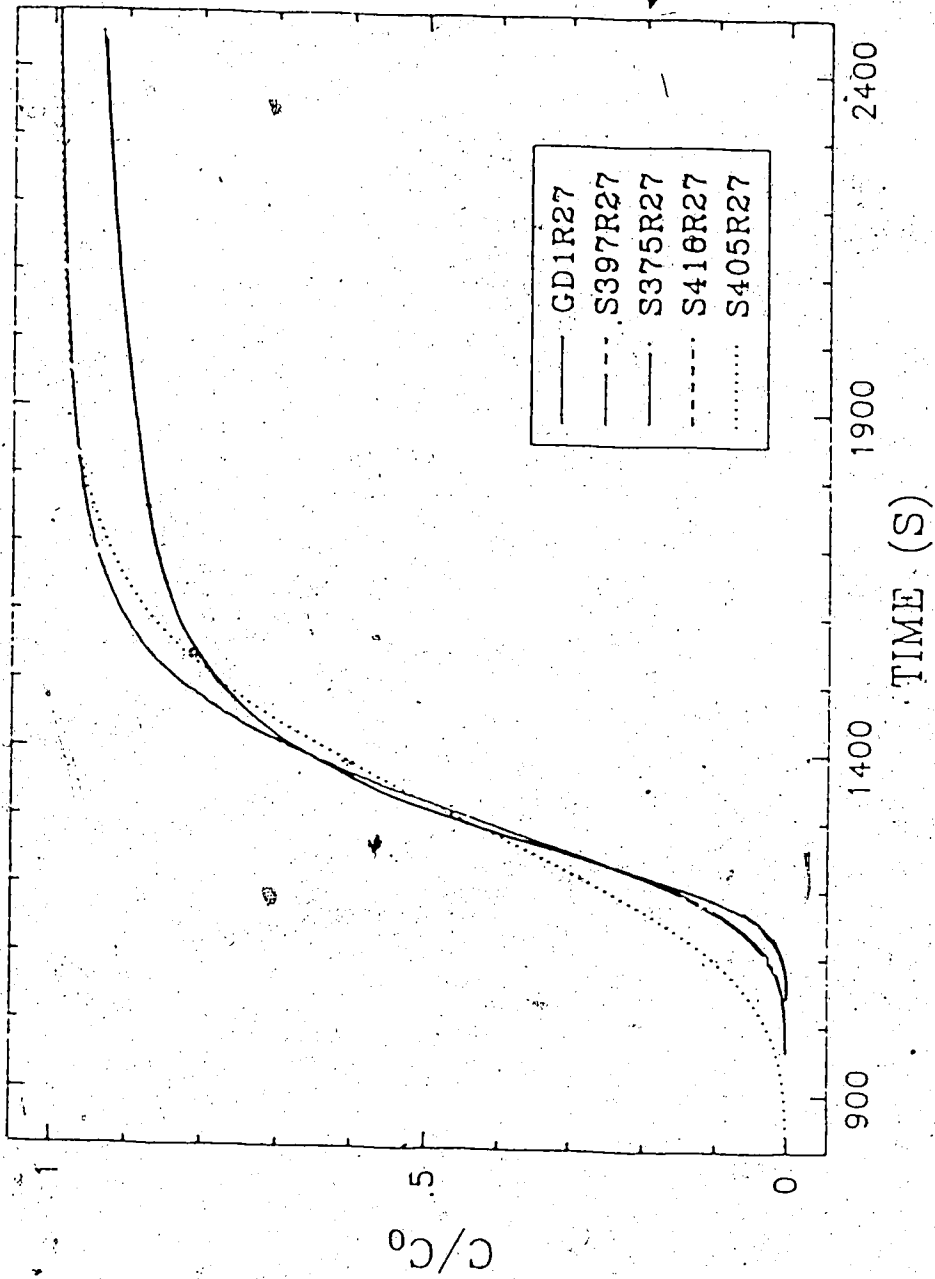


Figure 55: KB Variations

4.3 CONCLUSIONS AND RECOMMENDATIONS

The principal conclusion is that the rate of dispersion at high Peclet number is underestimated by models available in the literature, and this shortcoming is not due entirely to transient or non-local dispersion phenomena. The transition point is around a Pe_p of 150; below this, dispersion may be estimated using the standard Fried and Combarous (1971) dispersion models, although that cannot be proved with these data as all runs had some dispersion at high Peclet number.

The $Pe_p \ln(\phi Pe_p)$ dependence of the Koch & Brady (1985) model is the ruling term for the higher Peclet number region, as shown by the success there for the hybrid KB model. A simple model for longitudinal dispersion for Pe_p over 150 is just that term. However, the Koch & Brady model seems to overestimate dispersion at moderate Peclet (50 to 150), and underestimate at high (greater than 150). It may be very fruitful to continue with an adjustable Koch & Brady model, reducing the contribution of the natural log term stated above while increasing its value at high Peclet. e.g. Instead of the (1,1.5) pair tried here, a wider range may be employed to better effect. A transition region may be considered, between the high and low Peclet number regions. The functional form seems to be justified.

For the high Peclet number (over approximately 150) domain, longitudinal dispersion is adequately described by a Fried & Combarous type correlation, except that the value for α_1 is

around 4.5, or slightly greater, instead of their advised number of 1.8 ± 0.4 . This is roughly equivalent to using the natural log term described above, as the value of $\ln(\phi Pe_p)$ ranges from 4.3 to 8 for Pe_p in the range of 200 to 8000. The FC-KB model was used to take advantage of that observation.

The effect of using transient values for the longitudinal dispersion coefficient primarily was to reduce the total amount of dispersion. It did very little to increase the amount of tailing. This test was done in a qualitative manner by using a time dependent factor on the dispersion coefficient; the non-local models given in Koch & Brady (1987 a & b) have not been tested here. An offshoot model, assigning a path length dependent value to the dispersion coefficient, exhibited the same result as did the transient model; it simply decreased the total amount of dispersion.

Deconvolution may be reliably, if somewhat tediously, performed using the blank identification method given here. The results are much more stable and consistent than if discrete deconvolution is used.

The choice of boundary condition at the inlet, as either fixed equal to the feed concentration or varying as the Danckwerts condition, did not make a significant difference in the results. The effect is swamped by the choice of the adjustable parameters for whatever dispersion model is being employed.

The choice of definition for average particle diameter makes a very minor difference in the predicted breakthrough, and that

difference is swamped by the differences between the results for the variety of dispersion models. The effect of varying ratio of maximum to minimum bead diameter would be more significant, especially if mixtures are considered where the smaller beads fit in the small voids between larger beads. That was not the experimental condition for this work. For beads of roughly uniform size, the choice of definition of average particle diameter is immaterial.

As this study shows the high Peclet number region to be better modelled by using the longitudinal dispersion coefficient as proportional to Pe_p by a larger factor than previously known, a study aimed at obtaining exact values for this region is warranted. A comparison of the form of constant multiplied by Pe_p with the form of a constant times $\ln(\phi * Pe_p) * Pe_p$, where the values for the constant are different for low, transition and high Peclet regimes, is suggested.

It would be very interesting to try the Koch & Brady adjustable model for dispersion in beds of porous beads. Given that it has some success here with impermeable glass spheres, the one term in his model whose functional form was not tested is the one for porous particles.

Transverse dispersion effects may be studied using the same core design but much longer cores; that dispersive action takes place in the one dimensional (exit) flow regime where the concentration profile is roughly parabolic. Entrance effects would not be picked up, however.

Large packed beds may make collecting the data easier, at least in the sense that the step of deconvolution may be avoided. Using pressurized gas to force the flow may give steadier flow than HPLC pumps can provide.

REFERENCES

- Adler, P.M. and H. Brenner, "Transport Processes in Spatially Periodic Capillary Networks -I. Geometrical Description and Linear Flow Hydrodynamics", P.C.H. PhysicoChemical Hydrodynamics, 5(3/4):245-268, 1984
- Adler, P.M. and H. Brenner, "Transport Processes in Spatially Periodic Capillary Networks -II. Taylor Dispersion with Mixing, Verticles", P.C.H. PhysicoChemical Hydrodynamics, 5(3/4):269-285, 1984
- Adler, P.M. and H. Brenner, "Transport Processes in Spatially Periodic Capillary Networks -III. Nonlinear Flow Problems", P.C.H. PhysicoChemical Hydrodynamics, 5 (3/4):287-297, 1984
- Allen, T., *Particle Size Measurement*, 3rd Edition, Chapman and Hall, New York, 1981
- Ananthakrisnan, V., W.N. Gill and A.J. Barduhn, "Laminar Dispersion in Capillaries. Part 1: Mathematical Analysis", A.I.Ch.E. J., 11 (6):1063-1072, November 1965
- Aris, R., "On the Dispersion of a Solute in a Fluid Flowing Through a Tube", Proc. Roy. Soc. (London), 235A:67-77, 1956
- Babcock, R.E., D.W. Green and R.H. Perry, "Longitudinal Dispersion Mechanisms in Packed Beds", A.I.Ch.E. J., 12 (5):922-927, September 1966
- Bachmat, Y. and J. Bear, "The General Equations of Hydrodynamic Dispersion in Homogeneous, Isotropic, Porous Mediums", J. Geophys. Res., 69 (12):2561-2567, 1964
- Baker, L.E., "Effects of Dispersion and Dead-End Pore Volume in Miscible Flooding", S.P.E.J., June 1977:219-227
- Bear, J., *Dynamics of Fluids in Porous Media*, American Elsevier, New York, 1972

- Bear, J., "On the Tensor Form of Dispersion in Porous Media", *J. Geophys. Res.*, 66 (4):1185-1197, 1961
- Benenati, R.F. and C.B. Brosilow, "Void Fraction Distributions in Beds of Spheres", *A.I.Ch.E. J.*, 8(3):359-361, 1962
- Bhatia, Q.S., A. Ali and W.N. Gill, "Comparison of Approximate Methods for Solving Non-Linear Convective Diffusion Problems", *Chem. Eng. Commun.* 25:173-181, 1984
- Bird, R.B., W.E. Stewart and E.N. Lightfoot, *Transport Phenomena*, John Wiley and Sons, Toronto, 1960
- Blackwell, R.J., "Laboratory Studies of Microscopic Dispersion Phenomena", *S.P.E.J.*, March 1962:1-8
- Brenner, H., "Dispersion Resulting from Flow Through Spatially Periodic Porous Media", *Phil. Trans. Roy. Soc. (London)*, 297:11-133, July 1980
- Brenner, H., "The Diffusion Model of Longitudinal Mixing in Beds of Finite Length. Numerical Values", *Chem. Eng. Sci.*, 17:229-243, 1962
- Brigham, W.E., P.W. Reed and J.N. Dew, "Experiments on Mixing During Miscible Displacement in Porous Media", *S.P.E.J.*, March 1961:1-8
- Carberry, J.J. and R.H. Bretton, "Axial Dispersion of Mass in Flow Through Fixed Beds", *A.I.Ch.E. J.*, 4(3):367-375, 1958
- Carbonell, R.G., "Effect of Particle Size Distribution and Flow Non-Uniformities on Dispersion in Porous Media: Application to Oil Shale Retorts", *Proc. 2nd Multiphase Flow and Heat Transfer Symp.*, T. Veziroglu, Ed., 1979a, p. 2379
- Carbonell, R.G., "Effect of Pore Distribution and Flow Segregation on Dispersion in Porous Media", *Chem. Eng. Sci.*, 34:1031-1039, 1979b

- Carbonell, R.G., "Flow Non-Uniformities in Packed Beds: Effect on Dispersion", Chem. Eng. Sci., 35:1347-1356, 1980
- Carbonell, R.G. and S. Whitaker, "Dispersion in Pulsed Systems II. Theoretical Development for Passive Dispersion in Porous Media", Chem. Eng. Sci., 38(11):1795-1802, 1983
- Casulli, V. and D. Greenspan, "Numerical Simulation of Miscible and Immiscible Fluid Flows in Porous Media", S.P.E.J., October 1982:635-646
- Chandrasekhara, B.C., N. Rudraiah and S.T. Nagaraj, "Velocity and Dispersion in Porous Media", Int. J. Engng. Sci., 18:921-929, 1980
- Chandrasekhara, B.C. and D. Vortmeyer, "Flow Model for Velocity Distribution in Fixed Porous Beds under Isothermal Conditions", Thermo- and Fluid Dynamics, 12:105-111, 1979
- Chang, S. and J.C. Slattery, "A Linear Stability Analysis for Miscible Displacements", Transport in Porous Media, In Press, 1988
- Chen, H.R. and L.P. Blanchard, "Behavior of Macromolecules in Dilute Solutions: I - Longitudinal Dispersion", Can. J. Chem. Eng., 53:228-230, April 1975
- Chen, H.R. and L.P. Blanchard, "Behavior of Macromolecules in Dilute Solutions: II - On the Axial Dispersion Coefficient", Can. J. Chem. Eng., 53:476-480, October 1975
- Chen, J., "Pore Scale Difference between Miscible and Immiscible Viscous Fingering in Porous Media", A.I.Ch.E. J., 33(2):307-311, 1987
- Chen, T. and J.T. Hsu, "Prediction of Breakthrough Curves by the Application of Fast Fourier Transform", A.I.Ch.E. J., 33(8):1387-1390, August 1987
- Cheng, D.C.H. and E. Gulari, "Micellization and Intermicellar Interactions in Aqueous Sodium Dodecylbenzene Sulfonate Solutions", J. Coll. Interfac. Sci., 90(2):410-423, 1982

- Cheng, P., "Geothermal Heat Transfer", in *Handbook of Heat Transfer Applications*, 2nd Edition, (Rohsenow, W.M., J.P. Hartnett and E.N. Ganic, Editors), McGraw-Hill, Toronto, 1985
- Cheng, P. and C.T. Hsu, "Applications of Van Driest's Mixing Length Theory to Transverse Dispersion in Forced Convective Flow Through a Packed Bed", *Int. Comm. Heat Mass Transfer*, 13:613-625, 1986
- Chuoque, R.L., P. van Meurs and C. van der Poel, "The Instability of Slow, Immiscible, Viscous Liquid-Liquid Displacements in Permeable Media", *Trans. Am. Inst. Min. Met. Pet. Eng.*, 216:188, 1959
- Cluff, R. and J. Hawkes, "Zone Dispersion In Packings of Impermeable Spheres", *J. Chromatographic Sci.*, 14:248-255, May 1976
- Coats, K.H. and B.D. Smith, "Dead-End Pore Volume and Dispersion in Porous Media", *S.P.E.J.*, March 1964:73-84
- Cohen, Y. and A.B. Metzner, "Wall Effects in Laminar Flow of Fluids through Packed Beds", *A.I.Ch.E. J.*, 27(5):705-715, 1981
- Crane, F.E., H.A. Kendall and G.H.F. Gardner, "Some Experiments on the Flow of Miscible Fluids of Unequal Density Through Porous Media", *S.P.E.J.*, December 1963:277-280
- Dagan, D., "Perturbation Solutions of the Dispersion Equation in Porous Media", *Water Resour. Res.*, 7(1):135-142, February 1971
- Danckwerts, P.V., "Continuous Flow Systems: Distribution of Residence Times", *Chem. Eng. Sci.*, 2:1-3, 1953
- Deans, H.A., "A Mathematical Model for Dispersion in the Direction of Flow in Porous Media", *S.P.E.J.*, March 1963:49-52
- de Ligny, C.L., "Coupling Between Diffusion and Convection in Radial Dispersion of Matter By Fluid Flow Through Packed Beds", *Chem. Eng. Sci.*, 25:1177-1181, 1970

- Dieulin, A., G. Matheron and G. de Marsily, "Growth of the Dispersion Coefficient with the Mean Travelled Distance in Porous Media", *Sci. Total Environ.*, 21:319-328, 1981
- Diffey, B.L., F.M. Hall and J.R. Corfield, "The ^{99m}Tc-DTPA Dynamic Renal Scan with Deconvolution Analysis", *J. Nuclear Med.*, 17(5):352-355, 1976
- Dullien, F.A.L., *Porous Media: Fluid Transport and Pore Structure*, Academic Press Inc., New York, 1979
- Edwards, M.F. and J.F. Richardson, "Gas Dispersion in Packed Beds", *Chem. Eng. Sci.*, 23:109-123, 1968
- Eidsath, A., R.G. Carbonell, S. Whitaker and L.R. Herrmann, "Dispersion in Pulsed Systems -III. Comparison Between Theory and Experiment for Packed Beds", *Chem. Eng. Sci.*, 38(11):1803-1816, 1983
- Eldor, M. and G. Dagan, "Solution of Hydrodynamic Dispersion in Porous Media", *Water Resour. Res.*, 88(3):1316, 1972
- El-Mariah, A.A.R., Z.H. Kafafi and E.A. Moussa, "An Amperometric Study of the Aggregation of Some Acid Dyes", *Indian J. Chem.*, 23A:904-906, 1984
- Fair, G.M. and L.P. Hatch, "Fundamental Factors Governing Streamline Flow of Water Through Sands", *J. Amer. Water Works Assoc.*, 25 (11):1151-1565, 1933
- Fand, R.M., T.E. Steinberger and P. Cheng, "Natural Convection Heat Transfer from a Horizontal Cylinder Embedded in a Porous Medium", *Int. J. Heat Mass Transfer*, 29(1):119-133, 1986
- Fatt, I. and Goodnight, R.C., "Surface Concentration Buildup During Diffusion in Porous Media with Dead End Pore Volume", *J. Phys. Chem.*, 67:949-950, 1963
- Fatt, I., Goodnight, R.C. and W.A. Klikoff, "Nonsteady State Fluid Flow and Diffusion in Porous Media Containing Dead End Pore Volume", *J. Phys. Chem.*, 64:1162-1168, 1960

Fattah, Q.N. and J.A. Hoopes, "Dispersion in Anisotropic, Homogeneous Porous Media", *J. Hydraul. Eng.*, 111:810-827, May 1985

Fried, J.J., *Groundwater Pollution*, Elsevier, Amsterdam, 1975

Fried, J.J. and M.A. Combarous, "Dispersion in Porous Media", *Adv. Hydrosci.*, 7:169-282, 1971

Garder, A.O. Jr., D.W. Peaceman and A.L. Pozzi Jr., "Numerical Calculation of Multidimensional Miscible Displacement by the Method of Characteristics", *S.P.E.J.*, March 1964:26-36

Gill, W.N. and R. Sankarasubramanian, "Exact Analysis of Unsteady Convective Diffusion", *Proc. Roy. Soc. London Ser. A*, 316:341-350, 1970

Goddard, R.R., "Fluid Dispersion and Distribution in Porous Media Using the Frequency Response Method with a Radioactive Tracer", *S.P.E.J.*, June 1966:143-152

Govindarao, V.M.H. and G.F. Froment, "Voidage profiles in Packed Beds of Spheres", *Chem. Eng. Sci.*, 41(3):533-539, 1986

Greenkorn, R.A., *Flow Phenomena in Porous Media*, Marcel Dekker, Inc., New York, 1983

Greenkorn, R.A., "Steady Flow Through Porous Media", *A.I.Ch.E. J.*, 27(4):529-545, 1981

Greenkorn, R.A. and D.P. Kessler, "Dispersion in Heterogeneous Anisotropic Porous Media", *Ind. and Eng. Chem.*, 61(9):14-32, September 1969

Griffiths, A., "On the Movement of a Coloured Index Along a Capillary Tube, and its Application to the Measurement of the Circulation of Water in a Closed Circuit", *Proc. Phys. Soc. London*, 23:190, 1911

Guin, J.A., D.P. Kessler and R.A. Greenkorn, "The Dispersion

- Tensor in Anisotropic Porous Media", *Ind. Eng. Chem. Fundam.*, 11(4):477-482, 1972
- Gunn, D.J., "Theory of Axial and Radial Dispersion in Packed Beds", *Trans. Instn. Chem. Engrs.*, 47:T351-T359, 1969
- Gunn, D.J. and R. England, "Dispersion and Diffusion in Beds of Porous Particles", *Chem. Eng. Sci.*, 26:1413-1423, 1971
- Gunn, D.J. and C. Pryce, "Dispersion in Packed Beds", *Trans. Instn. Chem. Engrs.*, 47:T341-T350, 1969
- Haber, S. and R. Mauri, "Boundary Conditions for Darcy's Flow Through Porous Media", *Int. J. Multiphase Flow*, 9(5):561-574, 1983
- Han, N., J. Bhakta and R.G. Carbonell, "Longitudinal and Lateral Dispersion in Packed Beds: Effects of Column Length and Particle Size Distribution", *A.I.Ch.E. J.*, 31(2):277-288, 1985
- Harleman, D.R.F. and R.R. Rumer, "Longitudinal and Lateral Dispersion in an Isotropic Porous Medium", *J. Fluid Mech.*, 16:385-394, 1963
- Hassinger, R.C. and D.V. von Rosenberg, "A Mathematical and Experimental Examination of Transverse Dispersion Coefficients", *S.P.E.J.*, June 1968:195-204
- Hatton, T.A. and E.N. Lightfoot, "On the Significance of the Dispersion Coefficient in Two-Phase Flow", *Chem. Eng. Sci.*, 37(9):1289-1307, 1982
- Hayes, R.E. and P.A. Tanguy, "An Adaptive Domain Decomposition Method for Simulation of Transport in Porous Media", *Transport in Porous Media*, In Press, 1988
- Herzig, J.P., D.M. LeClerc and P. Le Goff, "Flow of Suspensions Through Porous Media - Application to Deep Filtration", *Ind. Eng. Chem.*, 62(5):8-35, May 1970
- Hiemenz, P.C., *Principles of Colloid and Surface Chemistry*, Marcel

- Dekker Inc., New York, 1977
- Jeffrey, D.J., "Conduction Through a Random Suspension of Spheres", Proc. R. Soc. Lond., 335:355-367, 1973
- Kalpakci, B., E.E. Klaus, J.L. Duda and R. Nagarajan, "Flow Characteristics of Surfactant Solutions in Porous Media and Their Role in Permeability Modification", S.P.E.J., December 1981:709-720
- Kehinde, A.J., R.R. Hudgins and P.L. Silveston, "Measurement of Axial Dispersion in Packed Beds at Low Reynolds Numbers by Imperfect Pulse Chromatography", J. Chem. Eng. Japan, 16(6):476-482, 1983
- Klingman, K.J. and H.H. Lee, "Alternating Flow Model for Mass and Heat Dispersion in Packed Beds", A.I.Ch.E. J., 33(3):366-381, 1987
- Koch, D.L. and J.F. Brady, "Dispersion in Fixed Beds", J. Fluid Mech., 154:399-427, 1985
- Koch, D.L. and J.F. Brady, "A Non-Local Description of Advection-Diffusion with Application to Dispersion in Porous Media", J. Fluid Mech., 180:387-403, 1987a
- Koch, D.L. and J.F. Brady, "Nonlocal Dispersion in Porous Media: Nonmechanical Effects", Chem. Eng. Sci., 42(6):1377-1392, 1987b
- Kramers, H. and G. Albreda, "Frequency Response Analysis of Continuous Flow Systems", Chem. Eng. Sci., 2:173, 1953
- Kreft, A. and A. Zuber, "On the Physical Meaning of the Dispersion Equation and Its Solutions For Different Initial and Boundary Conditions", Chem. Eng. Sci., 33:1471-1480, 1978
- LeGoff, P., D. LeClerc and J. Dodds, "The Structure of Packed Beds: Continuity of Research in Nancy and Some New Results", Powder Tech., 42:47-53, 1985
- Li, W. and R.P. Canale, "Dispersion from Sources in Non-Uniform

Seepage Flow", J. Hydraulics Div. Proc. A.S.C.E., No. HY 3:65-79, May 1967

Ljung, L., *System Identification - Theory for the User*, Prentice Hall, Englewood Cliffs, New Jersey, 1987

MacDonald, I.F., M.S. El-Sayed, K. Mow and F.A.L. Dullien, "Flow Through Porous Media- the Ergun Equation Revisited", Ind. Eng. Chem. Fund., 18:199-208, 1979

McKeown, G.G. and J.L. Thomson, "The Polarographic Reduction of Amaranth", Canadian J. Chemistry, 32:1025-1032, 1954

Miyauchi, T. and T. Kikuchi, "Axial Dispersion in Packed Beds", Chem. Eng. Sci., 30:343-348, 1975

Mohsen, M.F.N. and M.A. Baluch, "An Analytical Solution of the Diffusion Convection Equation Over a Finite Domain", Appl. Math Modelling, 7:285-287, August 1983

Ng, K.M. and A.C. Payatakes, "Critical Evaluation of the Flow Rate - Pressure Drop Relation Assumed in Permeability Models", A.I.Ch.E. J., 31(9):1569-1571, 1985

Niemann, E.H., M.S. Thesis, Purdue University, Lafayette, Indiana, 1969

Nunge, R.J. and W.N. Gill, "Mechanisms Affecting Dispersion and Miscible Displacement", *Flow Through Porous Media*, 6th Ind. and Eng. Chem. Symp., June 9-11, 1969, pp. 180-196

Ogata, A. and R.B. Banks, "A Solution of the Differential Equation of Longitudinal Dispersion in Porous Media", U.S. Geological Survey Professional Paper, 411-A, 1961

Ogata, K., *Modern Control Engineering*, Prentice Hall, Englewood Cliffs, New Jersey, 1970

Paine, M.A., R.G. Carbonell and S. Whitaker, "Dispersion in Pulsed Systems - I. Heterogeneous Reaction and Reversible Adsorption in Capillary Tubes", Chem. Eng. Sci., 38(11):1781-1793, 1983

- Parker, J.C., 'Analysis of Solute Transport in Column Tracer Studies', Soil Sci. Soc. Am. J., 48:719-724, 1984
- Patel, K.M., *Ph. D. Thesis*, University of Bath, 1983
- Patel, K.M. and M. Greaves, "Surfactant Dispersion in Porous Media", Chem. Eng. Res. Des., 65:12-22, 1987
- Patel, R.D. and R.A. Greenkorn, "On Dispersion in Laminar Flow Through Porous Media", A.I.Ch.E. J., 16(2):332-334, 1970
- Peaceman, D.W., "Improved Treatment of Dispersion in Numerical Calculation of Multidimensional Miscible Displacement", S.P.E.J., September 1966:213-216
- Peaceman, D.W. and H.H. Rachford, Jr., "Numerical Calculation of Multidimensional Miscible Displacement", S.P.E.J., December 1962:327-339
- Pearson, J.R.A., "A Note on the Danckwerts' Boundary Conditions for Continuous Flow Reactors", Chem. Eng. Sci., 10:281-284, 1959
- Perkins, T.K. and O.C. Johnston, "A Review of Diffusion and Dispersion in Porous Media", S.P.E.J., March 1963:70-84
- Pozzi, A.L. and R.J. Blackwell, "Design of Laboratory Models for Study of Miscible Displacement", S.P.E.J., March 1963:28-40
- Prasad, V., F.A. Kulacki and A.V. Kulkarni, "Free Convection in a Vertical, Porous Annulus with Constant Heat Flux on the Inner Wall - Experimental Results", Int. J. Heat Mass Transfer, 29(5):713-723, 1986
- Raimondi, P., G.H.F. Gardner and C.B. Patrick, "Effect of Pore Structure and Molecular Diffusion on the Mixing of Miscible Liquids Flowing in a Porous Media", A.I.Ch.E. -S.P.E. Joint Symposium, San Francisco, 1959
- Ramirez, W.F., P.J. Schuler and F. Friedman, "Convection,

- "Dispersion and Absorption of Surfactants in Porous Media", S.P.E.J., December 1980:430-438
- Rasmuson, A., "Diffusion and Sorption in Particles and Two - Dimensional Dispersion in a Porous Medium", Water Resour. Res., 17(2):321-328, April 1981
- Rasmuson, A., "Exact Solution of a Model for Diffusion in Particles and Longitudinal Dispersion in Packed Beds: Numerical Evaluation", A.I.Ch.E. J., 31(3):518-519, 1985
- Rasmuson, A., "Exact Solution of Some Models for the Dynamics of Fixed Beds using Danckwerts' Inlet Condition", Chem. Eng. Sci., 41(3):599-600, 1986
- Rasmuson, A. and I. Neretnieks, "Exact Solution of a Model for Diffusion in Particles and Longitudinal Dispersion in Packed Beds", A.I.Ch.E. J., 26(4):687-691, 1980
- Reis, J.F.G., E.N. Lightfoot, P.T. Noble and A.S. Chiang, "Chromatography in a Bed of Spheres", Sep. Sci. Tech., 14:367-394, 1979
- Ridgeway, K. and K.J. Tarbeck, "Radial Voidage Variation in Randomly Packed Beds of Spheres of Different Sizes", J. Pharmacy and Pharmacology, 18(suppl.):168s-175s, 1966
- Riekert, L., "The Relative Contribution of Pore Volume Diffusion and Surface Diffusion to Mass Transfer in Capillaries and Porous Media", A.I.Ch.E. J., 31(5):863-864, 1985
- Rose, D.A., "Hydrodynamic Dispersion in Porous Materials", Soil Science, 123(5):277-283, 1977
- Rudraiah, N. and D. Vortmeyer, "The Effect of Aspect Ratio on Longitudinal Diffusivity in a Porous Medium of Rectangular Cross-Section", Int. Comm. Heat Mass Transfer, 12:313-322, 1985
- Saffman, P.G., "Dispersion Due to Molecular Diffusion and Macroscopic Mixing in Flow Through a Network of Capillaries", J. Fluid Mech., 7:194-208, 1960

Saffman, P.G., "Dispersion in Flow Through a Network of Capillaries", Chem. Eng. Sci., 11:125-129, 1959

Saffman, P.G. and Sir G. Taylor, "The Penetration of a Fluid into a Porous Medium or Hele-Shaw Cell Containing a More Viscous Liquid", Proc. Roy. Soc. (London), A245:312, 1958

Satter, A., Y.M. Shum, W.T. Adams and L.A. Davis, "Chemical Transport in Porous Media with Dispersion and Rate Controlled Adsorption", S.P.E.J., 20(3):129-138, June 1980

Scheidegger, A.E., *The Physics of Flow Through Porous Media*, University of Toronto Press, Toronto, Canada, 1963

Schowalter, W.R., "Stability Criteria for Miscible Displacement of Fluids from a Porous Medium", A.I.Ch.E. J., 11(1):99-105, January 1965

Schwartz, F.W., "Macroscopic Dispersion in Porous Media: The Controlling Factors", Water Resources Res., 13(4):743-752, 1977

Settari, A., "Development and Application of Variational Methods for Simulation of Miscible Displacement in Porous Media", S.P.E.J., June 1977:228-246

Shergold, F.A., "The Effect of Sieve Loading on the Results of Sieve Analysis of Natural Sands", J. Soc. Chem. Ind. Trans. Comm., 65:245-249, 1946

Smith, L. and F.W. Schwartz, "Mass Transport 1: Stochastic Analysis of Macroscopic Dispersion", Water Resources Res., 16(2):303-313, 1980

Spiegel, M.R., *Theory and Problems of Vector Analysis*, Schaum's Outline Series, McGraw-Hill, 1974

Stalkup, F.I. Jr., *Miscible Displacement*, Monograph, Volume 8, A.I.M.E., S.P.E.J., Henry L. Doherty Series, New York, 1983

- Stanek, R. and J. Szekely, "The Effect of Non-Uniform Porosity in Causing Flow Maldistributions on Isothermal Packed Beds", *Can. J. Chem. Eng.*, 50:9-14, 1972
- Stephenson, J.L. and W.E. Stewart, "Optical Measurements of Porosity and Fluid Motion in Packed Beds", *Chem. Eng. Sci.*, 41(8):2161-2170, 1986
- Taigbenu, A. and J.A. Liggett, "An Integral Solution for the Diffusion-Advection Equation", *Water Resources Research*, 22(8):1237-1246, 1986
- Taylor, Sir G., "Dispersion of Soluble Matter in Solvent Flowing Slowly Through a Tube", *Proc. Roy. Soc. London*, 219A:186-203, 1953
- Taylor, Sir G., "Conditions Under Which Dispersion of a Solute in a Stream of Solvent Can be Used to Measure Molecular Diffusion", *Proc. Roy. Soc. London*, 225A:473-477, 1954
- Thuraisingham, S.T. and G.D. Towner, "A Simple Non-Destructive Method for Studying Longitudinal Dispersion Profiles", *Chem. Eng. Sci.*, 33:141-143, 1978
- Tinghui, L., T. Matsuura and S. Sourirajan, "Effect of Membrane Materials and Average Pore Sizes on Reverse Osmosis Separation of Dyes", *Ind. Eng. Chem. Prod. Res. Dev.*, 22:77-85, 1983
- Trogus, F.J., T. Sophany, R.S. Schecter and W.H. Wade, "Static and Dynamic Adsorption of Anionic and Non-Ionic Surfactants", *S.P.E.J.*, October 1977:337-344
- Ultman, J.S. and D.W. Weaver, "Concentration Sampling Methods in Relation to the Computation of a Dispersion Coefficient", *Chem. Eng. Sci.*, 34:1170-1172, 1979
- Vafai, K., "Convective Flow and Heat Transfer in Variable Porosity Media", *J. Fluid Mech.*, 147:233-259, 1984
- Vafai, K. and C.L. Tien, "Boundary and Inertia Effects on Convective Mass Transfer in Porous Media", *Int. J. Heat Mass Transfer*, 25(8):1183-1190, 1980

- Vafai, K. and C.L. Tien, "Boundary and Inertia Effects on Flow and Heat Transfer in Porous Media", *Int. J. Heat Mass Transfer*, 24:195-203, 1981
- Valentinuzzi, M.E. and E.M. Montaldo Volachec, "Discrete Deconvolution", *Med. Biol. Eng.*, 13:123-125, 1975
- van der Poel, C., "Effect of Lateral Diffusivity on Miscible Displacement in Horizontal Reservoirs", *S.P.E.J.*, Dec 1962:317-326
- Van Zee, G.A., W.M.M. Schinkel and O.H. Bosgra, "Estimation of the Transfer Function, Time Moments and Model Parameters of a Flow Process", *A.I.Ch.E. J.*, 33(2):341-346, 1987
- Vergnes, F., "A Simple and Practical Method for the Determination of the Peclet Number in the Longitudinal Model", *Chem. Eng. Sci.*, 31:88-90, 1976
- Vortmeyer, D. and J. Schuster, "Evaluation of Steady Flow Profiles in Rectangular and Circular Packed Beds By a Variational Method", *Chem. Eng. Sci.*, 38(10):1691-1699, 1983
- Warren, J.E. and F.F. Skiba, "Macroscopic Dispersion", *S.P.E.J.*, Sept. 1964:215-230
- Whitaker, S., "Advances in the Theory of Fluid Motion in Porous Media", I. and E.C., 61:14-28, 1969
- Whitaker, S., "Diffusion and Dispersion in Porous Media", *A.I.Ch.E. J.*, 13(3):420-427, May 1967
- Whitaker, S., "The Equations of Motion in Porous Media", *Chem. Eng. Sci.*, 21:291-300, 1966
- Wright, N.A., D.C. Villalantl and M.F. Burke, "Fourier Transform Deconvolution of Instrument and Column Band Broadening in Liquid Chromatography", *Anal. Chem.*, 54:1735-1738, 1982
- Wylie, C.R. and L.C. Barrett, *Advanced Engineering Mathematics*,

5th Edition, McGraw-Hill, New York, 1982.

Yellig, W.F. and L.E. Baker, "Factors Affecting Miscible Flooding Dispersion Coefficients", J. Can. Pet. Technol., (Oct - Dec 1981), Montreal, pp. 69-75.

APPENDIX A

The following plots contain the original run and blank data that were combined to give the deconvolved results presented in the third chapter. A similar naming convention is used here; the run data file names begin with "GOR", the blanks with "GOB", the deconvolved runs with "GD", and the simulation runs with "S". These raw data have been smoothed and the initial point of the breakthrough identified before plotting. The smoothing was performed although the noise on the original data was very low.

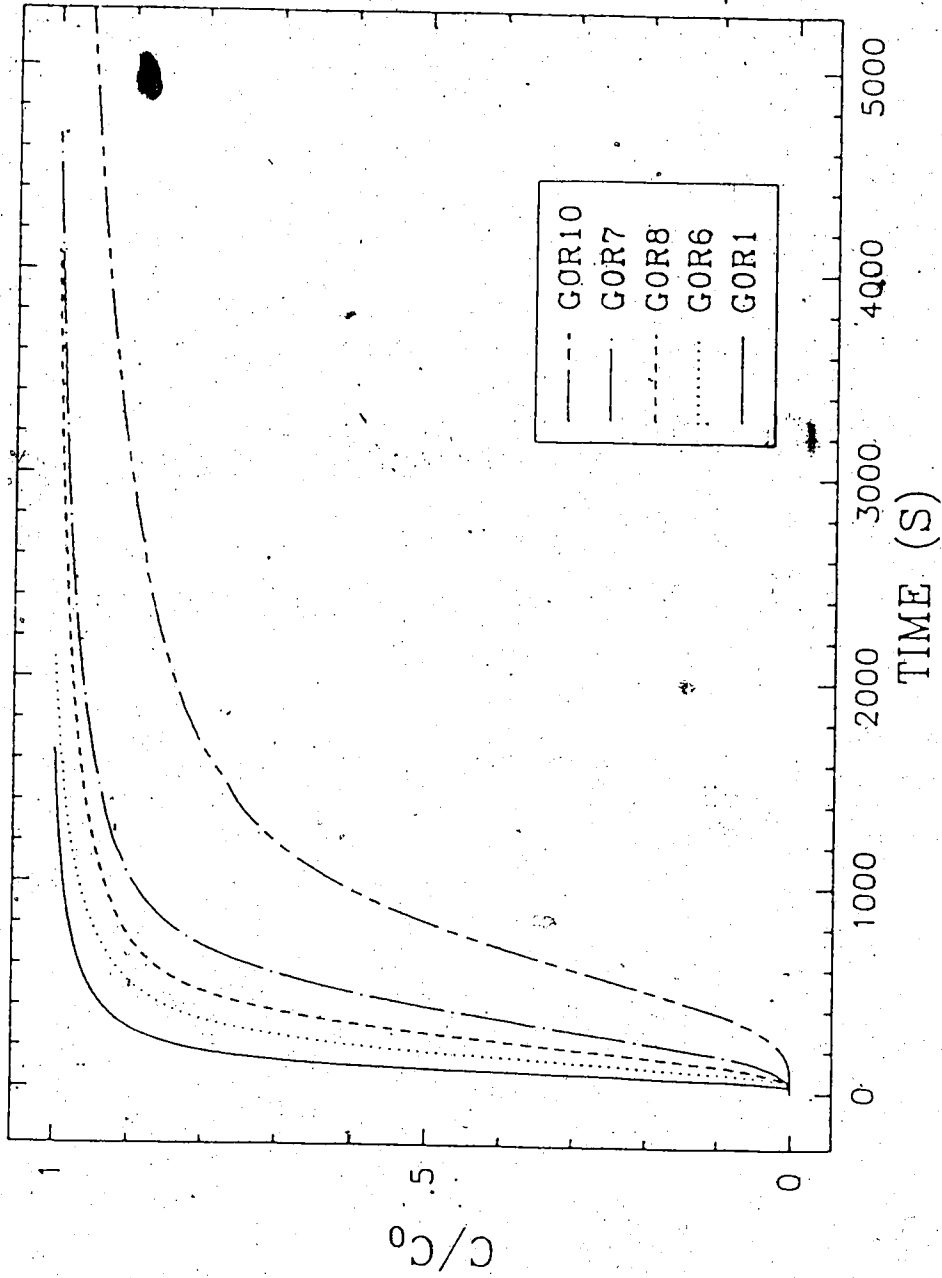


Figure A.1: Raw Data for 3x1 Inch Core

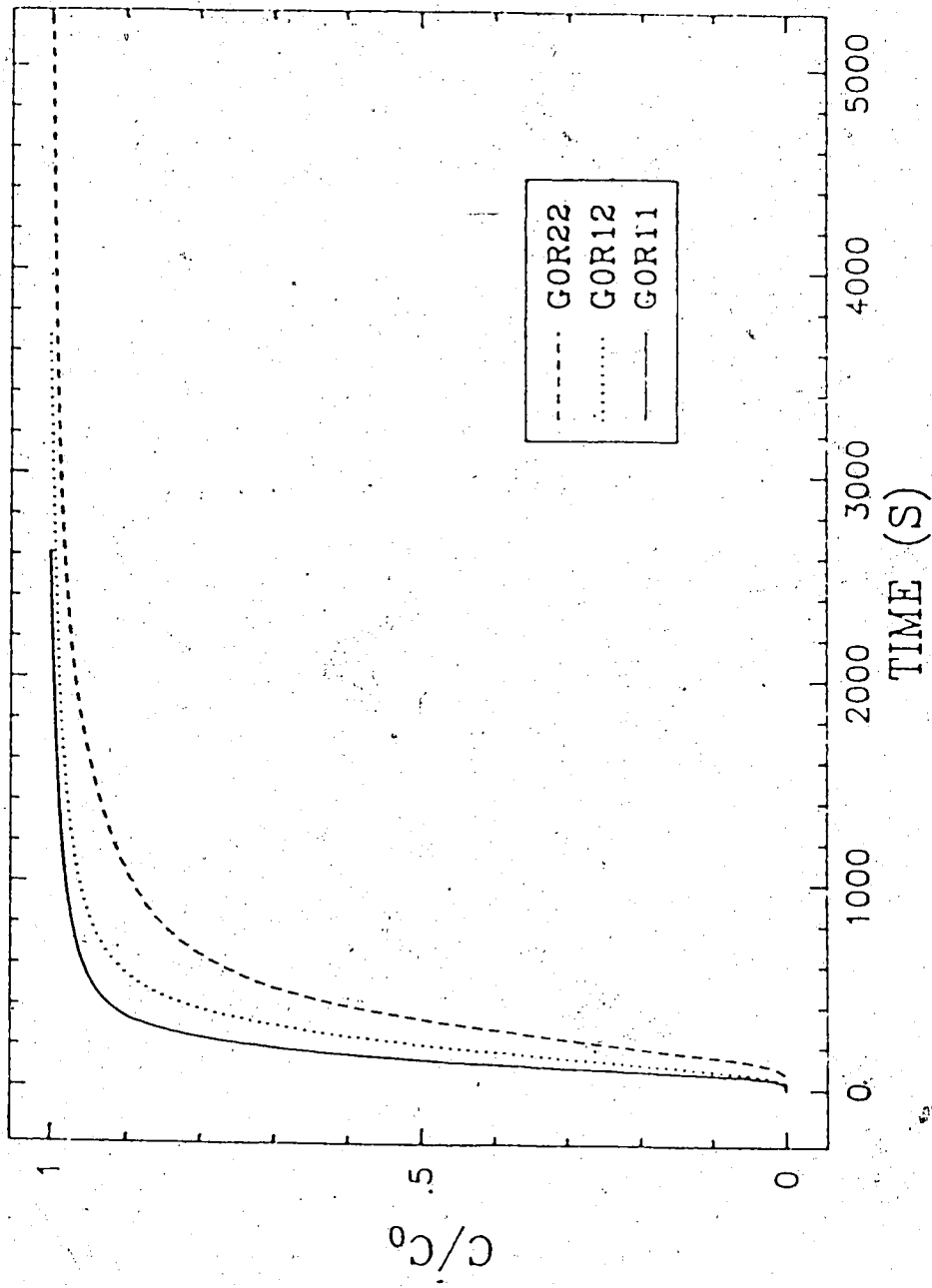


Figure A.2: Raw Data for 3x1.5 Inch Core

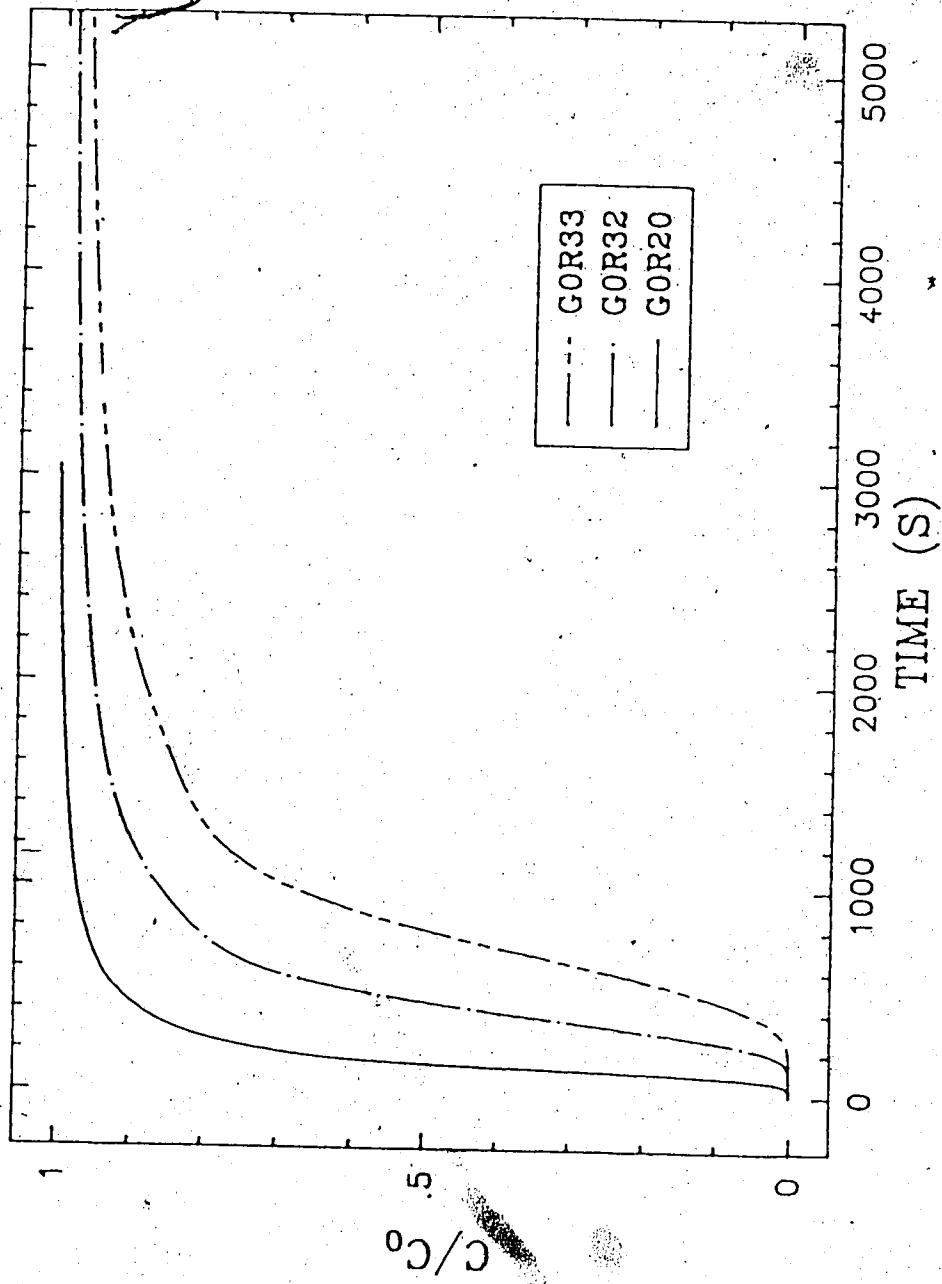


Figure A.3: Raw Data for 6x1 Inch Core

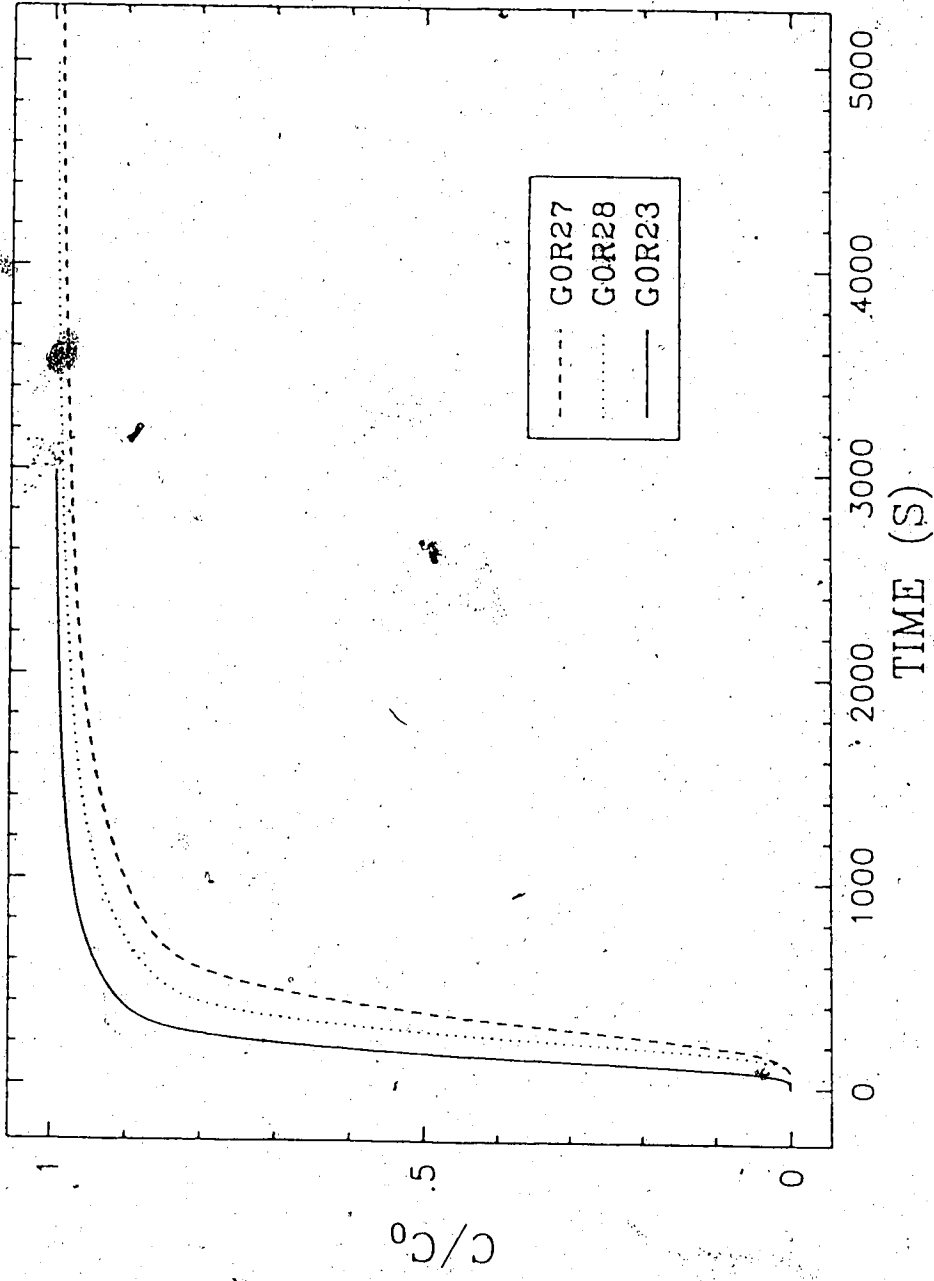


Figure A.4: Raw Data for 6x1.5 Inch Core

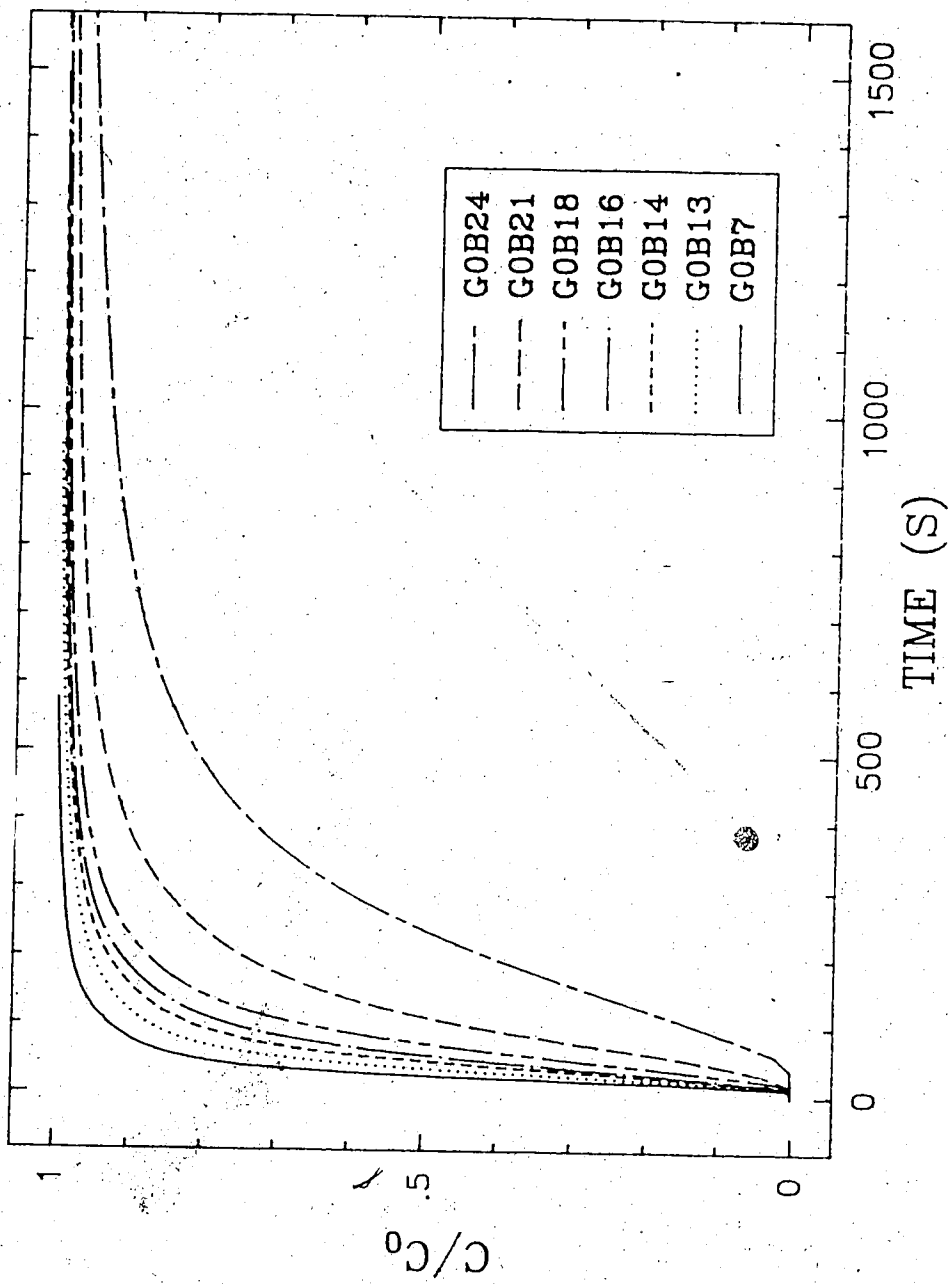


Figure A.5: Raw Data for Blank Runs

